One-dimensional chiral topological insulators in ladder models

Tyler Hewitt

Supervisor: Dr. Sam Carr

Division of Natural Sciences - School of Physics and Astronomy
Physics of Quantum Materials Group
University of Kent

This dissertation is submitted for the degree of
Doctor of Philosophy

November 2023

Declaration

I declare that the content of this thesis, titled "One-dimensional chiral topological insulators in ladder models" is entirely my own, and has not been submitted for the purposes of a qualification at any other institution or for any other degree. The content comprising chapters 3, 4, 5, and 6 has been adapted and extended from Matveeva, P., Hewitt, T., Liu, D., Reddy, K., Gutman, D., and Carr, S. T (2022). All data is my own, unless explicitly stated otherwise. All instances where use has been made of other work have been cited.

Tyler Hewitt
November 2023

Acknowledgements

For his infinite patience and wisdom I would wholeheartedly like to thank my supervisor of many years Dr. Sam Carr. He has seen me through a multitude of challenges and a number of degrees, this thesis being the final one. I have deeply valued our work, collaborations, and the physics we have done together. Additional thanks to the PQM group for the many interesting seminars and discussions.

The next major acknowledgement goes to my mother for supporting me, in so many ways, through these various degrees especially this PhD. Her love, consistent words of support especially in the difficult times, her wisdom on life, and mountains of patience have seen me through and made this possible.

Special mentions to the members of UKC Men's lacrosse, Canterbury City Lacrosse Club, and Christchurch Lacrosse for the many hours of distraction on and off the pitch and for the friends made. Specific honorable mentions to Joey B. and Josh M.

Another special thanks to the members of office 208 that have come and gone, including Leon, Oni, Henry, John P., Tym, John M., Joe, Alix, Oriella, Chloe, and Katie. I am especially grateful for the shared PhD experience, productive and not, the work would not have been as pleasureable without these people.

And finally my upmost gratitude and appreciation to my friends Charles T., Lizzie E., Andrew B., Will S., and Harry H. for the support and sanity.

Abstract

The topological insulator state describes a quantum state of matter that hosts topologically protected conductive edge modes, similar to the quantum spin Hall state but without the necessary applied fields. The coupling of topology to condensed matter theory in the context of topological insulators has produced the periodic table of topological insulators and superconductors. The ever popular SSH chain has become the prototypical model for describing simple topological properties in one-dimension. It is widely known that this model, in its modern form, hosts symmetry protected end states that are at zero energy. This model has supported mountains of research.

In this thesis we will use two deformed SSH model chains to constuct ladder models that are topological insulators in each of the chiral universality classes (AIII, BDI, CII, DIII, and CI). We systematically construct these models from general forms to specific forms examining their energy and wavefunction spectrums, leading easily to the conclusion of their topological nature. These constructions are motivated by the finding that the winding number has a sign ambiguity. This ambiguity leads to two forms of the chiral symmetry operator and subsequently two forms of the ladder, one adhering to the BDI and CII universality classes, and one for the DIII and CI classes. We are able to analytical derive expressions for the edge states in each chiral class ladder model and demonstrate the symmetry properties of each are encoded in these states. Additionally we show that, as a consequence of the sign ambiguity, for a weak interchain coupling, the winding numbers of the individual chains can be added leading to an index of 2, in the case of the BDI and CII class models, or subtracted giving an index of 0 in the case of the DIII and CI models. The conclusions and properties from this section of work is completely general and applicable to other chiral models.

In the final section of research we show via diagrammatic arguments and mean field theory the existence of a $\mathbb{Z}_2$ symmetry breaking bond density wave ground state in an SSH-like model with density-density interactions and a reduced filling fraction. The reduced filling fraction stabilizes a topological ground state where interactions would normally not permit one to exist. We further demonstrate this ground state occurs as a result of mean field rather than strong correlation effects. The ground state model turns out to be the noninteracting SSH4 model which we show has quantized Zak phases of individual bands confirming the topological nature of the model in a reduced filling fraction regime.

Publication: P. Matveeva, T. Hewitt, D. Liu, K. Reddy, D. Gutman, and S. T. Carr, 'One-dimensional noninteracting topological insulators with chiral symmetry', Phys. Rev. B., vol. 107, no. 7, Feb. 2023.

Table of contents

List of figures

List of tables

Chapter 1

Introduction

While symmetry has been a strong member of physics for centuries, topology is a relatively recent addition. These two concepts have become an entangled entity propelling physics research forward in a number of areas. In the last twenty years or so, topology has become a driving force behind our understanding of a range of fields in physics from elementary particles through exotic phases of matter [1]. In the field of condensed matter theory topology is playing a central role in how we classify phases and their properties [2, 3]. Novel work in discoveries of topological phases which has laid the ground work for much of condensed matter research today garnered Nobel prizes in Physics, notably in 2016[1]. In the context of electronic solid state physics this classification via topological indexes emerged with the integer quantum Hall effect [4] where the quantized Hall voltage is the topological quantum number which, in this case acts as the topological invariant of the model. The applied magnetic field in the integer quantum Hall model results in broken time-reversal symmetry and Landau levels opening a energy spectral gap in the bulk of the two-dimensional sample. The topological invariant in this case is the first Chern number, the typical invariant for odd-dimensional systems. The Chern number forces this gap to close at the boundaries causing protected chiral edge modes to emerge [5]. These modes are topological causing them to be robust against any symmetry preserving perturbations and are electronically conductive. We have come to understand that an applied magnetic field isn't necessary to induce robust conductive edge states, e.g. the quantum spin Hall effect discovered by Kane and Mele [6]. If one engineers the topology of the occupied bands correctly, robust edge states emerge. The name topological insulator was given to such models, and research into these nontrivial topological states has become a strong branch of condensed matter theory and materials science.

A major contribution to these theories and materials has been understanding the role of symmetry in these models, which led to a plethora of different invariants to classify phases in noninteracting electronic systems. It was previously thought that the integer quantum Hall state was the only phase that cannot be smoothly deformed into a trivial band insulator without breaking one of the protecting symmetries, although in higher

[1]Given to Thouless, Haldane, and Kosterlitz for 'Theoretical discoveries of topological phase transitions and topological phases of matter'.

dimensions it is possible. It was later found that by instituting a symmetry on the model, such as time-reversal, distinct phases arose that also could not be deformed to the trivial state or each other. A famous example is the quantum spin Hall state already mentioned, which relies on spin-orbit interactions to host helical edge modes topologically protected against scattering. As research progressed realistic models were proposed [7, 8], followed very shortly by experiments [9] confirming their states. These nontrivial properties have sparked a wave of research into topological phases of matter and their practical applications. While these quantum Hall models lie in two-dimensions, there has been a lot of work on three-dimensional topological insulator states which spurred work both theoretically [10–13] and experimentally [14–17]. However there has been much interest recently in 1D models, with advances in experimental techniques allowing these systems to be realized. This thesis will focus on this dimensional regime.

This burgeoning interest in topological states has given researchers the well quoted 'periodic table of topological insulators and superconductors' [18, 19]. This table and the associated research has shown that dimensionality and symmetries are the only factors necessary to determine whether an insulator state is a topological insulator or a trivial one. The symmetries used in the classification, which come from random matrix theory [20], are time-reversal, particle-hole, and the combination of the two known as chiral symmetry. The topological indices of the ground states have three categories, the $\mathbb{Z}$ index like the Chern number, the $\mathbb{Z}_2$ index like those proposed by Kane and Mele and the subsequent models, and finally the null category of nontopological models. These indexes arise from homotopy groups of the spaces of ground states [21, 22]. The landscape of topological insulators is extensive, more developed in 2D and 3D theoretical and experimental models and materials, so we look towards the one-dimensional models where we can ask the specific question, is it possible to construct a 1D topological insulator in the same vein as the quantum spin Hall state? This dimension is interesting because of its affordability for both intuitive pictures and increasing popularity with the advent of tunable trapped ion and cold atom experiments.

In this thesis we use the ever popular 1D Su-Schrieffer-Heeger (SSH) model [23] as a building block to construct ladder models in all five chiral universality classes and demonstrate topological insulator properties in each model class. The SSH model is the simplest 1D topological insulator hosting zero energy edge modes, where similar models have been experimentall realized [24, 25]. Crucially we follow a recipe similar to that used by Kane and Mele [6] to construct a 2D topological insulator. Their procedure is to take two time-reversed copies of a particular Haldane [26] model and couple them together making the model time-reversal symmetric. One chain has a Chern number of +1 and the other -1 so that in the coupled system the total Chern number is 0. Despite this, the topological properties of the system can still be characterized if one uses a different $\mathbb{Z}_2$ index. We will pay particular attention to the quantum spin Hall model as it was initially proposed by Kane and Mele [27] because we utilize the same methodology to construct our models. We use the exact same procedure however working in 1D using deformed SSH chains and the winding number topological index. The deformed SSH chain belongs to the chiral symmetry preserving AIII class with time-reversal and particle-hole symmetries being broken. As

before, taking two time-reversed copies of these AIII chains and coupling them together to form a ladder restores the time-reversal and particle-hole symmetries.

One of the crucial differences is that the Chern number is odd under time-reversal symmetry (acquires an opposite sign), the 1D winding number is not. We will use this fact to couple the AIII chains in two unique ways giving the BDI and CII, and DIII and CI class models respectively. Before coupling both chains have a winding number of $\nu = 1$, however when weakly coupled the winding number is not necessarily 2, it can also be 0. This ambiguity, as we will explore in more depth, arises from the winding number being odd under lattice relabeling. The winding number is therefore only defined up to a sign, which permits two different interchain coupling forms. Such a fact is a main thread through this thesis, we will couple topology and symmetry to construct novel nontrivial phases.

Topological insulators have been topics of research for decades and there are a number of well cited reviews that cover the extent of the topic from various lenses, [28, 29], as well as several detailing the classification of topological insulators and superconductors [30, 30]. There are several texts on the subject as well, [31] and [32], tackling it from the perspective of the Dirac equation. In terms of classification there are a number of notable reviews [19, 33].

While noninteracting phases come with well documented classification and understanding, interacting topological insulators are much less so. In general, interactions typically destroy a topological state hosted in a single particle regime. New research [34] however proposes that a reduced filling fraction and repulsive nearest neighbor interactions can restore a topological state disrupted by strong interactions [35, 36], although this is not so surprising as such models can be mapped to the spin-$1/2$ XXZ chain [37]. Taking a different avenue for the SSH model, we apply interactions and reduced filling fraction, we show that via a mean field approach the system falls into a $\mathbb{Z}_2$ symmetry breaking topological bond density wave phase. Typically topological models with degenerate spectra are characterized by the Wilczek-Zee phase topological number [38, 39], however in the mean field approximation the Zak phase provides an analogous role. Our work in this thesis contributes to a group of work analyzing fractional topological insulators induced via interactions by a number of techniques [40–48].

To put this work into a broader context, these models are enticing because of their experimental viability with cold atomic gases in optical lattices. These systems can realize band structures and permit accurate tunability of system parameters [49–53]. Luckily for this thesis, there has been good work simulating one-dimensional ladders [54–64] and these experiments have been able to detect chiral edge currents [65] (like the Hall effect) and even skipping orbits [66, 67] which are typically very hard to detect.

1.1 Thesis structure

This thesis has two main sections, the theoretical background and the novel research and results. Chapters 2 and 3 provide the necessary introductions to topological insulators, the SSH model, and calculating winding numbers. Secondly chapters 3, 4, 5, 6, and 7 present the

novel research of this thesis. Lastly chapter 8 wraps the work with a summary, conclusion, and projected future work based on the given research.

One may notice that chapter 3 has been listed in both sections. This chapter acts in a hybrid fashion, both giving the necessary information to understand the winding number as a topological invariant in lattice models and presents a surprising result regarding a sign ambiguity. This result acts as a stepping off point for the following chapters.

Briefly, chapter 4 presents our methodology for constructing topological insulator models by coupling two SSH model chains together. We use symmetry arguments to design and build these models to adhere to the known universality classes. Using these models we proceed to chapter 5 to construct the real space lattices for each model and offer energy spectrum results identifying hallmark signs of topological insulator phases including gapped band structures and zero energy edge modes. Chapter 6 examines the edge states associated to these zero energy modes both numerically and analytically, and demonstrates the robust symmetry protected properties of these states in each class. This section wraps up and validates the methodology that topological insulators can be, carefully, constructed by 'stacking' SSH chains.

Chapter 7 takes a different path than the previous chapters and presents results for an SSH-like chain with repulsive interactions at a reduced filling fraction of $\upsilon = 1/4$. While this research is heavily motivated by Barbarino et al we take a slightly different approach by using mean field theory. We find the mean field theory results in a simpler toy model, named SSH4 [68], and subsequently show the description of a $\mathbb{Z}_2$ symmetry breaking bond density wave state. We show via Zak phase calculations the lower band of the SSH4 model is quantized in the topological regime and 0 for the trivial phase. The results show that the topological phase at the reduced filling fraction can be attributed to mean field effects of the interactions and not strong correlation effects.

Chapter 2

Background

In this chapter we lay the necessary background material to understand the results presented in this thesis. We start by introducing the SSH model and its essential features as we use it as the foundation for constructing our models. Particular attention is paid to the nontrivial topological insulator phase which presents with symmetry protected edge states and a quantized winding number. As with much of physics, symmetry plays an important and essential role in the SSH model as well as the work presented here. We will look at the nature of time-reversal, particle-hole and chiral symmetries, and their necessity in the categorization of models which fall under the universality class system. These concepts will be utilized to construct our ladder models in the later chapters.

2.1 SSH model and the Topological Insulator state

The Su-Schrieffer-Heeger (SSH) model stands as the prototypical model demonstrating physical properties attributed to the topological insulator state. It is interesting to note that this model, as presented in the original paper, was an analogue of a polyacetylene chain investigating phonons and a symmetry broken phase. This model has evolved as the simplest model to demonstrate the power of topology in condensed matter and the unique topological insulator phase. Current literature describes the SSH model as electrons (or spinless fermions) hopping on a one-dimensional lattice with alternating (i.e. staggered) hopping amplitudes.

We take the time to introduce the main features of the SSH model because it acts as the building block model, conveniently describing a 1D topological insulator state, and of the research presented in this thesis. In this chapter we will present the SSH lattice model and solve its Hamiltonian to examine the energy spectrums across several coupling regimes to see the trivial and nontrivial phases. The concepts of single particle Hamiltonians, bulk-boundary correspondence, chiral symmetry, gapless edge states, and the winding number topological invariant will be introduced as well. We will also briefly discuss symmetries and universality classes as we utilize these concepts to construct our models in later chapters.

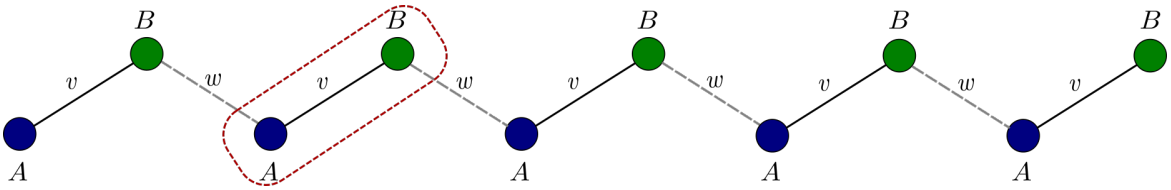

Fig. 2.1 Lattice diagram for the SSH model. Unit cells, encircled by the red dotted line, consist of two sublattice sites, an A site and a B site. Intracell coupling is given by v and the intercell coupling is given by w.

It is worth noting that the SSH model as a topological insulator has some detractors but here we define the unit cell specifically so these topological properties arise and it cannot be deformed to the atomic flat band limit. By defining the unit cell in this way we remove any ambiguity about the topology.

A single chain SSH model is a tight-binding model that consists of connected unit cells with two internal states, Fig. 2.1. The sites within the unit cell are labeled A and B, a notation that will be used through the extent of this thesis. The internal structures of the unit cell are known as sublattices. The model Hamiltonian (in position/site representation),

$$\hat{H}_{SSH} = v\sum_{n=1}^{N}(c_{nA}^{\dagger}c_{nB} + c_{nB}^{\dagger}c_{nA}) + w\sum_{n=1}^{N-1}(c_{nB}^{\dagger}c_{n+1,A} + c_{n+1,A}^{\dagger}c_{nB}) \tag{2.1}$$

where v and w are the intra- and inter- cell couplings, respectively, and the sum is over all unit cells (N) and n is the cell index. The operator $c(c^{\dagger})$ denote the annihilation(creation) operators on that particular unit cell (n) and sublattate (A,B). We constrain these hoppings to be real and positive. It should be noted that if these couplings are complex, the phases can be 'gauged' away by redefining the basis states with an additional phase.

We neglect any interactions and spin degrees of freedom, focusing only on the single particle Hamiltonian states. We are interested in the zero temperature and zero chemical potential dynamics of the fermions near or at the ground state(s). We consider the situation of half filling - all negative energy eigenstates are singly occupied as a result of the Pauli exclusion principle. This model is characteristic of simple realistic systems such as polyacetylene where the carbon atoms contribute a single conduction electron, i.e. one particle per unit cell. Throughout this thesis we will consider the bulk to be translationally invariant.

The real space SSH Hamiltonian matrix for a 3 cell system in the basis $\{A_1, B_1, A_2, B_2, A_3, B_3\}$ is given by,

$$\hat{H}_{SSH} = \sum_{n}^{3} C_n^{\dagger}\hat{h}C_n \tag{2.2}$$

where $C_n^{\dagger}(C_n)$ is the one-dimensional vector of creation(annihilation) operators, respectively. The operator $\hat{h}$ is the matrix,

$$\hat{h} = \begin{pmatrix} 0 & v & 0 & 0 & 0 & 0 \\ v & 0 & w & 0 & 0 & 0 \\ 0 & w & 0 & v & 0 & 0 \\ 0 & 0 & v & 0 & w & 0 \\ 0 & 0 & 0 & w & 0 & v \\ 0 & 0 & 0 & 0 & v & 0 \end{pmatrix} \tag{2.3}$$

It is convenient to define the external degrees of freedom of the state as the cell index (n) and the internal degrees as the sublattice index $\{A, B\}$. We work with open boundary conditions because the topological phase does not arise with periodic boundaries [69]. The state is then easily represented by a tensor basis,

$$|n, \alpha\rangle \rightarrow |n\rangle \otimes |\alpha\rangle \in \mathcal{H}_{ext.} \otimes \mathcal{H}_{int.} \tag{2.4}$$

where $\mathcal{H}_{ext/int}$ are the Hilbert spaces of their respective domains. The energy spectrum for a 10 unit cell system shows a series of gapped states at zero energy when $v < w$, Fig 2.2. These states are absent in the opposing regime ($v > w$), which suggests a change in phase. In the thermodynamic limit this quantum phase transition point is at $\epsilon = 0$, i.e. $v = w$. We will show later in this chapter these zero energy states are doubley degenerate symmetry protected edge modes. While both phases appear to be insulating, we will show they are different and can be classified distinctly. These zero energy states are a hallmark property of the topological insulator phase and will be a property we look for when we construct more complex models in later chapters.

We shift focus here to examine the band structure of this model which tells us the electron dynamics by utilizing the translational invariance and periodic nature of the lattice, and Bloch's theorem to define the appropriate Fourier operators to transform the Hamiltonian to reciprocal momentum space,

$$c_n = \frac{1}{\sqrt{N}} \sum_{kn}^{BZ,N} e^{ikn} c_k \tag{2.5}$$

$$c_n^\dagger = \frac{1}{\sqrt{N}} \sum_{kn}^{BZ,N} e^{-ikn} c_k^\dagger \tag{2.6}$$

where k is the crystal momentum and we have set the lattice constant to be 1, i.e. k is dimensionless. This gives,

$$\hat{H}(k) = \sum_{k}^{BZ} C_k^\dagger \hat{h}(k) C_k \tag{2.7}$$

where,

$$\hat{h}(k) = \begin{pmatrix} 0 & v + we^{-ik} \\ v + we^{ik} & 0 \end{pmatrix} \tag{2.8}$$

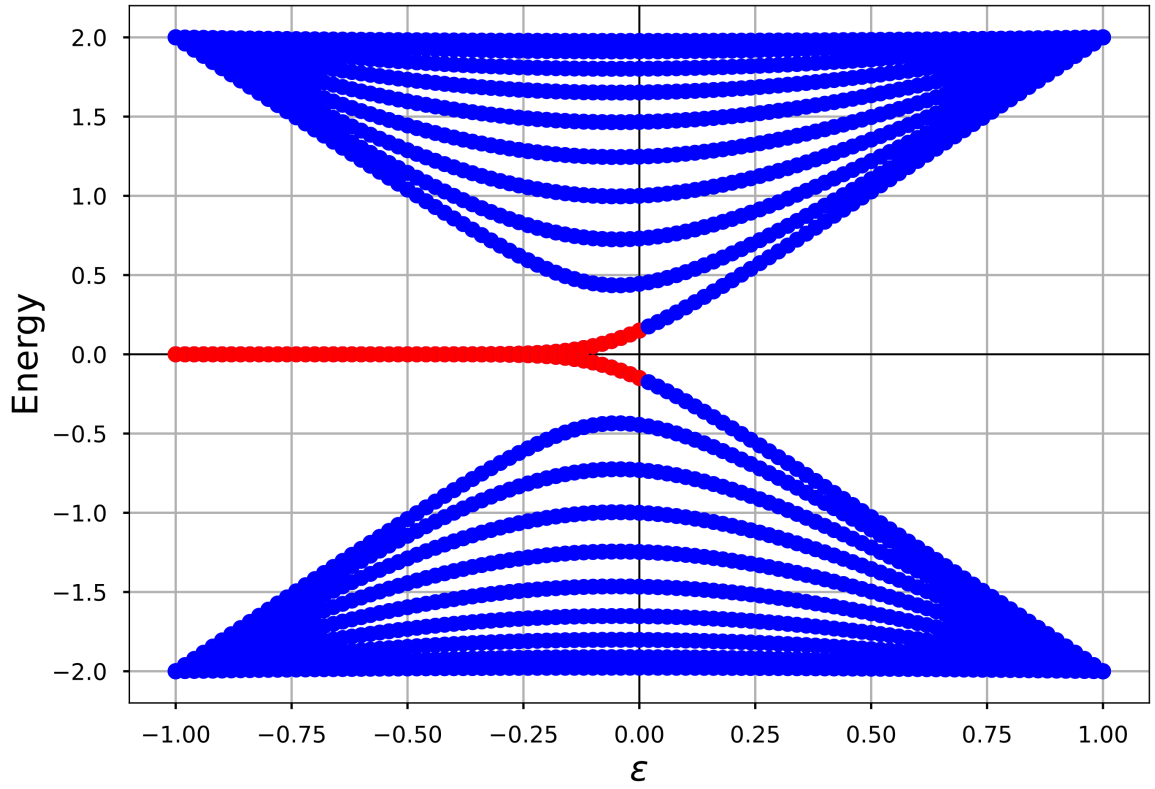

Fig. 2.2 Energy spectrum of the SSH model as a function of ϵ where ϵ acts to parameterize v and w relative to each other, i.e. $v = 1+\epsilon$ and $w = 1-\epsilon$. Zero energy states are indicated by the red data points.

The 2x2 nature of $\hat{H}_{SSH}$ can be decomposed into Pauli matrix components with some Bloch sphere dependence $d(k)$,

$$\hat{h}(k) = \vec{d}(k)\vec{\sigma} = d_x(k)\sigma_x + d_y(k)\sigma_y + d_z(k)\sigma_z \tag{2.9}$$

where $\vec{d}(k)^T = \{d_0(k)\ \ d_x(k)\ \ d_y(k)\ \ d_z(k)\}$ and $\vec{\sigma}$ is the set of Pauli matrices $(\sigma_0\ \ \sigma_x\ \ \sigma_y\ \ \sigma_z)$. From equation (2.8) we see that $d_x = v + wcos(k)$, $d_y = wsin(k)$ and $d_0 = d_z = 0$. We examine the dispersion relation of this model by choosing a plane wave wavefunction to use in the time-independent Schrödinger equation. Such a wave is an eigenstate of energy in position space and has internal degrees of freedom to represent the A and B sublattices.

Solving (2.8) for the energy eigenvalues,

$$E(k) = \pm\sqrt{v^2 + w^2 + 2vwcos(k)} \tag{2.10}$$

gives a dispersion relation between the energy of the system as a function of the crystal momentum k across the first Brillouin zone, i.e. $k = [-\pi, \pi)$.

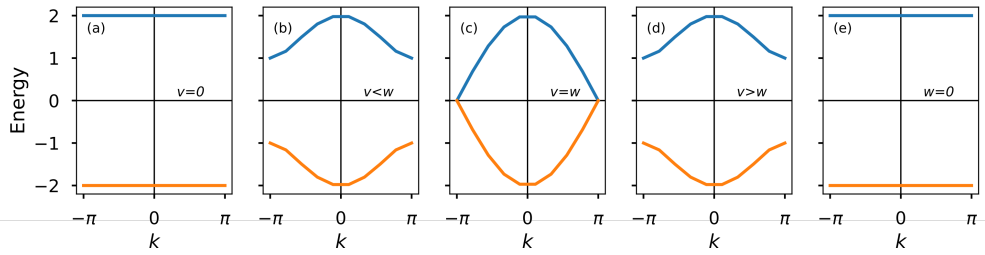

Fig. 2.3 Band structures for the SSH model, Eq. (2.10), for five different hopping parameter sets: (a) $v = 0.0$ and $w = 2.0$; (b) $v = 0.5$ and $w = 1.5$; (c) $v = 1.0$ and $w = 1.0$; (d) $v = 1.5$ and $w = 0.5$; (e) $v = 2.0$ and $w = 0.0$. The crystal momentum k spans the Brillouin zone $[-\pi, \pi)$. Plots (a), (b), (d), and (e) describe insulating phases while plot (c) shows a metal phase.

2.1.1 Band structures

The dispersion relation gives us information about the electron dynamics of the model such as phase and degeneracies in terms of energy bands. As the unit cell consists of two sites there will be two bands in the dispersion relation. We show the energy band spectrum for five parameter sets, see Figs. 2.3. When bands cross the Fermi level there are conductive states, i.e. the electrons are moving, however when the bands are fully gapped the system is in an insulating phase. The valence electrons in the states below the Fermi level require energy to 'jump' the gap to the empty conduction band.

The spectrums show that as long as the hopping amplitudes are not equal, i.e. $v \neq w$ (Figs. 2.3(a), (b), (d), (e)), the bands are gapped with a separation of $2E(k)$. We observe that in the absence of staggered hoppings, i.e. if $v = w$, (Fig. 2.3(c)) the bands touch at the Brillouin zone terminal limits ($k = \pm\pi$), these Fermi points describe a conductive metal state. In this regime there exist small energy plane waves in the bulk that can transport electrons across the length of the chain. We observe that as the difference in relative hopping amplitudes increases, the more energetically favorable the system becomes because the lower bands continue to drop in energy.

In the limit that one of the hopping amplitudes becomes 0, $v = 0$ or $w = 0$ (Figs. 2.3(a), (e)), the bands become flat and the physical chain enters a dimerization state. This series of band structures tells us that as the parameters change from $v > w$ to $v < w$, where v and w are positive, we see that the gap closes. This strongly indicates the existence of a quantum phase transition.

The signature of a phase transition in this 1D system will be a closing and opening of the spectral gap at some value of the momentum k. This phase transition is between the trivial $v > w$ and topological phase $v < w$ and occurs when $v = w$, as shown in the plots. The conditions for when the energy is zero is easily calculated from the dispersion relation Eq. (2.10).

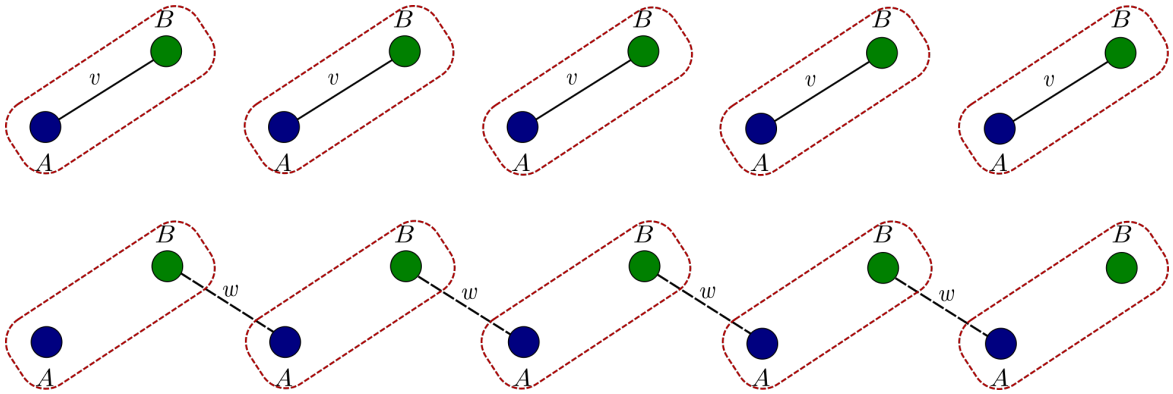

Fig. 2.4 Possible dimers of the SSH model in the strong coupling limits. Top chain shows a $w = 0$ dimer state, a series of unit cells. Bottom chain shows a $v = 0$ dimer state, a series of dimers with isolated edge sites, one on each end of the chain.

2.1.2 Edge states

While the bulk part of the SSH chain gives a lot of information about the system, the edges present the most interesting properties of the SSH model. The distinction between the bulk and the boundary edge in the thermodynamic limit lies in the behaviour of the energy eigenstates in each region. As we will show, the bulk eigenstates are spread through the system while the edge eigenstates are localized on at the boundaries. We will begin our discussion of edge states in the fully dimerized limit where the edges are very distinguishable from the bulk in the topologically nontrivial phase.

Outside the full dimer limit $v = 0$ the edge is not sharply defined leading to hydrization of the left and right edges. This thesis will focus very majorily on the topological phase of the presented models. Isolated edge states have become a hallmark indicator of topological insulators, the number of edge states can be used as a topological invariant. We introduce them here as they are a key component of later discussions in this thesis. These edge states only arise with open boundary conditions and thus the topological phase occurs in this configuration and does not emerge with periodic boundary conditions as there is no edge.

Fully dimerized limits

One of the key properties that makes the SSH model so powerful is its simplicity in the limit cases where v or w are 0, see Fig. 2.4. In these limits the chain falls apart into a series of disconnected dimers. The form of these dimers depends on the which coupling is 0. In the $w = 0$ (Fig. 2.3(e)) configuration all of the sites are paired up in their original unit cells. The energy eigenstates will therefore be some even or odd superposition of the sublattices in each cell, i.e.,

$$v = 1, w = 0: \quad \hat{H}(|n, A\rangle \pm |n, B\rangle) = \pm(|n, A\rangle \pm |n, B\rangle) \tag{2.11}$$

We see that this bulk state has energy $\pm v$ where $\hat{H}(k)$ is independent of the wavenumber, i.e. $\hat{H}(k) = \sigma_x$. However in the $v = 0$ (Fig. 2.3(a)) limit the bulk consists of dimers of neighboring cells but there are singular isolated sites at each end of the chain, an A site on the left edge and a B site on the right edge, Fig. 2.4. In this case there must be two degenerate zero energy eigenstates [70] that exist on these isolated edge sites, as there is no onsite potential,

$$v = 0, w = 1: \quad \hat{H}(|n, B\rangle \pm |n+1, A\rangle) = \pm(|n, B\rangle \pm |n+1, A\rangle) \tag{2.12}$$

While the band is also flat in this case as well Fig. 2.3(a), the Hamiltonian has wavenumber dependence $\hat{H}(k) = cosk\sigma_x + sink\sigma_y$. In both dimer limits the energy eigenvalues are independent of momentum k, leading to the flat bands. Any particle added to the system will have an isolated wavefunction as it is unable to propogate through the chain due to zero velocity.

We will see that these zero energy modes, Eq. (2.13), exist in the middle of the spectral gap of the energy spectrum. They cannot be easily removed unless the gap is closed, i.e. bringing other states closer so the energy cost is much lower to move to a different energy state.

$$v = 0, w = 1: \quad \hat{H}\,|1, A\rangle = \hat{H}\,|N, B\rangle = 0 \tag{2.13}$$

These states exist in the fully dimerized chain in the topological phase of the model. However this dimer configuration has more eigenstates available due to the isolated zero energy end sites, leading to a simple example of an edge state.

We note that these edge states emerge for open boundary conditions. No edge states emerge for periodic boundaries.

Perturbed dimer limits

Starting in the topological dimer phase ($v = 0, w = 1$) we will add a small perturbation by turning on the v hopping parameter and see that as the chain becomes increasingly connected the edge state wavefunctions decay exponentially into the bulk of the chain. These states are no longer pinned to zero energy as well. The edge state wavefunctions will hybridize into even and odd superpositions, Figs. 2.5(a),(b). Moving slightly away from the dimerized limit results in states that are not fully localized on a single site at the edge. These near zero energy states decay exponentially into the bulk. In the finite system there is an overlap between the left and right edge state wavefunctions but in the thermodynamic limit there is zero overlap. In the non-dimer limit the wavefunction is spread through the entirety of the chain, with most of the amplitude in the bulk. These wavefunctions show nonvanishing amplitudes only on the A or B sublattice, depending on the edge, suggesting it is energetically favorable to have the particles only on one of the sublattices. We will see in the next section these unique properties are the consequence of chiral symmetry.

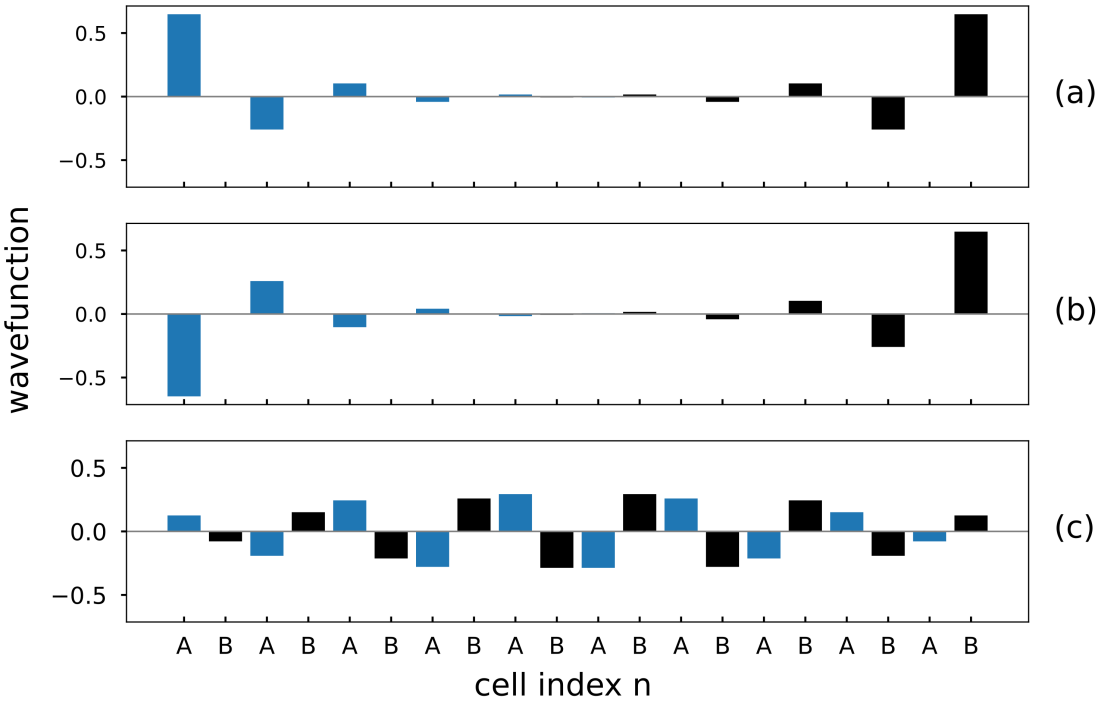

Fig. 2.5 Wavefunction spectra for the SSH model in the topological and trivial phases. Plots (a) and (b) present symmetric and antisymmetric near dimer edge state combinations with $v = 0.4$ and $w = 1.0$. Plot (c) shows the wavefunction for a trivial phase $v = 1.0$ and $w = 0.4$ where the amplitude is spread in the bulk.

2.1.3 SSH Winding number

The SSH model is a bipartite lattice, with the unit cells divided into two sites or sublattices and the Hamiltonian only has terms connecting A-B sites, and no terms connected A-A, B-B sites. In condensed matter physics we define chiral symmetry of a Hamiltonian as,

$$CHC^{\dagger} = -H \tag{2.14}$$

This symmetry commutes with the Hamiltonian H and therefore they can be diagonalized together. The Hamiltonian H will have no matrix elements between eigenstates of C with different eigenvalues. This allows us to segment the H into sectors labeled by their corresponding eigenvalues. The physics in each sector can be regarded as separate from another sector. The Hamiltonian can thusly be ordered into blocks which can be analyzed separately. A consequence of this commutation relation is the energy spectrums are symmetric or mirrored. Any state with energy E has a chiral symmetry 'partner' with energy $-E$. To be more concrete,

$$\hat{H}|\psi_n\rangle = E|\psi_n\rangle \Rightarrow \hat{H}C|\psi_n\rangle = -C\hat{H}|\psi_n\rangle = -CE|\psi_n\rangle = -EC|\psi_n\rangle \tag{2.15}$$

The SSH model has chiral symmetry which gives the off-diagonal structure of the Hamiltonian, Eq. (2.16). As the wavenumber k moves through the Brillouin zone, ($[-\pi, \pi)$), the endpoint of $\vec{d}(k)$ describes a closed path of radius w in the complex plane since there are no σ_0 or σ_z components in the Hamiltonian, Eq. (2.8).

We know that there are two phases as per the band structure plots, characterized by a quantum phase transition where the gap closes at $v = w$, which corresponds to a zero energy point at the origin $\vec{d} = 0$ in the complex plane. At this point the model is no longer an insulator but a metal, as previously stated. This describes a closed loop in this plane running through the Brillouin zone which describes a *'winding number'* about the origin and it is the primary invariant for chiral symmetric systems in odd dimensions. Simply, this describes the number count of loops around a given point (origin) as the vector cycles through the Brillouin zone.

Any loop that does not encircle the origin ($v > w$) can be deformed into any other loop not encircling the origin, Fig. 2.6. The principle also applies to loops that have the origin inside them ($v < w$). In essence the origin is the phase transition point, such that $\vec{d}(k)$ must pass through it to change phase. A loop that does not encompass the origin must pass through the origin i.e. the energy gap is closed and the bands touch (see Fig. 2.3(c)), in order to become a loop that encircles the origin. This is where the topology enters the picture, the winding number is a topological invariant used to describe and differentiate between quantum phases and will be used heavily in this thesis. It is important to note that if $d_z \neq 0$ then the rotation could be lifted out of the plane and thus the invariant changes.

Any closed loop that encompasses the origin can be adiabatically deformed to any other loop also encompassing the origin with the same winding number index. The same principle is true for loops not encompassing the origin. Insulating Hamiltonians are adiabatically equivalent if they can be adiabatically deformed into eachother.

The winding number can be calculated from the bulk momentum space Hamiltonian, Eq. (2.16), which is in the basis where the chiral symmetry operator is diagonal (σ_z),

$$\hat{H}(k) = \sum_{k}^{BZ} C_k^\dagger \hat{h}(k) c_k \quad \hat{h}(k) = \begin{pmatrix} 0 & \Delta(k) \\ \Delta^\dagger(k) & 0 \end{pmatrix} \quad \Delta(k) = d_x(k) - id_y(k) = v + we^{-ik} \tag{2.16}$$

The winding number ν can be written as a convenient integral by virtue of Cauchy's theorem from complex analysis. We can then define the winding number as [69] [71],

$$\nu = \frac{-i}{2\pi} \int_{BZ} \frac{d}{dk} (log(\Delta(k)))dk \tag{2.17}$$

where we have used the complex logarithm function $log(|\Delta|e^{iargh}) = log|\Delta| + iargh$. We take care to define the logarithm branch so the derivative is always well defined and the winding number is well quantized. For the SSH model the winding number takes the value of either 0 for the trivial phase ($v > w$), dominant intracell hopping) and 1 for the topological insulator

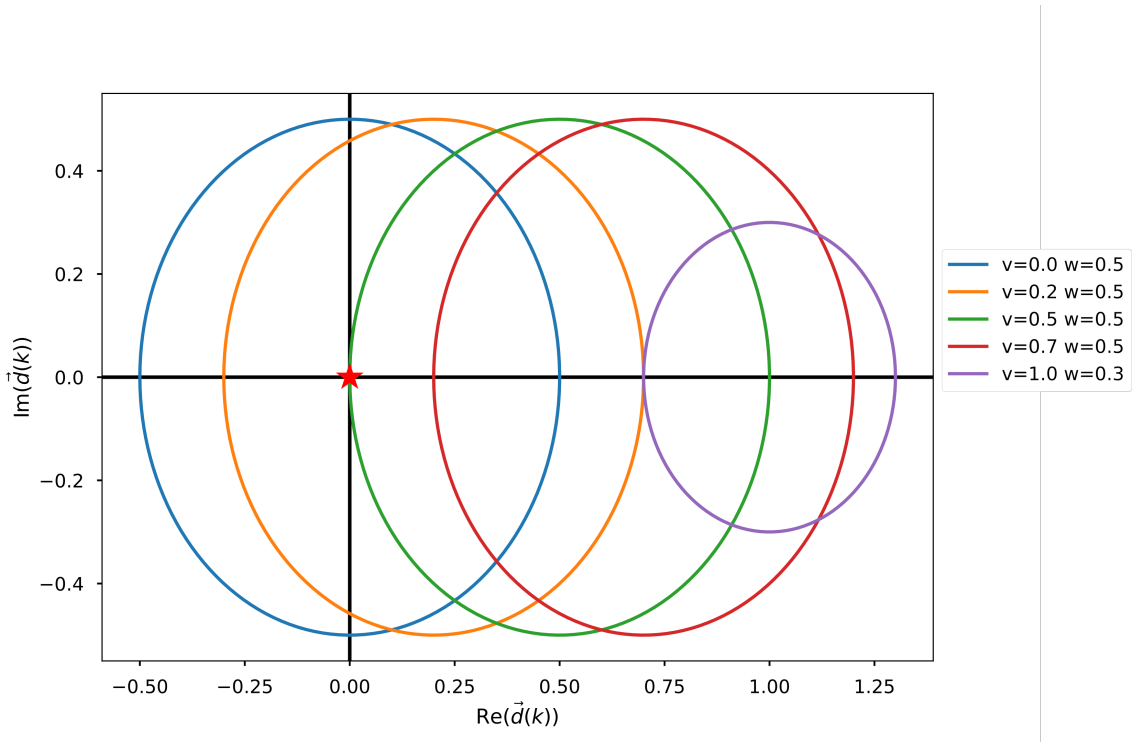

Fig. 2.6 Winding number of the SSH Hamiltonian vector $\vec{\Delta}(k)$, Eq. (2.9), through the complex (Bloch) plane. For $v < w$ the winding encirles the origin (marked by the red star). For $v > w$ the winding does not encircle the origin. Each circle has its origin at v with radius w.

phase ($v < w$), dominant intercell hopping). The winding number is obtained using the bulk Hamiltonian only. One can take some intuition about the winding number calculation by looking at the exponential of $\Delta(k)$. Since it is a linear combination of sinusoidal functions and the range of the Brillouin zone is 2π we know that the 'vector' represented by $\vec{d}(k)$ must form a complete circle. The number of rotations the vector makes over the span of the Brillouin zone is dependent, in this case, on the hoppings and therefore on the value of the exponential, e.g. $-ik$ will be one rotation, $-2ik$ will be two rotations, $-3ik$ will be three, etc. Longer range hoppings will give the higher integers in the exponential.

Two (or more) Hamiltonians are equivalent if they can be transformed into each other via an adiabatic process that respects the important symmetries. From this principle we can say that the winding number is a topological invariant which cannot change under adiabatic symmetry perserving deformations of the Hamiltonian. We then conclude that the two phases that occur in the SSH model, the trivial and topological phases are not adiabatically connected because they have different winding indexes, 0 and 1 respectively. In the case of the SSH model if chiral symmetry is broken the Hamiltonian may have diagonal terms, permitting adiabatic connections between the two phases as the vector can be lifted out of the plane and therefore can bypass the zero energy point.

The edge states can be connected to the bulk winding number in what is known as the bulk-boundary correspondence. We have seen that the number of zero energy edge states is

fixed and finite (in the thermodynamic limit) which are situated on a single sublattice. If we examine the low energy sector (lower band) of the left edge the winding number is 0 in the trivial case ($v > w$) and 1 when in the topological phase ($v < w$), Eq. 2.18. Since the winding number is calculated over the bulk Hamiltonian we can connect the bulk topological invariant to the boundary physics, i.e. number of edge states on a single edge.

$$\nu = \begin{cases} 0 & if \;\; v > w \\ undefined & if \;\; v = w \\ 1 & if \;\; v < w \end{cases} \tag{2.18}$$

At the point when the bands touch ($v = w$) the winding number becomes undefined due to the bands being degenerate. The bulk can be related to the edges via the bulk-boundary correspondence which connects the winding number to the edge states, the number of edge modes is related to the magnitude of the winding number. In summary, the winding number serves as a topological invariant that characterizes the presence and number of topologically protected edge modes in the SSH model. It establishes a direct correspondence between the bulk properties (captured by the winding number) and the edge properties of the system.

2.2 On the nature of symmetries

As we saw in the previous section chiral symmetry plays a key role in the characterization of the phases of the SSH model. Symmetry is one of the single most important concepts in physics. As a definition symmetry means a transformation that leaves the properties of the model unchanged. A sphere remains a sphere even after being rotated about. In condensed matter physics the most common symmetries in systems are time reversal symmetry, particle-hole symmetry, and chiral or sublattice symmetry. The idea of symmetry is quite simple, does a transformation on the system have any effect on the properties of that system. If the properties are unchanged the system is said to have that particular symmetry (i.e. rotating a circle by any angle returns the same circle). If the properties of the system do change then that particular symmetry is said to have been broken by the transformation. It has been well established by Atland and Zirnbauer (and others) [72–74, 20] that all random matrices can be classified into ten symmetry classes based on how the matrices respond to transformations. The random matrices can be interpreted as Hamiltonians of non-interacting fermionic systems.

The symmetry properties of a given model are encoded in the Hamiltonian of that system. The Hamiltonian needs to fulfill certain conditions to exhibit time reversal (T), particle hole/charge conjugation (P), and chiral/sublattice (C) symmetries. In the case of the SSH model we use the Hamiltonian matrix Eq. (2.16) to understand these symmetries. From a physical standpoint time-reversal will reverse the momentum of particles, particle-hole symmetry relates the dichotomy of the existence and absence of a particle particle. Finally chiral or sublattice symmetry relates the relabelling of sites in a unit cell, a property which is

of particular importance to this thesis. We will use these terms interchangeably as they are equivalent here. These conditions are [75, 69],

$$T : U_T K| \quad U_T K H^*(-k) U_T^\dagger K = H(k) \tag{2.19a}$$
$$P : U_P K| \quad U_P K H^*(-k) U_P^\dagger K = -H(k) \tag{2.19b}$$
$$C : U_C| \quad U_C H(k) U_C^\dagger = -H(k) \tag{2.19c}$$

These matrices U_N are unitary with no dependence on the (crystal) momentum k. Note the Hamiltonian is in the momentum-space basis and K is the complex conjugate operator. The time-reversal and particle hole symmetries have the property that $T^2 = P^2 = \pm 1$. The square of the operator matters because it tells us the operator can take two forms, each form bringing about different consequences. Additionally if both time-reversal symmetry and particle-hole symmetry exist then chiral symmetry must exist, $U_S = U_T U_C^*$. If only one exists, then chiral symmetry won't exist. The chiral symmetry operator only comes in +1 form. This gives 10 possible combinations of the operators, known as the ten-fold way [30].

In the case of an antiunitary operator that squares to -1, in our case $T^2 = -1$, we have an application of Kramers theorem [76]. The theorem describes a degeneracy that results from the commutation of the Hamiltonian with T of this form. The implication being that at 'high' time-reversal points of momenta ($k = 0, \pm\pi$) there are two orthogonal states with the same energy. We will see in later section the implications of this degeneracy in dispersion spectra. In general time-reversal symmetry creates a 'mirror' symmetric spectrum across the center of the Brillouin zone value. Particle-hole symmetry ($E \to -E$) forces a similar behaviour over the zero energy axis. The existence of chiral symmetry will constrain the spectra to adhere to the properties of time-reversal and particle-hole symmetries.

On the Nature of Universality Classes

There have been several successful approaches to classifying noninteracting fermionic topological quantum matter, notable Anderson localization [19, 77, 30], Topology (K-theory) [18], and quantum anomalies [78][1]. Collectively these approaches have born the current classification system known as the 'ten-fold' way. This scheme identifies five distinct forms of topological insulators (superconductors) in each dimension. In 1D these are AIII, BDI, CI, CII, and DIII. In the single particle basis the time-reversal and particle-hole symmetries are anti-unitarily realized symmetries. In contrast chiral/sublattice symmetry is unitary. As we will see in the next chapter time-reversal symmetry commutes with the single particle Hamiltonian while particle-hole and chiral symmetries anti-commute with it [33].[2].

The ten-fold way gives a simple system for the ten universality classes of noninteracting topological insulators and superconductors, their symmetries, and their topological index in each dimension. We restrict our focus to the 5 classes, Table 2.1, that have chiral symmetry,

[1]There have been advances on these approaches in the last decade, see [79] [80]

[2]There are extensive and indepth reviews of this classification system, details of which we leave to the literature [33, 72, 19]

Class	T^2	P^2	C^2	Topological index in 1D
AIII	0	0	1	$\mathbb{Z}$
BDI	1	1	1	$\mathbb{Z}$
CII	-1	-1	1	$2\mathbb{Z}$
DIII	-1	1	1	$\mathbb{Z}_2$
CI	1	-1	1	0

Table 2.1 Summary of chiral universality classes and their topological index in one-dimension.

because chiral symmetry will play a central role in the models developed here. The classification provides a framework to orient and guide the research presented here.

The universality classes are not defined by 'which symmetries does the model have' but rather 'what kinds of arbitrary symmetry terms do we add to our model'. These five chiral classes contain all possible combinations of symmetries. We show that the different combinations give different but observable properties in our models. Additionally the topological indexes provide information about the edge states as we will also show. Observe that the CI class is not topological in 1D. These classes will provide structure to our discussions as we present results for classed ladder models. For conveniece

The topologies $\mathbb{Z}$ and $\mathbb{Z}_2$ indicate whether the space of quantum ground states is partitioned into topological sectors labeled by an integer or a $\mathbb{Z}_2$ quantity, respectively. In the case of CII its inherent Kramers pairing the ground states always come in time-reversed pairs which forces the invariant to always be even. These topological invariants have been worked out for every class and dimension, in what is known as the ten-fold way [30].

Chapter 3

Winding number of 1D noninteracting gapped systems

This chapter will perform a hybrid purpose in that it will both provide necessary background information on winding number as a topological invariant in 2N-band models, and give a crucial result regarding a sign ambiguity in the definition of the winding number [81].

We will derive a general expression for the winding number calculable for noninteracting 2N-band models in 1D and discuss important details of chiral symmetry as they pertain to the lattice and the winding number. The winding number is defined in any odd dimension, therefore the results presented are applicable to any of these spaces.

There is a subtlety that arises in the winding number of a system with chiral symmetry, which is an ambiguity in the sign of the index in the topological phase. This finding underpins the construction of the combined model presented later in this thesis. We will discuss the significance of this ambiguity later in this chapter.

3.1 Winding number in 2N-band models

Here we need to expand our discussion of the winding number as a topological invariant in 1D noninteracting models with a specific focus on the nuances of chiral symmetry. The winding number is well studied and very often defined in the context of 2-band models (see previous sections) but a definition for any general N-band chiral model is not well know. We will give a detailed derivation of the winding number for a 2N-band model [82] and show that it is equivalent to the often used Q-matrix operators method [30].

In lattice models chiral symmetry is equivalent to a sublattice symmetry, i.e. swapping the 'labels' of the sublattice sites within a unit cell. This can be shown by defining new operators using the chiral operator given by equation (2.19c),

$$P_{A(B)} = \frac{1}{2}(1 \pm U_C) \tag{3.1}$$

In a bipartite lattice, like the SSH model, these operators are projectors onto the A or B sublattice and therefore have the properties of $P_A + P_B = 1$ and $P_A P_B = 0$. The projector

acting on a state only retains say the A-site components for P_A and zeros the B components. And vice versa for P_B. It is easy to see that changing the sign of the chiral operator simply swaps $P_A \leftrightarrow P_B$. It must be noted that if the chiral symmetry operator is not diagonal, as it is defined in this thesis, then an easy basis may not be as physically recognizable. Additionally we would like to explicitly say that we will use descriptions of change of sign of the chiral operator and relabeling the sublattices interchangably as these are equivalent.

The anticommutation of the chiral operator U_C with the Hamiltonian, $\{U_C, H\} = 0$, implies the same condition for the projection operators from equation (3.1),

$$P_A H P_A = P_B H P_B = 0 \tag{3.2}$$

In order for the above statements to be true the Hamiltonian must be block off-diagonal in our chosen basis in momentum space where,

$$\hat{H}(k) = \sum_{k}^{BZ} c_k^{\dagger} \hat{h}(k) c_k \tag{3.3}$$

This means there are no direct hoppings between like sites, i.e. no A-A or B-B site couplings. Therefore the Hamiltonian can be written,

$$\hat{h}(k) = \begin{pmatrix} 0 & \hat{\Delta}(k) \\ \hat{\Delta}^{\dagger}(k) & 0 \end{pmatrix} \tag{3.4}$$

From here the winding number of this model can be defined via,

$$\nu = \frac{-i}{2\pi} \int_{BZ} \partial_k i\phi(k) dk \tag{3.5}$$

with $\phi(k)$ being the complex phase of the determinant of $\hat{\Delta}(k)$ and is defined from the formula,

$$det\hat{\Delta}(k) = r(k) e^{i\phi(k)} \tag{3.6}$$

We find the above expressions to provide a more intuitive picture of the winding number integral, where we can define,

$$\phi(k) = arctan\left[\frac{Im[det\hat{\Delta}(k)]}{Re[det\hat{\Delta}(k)]}\right] \tag{3.7}$$

This expression for the winding number is very well known in the two-band model [69] but less developed for models with more than two bands. We note for clarity that the winding number is defined over all filled bands in the half-filled case. For an N-band model equation (3.5) is given in [82] but with limited detail. A detailed derivation for a general N-band model is provided in Appendix A and in Matveev et. al. [83]. This derivation shows that this method is valid, robust, and general. It is easy to see that by adding the determinant this expression is equivalent to the Q-matrix method for multiband systems

[19]. The integral in equation (3.5) tells us that the winding number index ν is determined by the number of poles $f(k) = \partial_k \phi(k)$ that lie in a unit circle and the number of times the $det\hat{\Delta}(k)$ winds around this pole in the complex plane.

The index of the winding number is invariant as long as any smooth adiabatic deformation doesn't result in the band gap closing, i.e. $det\hat{\Delta}(k) = 0$. The system will go through a phase transition if the gap closes, the path of the vector will have to cross through the pole. The winding number is well quantized and can wind around the pole any integer number of times, making it a $\mathbb{Z}$ topological index in the case of only chiral symmetry being present.

To construct the winding number for this type of system we follow Ryu et. al. [30] by building a projection *P(k)* onto the filled bands and use this projection to build the *Q(k)*-matrix. The off-diagonal structure of the *Q(k)*-matrix is a consequence of how the chiral symmetry is defined in the A-B basis.

The *Q(k)*-matrix is defined via these projection operators,

$$Q(k) = 1 - 2P(k) \tag{3.8}$$

$$P(k) = \sum_a |u_a(k)\rangle \langle u_a(k)| \tag{3.9}$$

This form of the projection operator is equivalent to equation (3.1) where we have summed over all filled bands a. The *Q(k)*-matrix is chiral symmetric i.e. $\{C, Q\} = 0$ where C is the chiral symmetry operator and in the basis where C is block diagonal, we have $C = \lambda\sigma_z$ where λ is a unitary matrix. The *Q(k)*-matrix is in the same basis as the Hamiltonian operator and is block off-diagonal,

$$Q(k) = \begin{pmatrix} 0 & q(k) \\ q^\dagger(k) & 0 \end{pmatrix} \tag{3.10}$$

where $q(k)$ is in the set of complex valued unitary matrices of dimension N, $q \in U(N)$. In our case $N = 2$ and there are 4 bands. The submatrix $q(k)$ describes a mapping between the Brillouin zone onto the space of two-dimensional unitary matrices $U(2)$. To be more clear we are mapping the Brillouin zone equivalent in 1D of a 1D sphere S^1. The corresponding homotopy group is non-trivial $\pi(U(1)) \cong \mathbb{Z}$. Finally we write the winding number in terms of the $q(k)$ submatrices,

$$\nu = \frac{i}{2\pi} \int_{BZ} tr[q^{-1}(k)\partial_k q(k)]dk \tag{3.11}$$

Luckily for an arbitrary unitary matrix, which $q(k)$ is, this invariant is given by the winding number of the determinant of the matrix. Thus we find,

$$tr[q^{-1}\partial_k q] = \partial_k log det[q] = i\partial_k \phi(k) \tag{3.12}$$

where we have used $det[q(k)] = e^{i\phi(k)}$. The above procedure requires the Hamiltonian to be diagonalized and eigenvectors calculated. The advantage of equation (3.5) is it is basis independent, does not require any diagonalization, relies only on the Hamiltonian being

block off-diagonal, and is completely equivalent to the Q-matrix method. This leads nicely to the formula which matches equation (3.5),

$$\nu = \frac{i}{2\pi}\int_{BZ} \partial_k \phi(k) dk \tag{3.13}$$

where $\phi(k)$ is defined as the complex phase of $q(k)$. While equivalent, this method does not provide an elegant intuative picture of the winding number.

We can then safely say that the chiral symmetry protects this index and is in fact required as the winding number needs this protection to be well-defined and quantized. Chiral symmetry is the only symmetry required for these conditions to occur, and the winding number ν cannot change unless the gap is closed. This statement is well founded [69]. We will see later that additional symmetries, which give the other chiral classes, can restrict the type of the index. In some cases the constraint causes the index to be 0, in other cases the index becomes $\mathbb{Z}_2$ or $2\mathbb{Z}$. While we have performed and described this derivation in 1D, these characteristics will exist in all odd dimensions where the winding number can be defined [84].

3.2 Winding number ambiguity

In this section we present the result that there is a sign ambiguity in the winding number which subsequently leads to two different forms of the chiral symmetry operator. These different forms become important when we construct the combined ladder model in the next chapter.

While the winding number is a well known topological invariant for 1D models and in general an application of Cauchy's integral formula [81] in complex analysis, we derived an interesting and surprising result when applied to lattice models with chiral symmetry. This result being that there is an ambiguity in the sign of the winding number in 1D, in other words it is only defined up to a sign. As shown in a previous section the winding number of the SSH model is +1 in the topological phase and 0 trivial phase. A negative winding number can be achieved by 'winding' the Hamiltonian vector in the opposite direction around the pole.

Relabeling the sublattices i.e. $A \rightarrow B$, $B \rightarrow A$ causes the hamiltonian (3.4) to become,

$$\hat{h}(k) = \begin{pmatrix} 0 & \hat{\Delta}(k)^\dagger \\ \hat{\Delta}(k) & 0 \end{pmatrix} \tag{3.14}$$

This transformation changes the determinant used in the winding number calculation such that $det\hat{\Delta}(k) \rightarrow (det\hat{\Delta}(k))^*$. The sign of the phase changes $\phi(k) \rightarrow -\phi(k)$, and hence the winding number gains a minus sign,

$$\nu \rightarrow -\nu \tag{3.15}$$

While this may seem inconsequential, such a transformation has a significant effect on the construction of our later models. This crucial notion arises from the labeling of the sublattices in the unit cell, which has no physical significance. The winding number is odd under a relabeling of these sublattices which is equivalent to changing the sign of the chiral symmetry operator. Chiral symmetry, Eq. (2.19c), is a unitary operator meaning there is an arbitrary phase attached to the operator. We can make a gauge choice that gets rid of this phase by explicitly defining $U_C^2 = 1$ [33], however while this definition fixes the gauge it does not uniguely define the operator as there is still a sign ambiguity, i.e. $U_C \to -U_C$. This means that the chiral symmetry operator is defined up to a sign and therefore there is no physical difference between a winding number of $\nu = +1$ and $\nu = -1$.

However due to how the winding number integral is defined, flipping the structure of the unit cell so $A \to B$ and vice-versa or application of the chiral symmetry operator, causes the sign of the winding number to change so that one can calculate -1 in the topological phase and 0 in the trivial phase. This simply amounts to performing the integral with $\hat{\Delta}^\dagger(k)$ which has the opposite signed phase. Geometrically this simply means the vector winds in the opposite direction now. Physically speaking, because the winding number is the winding of a phase, +1 and -1 are identical.

While such an ambiguity may be known to experts and those well versed in the subtleties of calculating geometric phases, this result does not seem to be present or discussed in the literature. Naturally a question then arises, what does this ambiguity mean when coupling multiple chains together? If one takes two models, each with its own winding number, ν_1 and ν_2 respectively, there will be two ways to couple them that still respect the chiral symmetry. One method results in a total winding number $\nu_{tot} = \nu_1 + \nu_2$ and the other gives $\nu_{tot} = \nu_1 - \nu_2$. It is no leap then to state models with differently signed winding numbers can be adiabatically deformed into each other without closing the energy gap.

Physical measurements can't distinguish individual sublattices, it can not tell the difference between a system that has $+\mathbb{Z}$ winding number or $-\mathbb{Z}$ winding number. Thus there is an ambiguity in the topological index $\mathbb{Z}$ such that $+\mathbb{Z} \leftrightarrow -\mathbb{Z}$ for $A \to B$ and $B \to A$. One of the main points we are making is that the winding number only makes sense up to a sign so that essentially $+1$ and -1 are the same topologically speaking. This is what gives rise to the two possible ways of constructing the chiral symmetry operator, one for AIII, BDI, and CII class models, and another for DIII and CI class models, which we will present in the next chapter.

It needs to be pointed out that the sign ambiguity in the winding number is unrelated to the sign ambiguity in the Chern number. In even dimensions the Chern number, equivalent to the winding number, is odd under time-reversal symmetry however the winding number is not. In this way a two-dimensional coupled system of time-reversed elements will always result in a Chern number of 0. Since the winding number does not have this restriction, the total value of the invariant can take a range of specific values that is dependent on the number of coupled chains in the system. It is surprising that given two subcomponents (i.e. chains) of a model both with winding number $\nu = 1$ the weakly coupled combined system of two chains can necessarily have a winding number of 0 or 2 depending on the form of the chains.

This result is not unique to one-dimension but is general to all odd dimensions where the winding number can be defined. See reference [83] and Appendix B for this derviation.

In the next chapter we will construct general ladder models of two chains (in momentum space) utilizing the sign ambiguity of the winding number to derive the two different forms of the chiral symmetry operator as well as the two forms for the time-reversal and particle-hole symmetry operators. These steps are crucial to construct the proper interchain couplings, and the full model.

Chapter 4

Constructing the combined (ladder) model

In this chapter we will construct a combined ladder model utilizing the winding number sign ambiguity towards answering the project aims, i.e. constructing the topological insulator phase by stitching together time-reversed SSH-like chains. Firstly we will build an SSH-like chain that is in the AIII universality class. Using this, five ladder models can be constructed corresponding to each of the chiral universality classes, see Table 2.1. As stated in the introduction we use the methodology laid out by Kane and Mele to construct the quantum spin Hall state to build our models by coupling two copies of a smaller model. We will use AIII chains as the smaller model to construct the ladder where the coupling will give the appropriate symmetry properties. The winding number ambiguity will be essential to building the ladder models and the symmetry operators.

4.1 AIII chain model

In this section we will construct the AIII class chain by deforming the SSH chain model. Using symmetry arguments and this AIII chain we will construct the combined ladder model for all five chiral universality classes (AIII, BDI, CII, DIII, CI).

The emergent characteristics of the SSH model, including the topological state and zero energy edge modes, are due to the inherent chiral symmetry, and will translate directly to the ladder models we will construct. The basic idea is that the chiral universality classes can be constructed easily using an SSH-like chain as a base and adding terms for the other symmetries.

We are interested strictly in the chiral symmetry universality classes, see Table 2.1. The specific topological insulator properties stem from the chiral symmetry, as shown in the SSH model. While the edge states of the SSH model have properties that can be attributed to time-reversal or particle-hole symmetry, the edge state itself exists because of the chiral symmetry and in most classes (AIII, BDI, and CII) is protected by this symmetry. We will

show that the DIII class model picks up protection in a different way. We will also show that the edge states carry some of the symmetry properties of the models.

The SSH model is arguably in the BDI topological class, with edge mode momentum of either 0 or π which maintains time-reversal symmetry [75]. When the SSH model is discussed in the literature, this is the form they mean. While there are counter arguments to this assertion, they only depend on the symmetries one decides to 'enforce'. Here we force the model to be in the BDI universality class with $\mathbb{Z}$ topology index. The BDI class has $T^2 = P^2 = C^1 = 1$ symmetries. As we want to maintain chiral symmetry, we proceed to break time-reversal symmetry to get to the AIII class model.The most general method would be to add phase factors on the intracell hopping v and the intercell hopping w, so that instead of being real quantities these hoppings would be complex, $v, w \in \mathbb{C}$.

These complex hoppings subsequently break the time-reversal symmetry (and therefore particle-hole) of the SSH model leaving only chiral symmetry intact, see equations (2.19a), (2.19b), and (2.19c). The new model is in the AIII universality class which only has chiral symmetry. It is worth noting that there is a subtlety in this case, as these hoppings, v and w, can be made real again by adding a gauge factor to the creation and annihilation operators of the Hamiltonian, i.e. $c_n \to e^{ian} c_n$. The chain can have time-reversal symmetry despite the complex hoppings as long as one defines the time-reversal symmetry operator correctly. However time-reversal symmetry in the chains is truly broken in the combined model.

We construct the matrix for a single AIII chain in momentum-space, which becomes the SSH model for real v and w,

$$H_{AIII} = \begin{pmatrix} 0 & v + we^{-ik} \\ v^* + w^* e^{ik} & 0 \end{pmatrix} \tag{4.1}$$

where the basis is given as $\Psi_k^T = \{A_k, B_k\}$. It is easy to check that this Hamiltonian only has chiral symmetry by showing it does not have time-reversal symmetry, Eq. (2.19a),

$$\hat{H}^*_{AIII}(-k) = \begin{pmatrix} 0 & v^* + w^* e^{-ik} \\ v + we^{ik} & 0 \end{pmatrix} \neq \hat{H}_{AIII}(k) \tag{4.2}$$

It is easy to see there is no unitary matrix that can fulfill the time-reversal symmetry in this case. We can think about this in terms of rotations of the bloch sphere in the $x - y$ plane, there is no rotation that can affect $H^*_{AIII}(-k)$ to return $H_{AIII}(k)$.

The dispersion plots and edge state spectrums are similar to those shown for the SSH model, see Figs. 2.3 and 2.5, and we can thus conclude that this AIII model is rigorous and can be used to construct topological ladder models. From here we have the fundamentals to construct the other chiral classes. In the next section we will build the combined models and show the existence of topological insulator phases in these models.

4.2 Constructing the combined (ladder) models

The main idea here is the hypothesis that we can construct all of the chiral symmetric universality classes via adding the correct symmetric terms to the AIII class Hamiltonian and the models will have topological insulator phases. This is done by coupling two spinless 1D time-reversed AIII chains. We are going to use this understanding to construct the proper symmetry operators for this coupled model. Understanding the symmetry operations for each class will allow us to understand the associated topological phases and indices.

Constructing the more complicated chiral models will involve adding terms that give the model time-reversal or particle-hole symmetry. We choose to add time-reversal terms to construct the models. We are permitted to do this because of the finite momentum of the edge states, resulting from the additional phase factors in the complex hoppings v and w. The methodology for coupling chains related by time-reversal symmetry is consistent with the procedure for constructing the quantum spin Hall insulator state, by coupling time-reversed partners. By adding coupling terms we can artifically keep or break symmetries to obtain the symmetry class we are interested in.

The momentum of the edge state is fixed at some value determined by the phases of v and w (i.e. finite) and not variable, we can add a second chain or 'leg' to the lattice model with the time-reversed momentum [83]. This time-reversed chain will have the opposite momentum but same energy. Taking an instance of both types of chains and coupling them together in a specific way makes the combined system adhere to time-reversal symmetry and chiral symmetry, and subsequently particle hole symmetry. We describe each chain as $\hat{h}_+$ and $\hat{h}_-$, where $\hat{h}_- = \hat{h}_+^*$, and both chains have the same unit cell basis. We emphasize that the hopping parameters on both chains are the same, $v_1 = v_2$ and $w_1 = w_2$ where 1, 2 represent the 'top' and 'bottom' chains respectfully for the sake this discussion.

The 2-chain uncoupled model now reads,

$$\hat{H}_{uncoupled}(k) = \begin{pmatrix} \hat{h}_+(k) & 0 \\ 0 & \hat{h}_-(k) \end{pmatrix} \tag{4.3}$$

where $\hat{h}_+$ is the AIII Hamiltonian, Eq. (4.1). This matrix, Eq. (4.3), represents two uncoupled chains each in the AIII class that are the time-reversed partners. For clarity we state the basis $c_k = \{c_{A,1,k}, c_{B,1,k}, c_{A,2,k}, c_{B,2,k}\}$. The basis is chosen such that matrix is diagonal in the chains, making an easy chiral basis. This is a 4x4 matrix where each element is a 2x2 matrix. From here we can now build and list the full operators for each symmetry for four of the five chiral classes.

The next step is to couple the chains in some way that gives the correct symmetry terms. This interchain rung coupling will act as a small perturbation on the two uncoupled chain system such that the topological properties of each chain should remain unaffected, i.e. they are weakly coupled. The properties of the coupled system will be the summation of both chains. In the current basis (A, B) this coupling fills the off-diagonal matrix elements, represented by $\hat{\Delta}(k)$. Similar to the $\hat{h}_\pm$ elements, $\hat{\Delta}(k)$ is a 2x2 matrix with quasimomentum-k dependence. The full 2-leg ladder Hamiltonian matrix is given as,

$$\hat{H}(k) = \begin{pmatrix} \hat{h}_+(k) & \hat{\Delta}(k) \\ \hat{\Delta}^\dagger(k) & \hat{h}_-(k) \end{pmatrix} \tag{4.4}$$

There will be restrictions on the form of the chain coupling matrix $\hat{\Delta}(k)$ which depend on which version of the symmetries $\hat{H}(k)$ adheres to, i.e. whether $T^2 = 1$ or -1 and $P^2 = 1$ or -1. We can think about this in reverse by saying that the nature of the $\hat{\Delta}(k)$ will force the full Hamiltonian $\hat{H}(k)$, Eq. (4.4), to be in one of the chiral classes. The symmetry operators consist of 2 parts, one acting on the internal structure of each 2x2 matrix denoted using S_n, and a second part acting on the structure of the condensed $\hat{H}(k)$ matrix denoted by σ_n. Both S_n and σ_n represent a matrix from the set of Pauli matrices.

4.2.1 Deriving symmetry operators

In this section we will derive all of the symmetry operators for the combined model for each universality class. It is well known that an SSH chain has winding number $\nu = 1$ in the topological nontrivial phase ($|w| < |v|$) and $\nu = 0$ for the trivial phase ($|w| > |v|$). The chiral symmetry operator for the natural A, B basis is S_z. Additionally due to the ambiguity in the sign of the winding number the nontrivial phase can also occur with $\nu = -1$ when the sites within the cells are flipped $A \leftrightarrow B$. This case would have a chiral symmetry operator of $-S_z$. Given this, we then have a choice of operator.

In regards to a single chain such a choice makes little difference to the physical and observable pictures. However an interesting scenario arises when multiple chains are coupled together because we have this choice of operator on each individual chain so the sign matters. Thus it stands to reason that the winding number of a two chain system would be the sum or difference of the winding numbers of both chains dependent on the sign of the chiral operators.

We can understand this more closely by examining the Hamiltonian of two uncoupled AIII chains. The first case is to have both chains take on the same signed chiral symmetry operator, where the total winding number is the sum of the winding number of the individual chains, i.e. $\nu = \nu_1 + \nu_2$. In the second case when the chiral operators differ by as sign the total winding number is the difference of the individual winding numbers, i.e. $\nu = \nu_1 - \nu_2$.

In the combined model we need to be more concrete and account for both the intracell chiral symmetry and the chain chiral symmetry. There are two possible forms for the chain coupling terms, which stem from the winding number sign ambiguity. We remind the reader that in the combined model the unit cell is now four sites, two on the top chain and two on the bottom, and we use the basis stated previously. Thus we will define a 'double' operator, with one acting in the chain basis and the other acting in the unit cell basis.

In the case that we choose for both chains to have the same chiral operator the combined operator can be written as $C_1 = S_z\sigma_0$ where S_z acts in the unit cell basis and σ_0 acts in the chain basis. Depending on the relative magnitudes of the hopping parameters $|v|$ and $|w|$ the total winding number can be 0 or 2, representing trivial phases and topological phases on both chains. In the case where the unit cell chiral operators have opposing signs, the

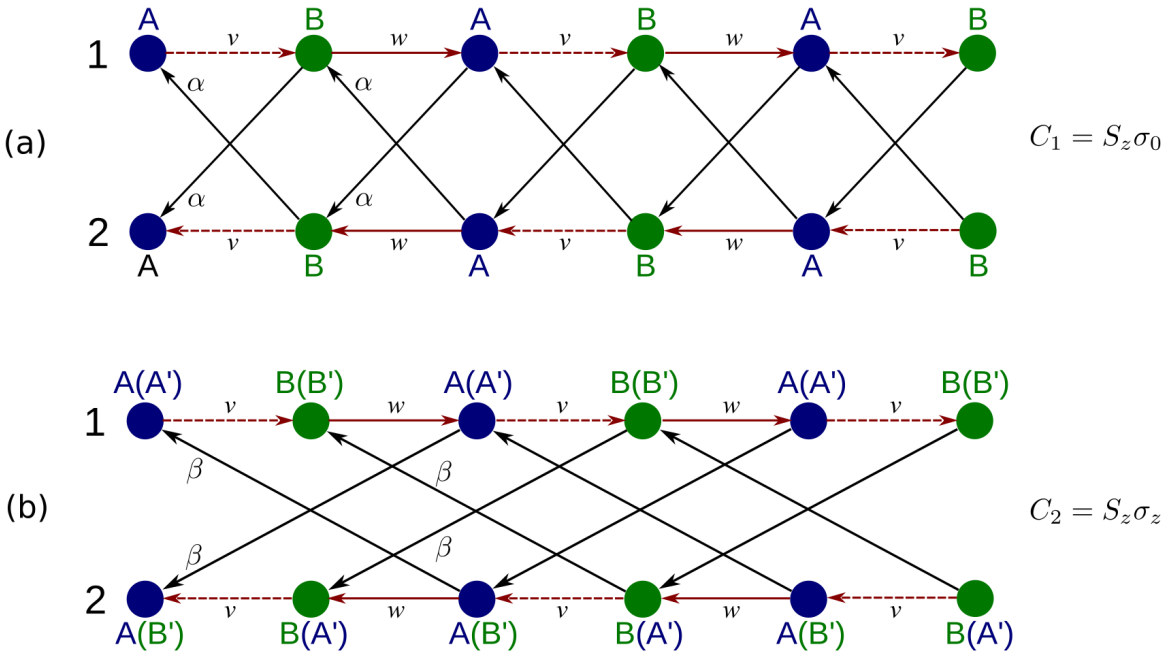

Fig. 4.1 Two ladder models of coupled deformed SSH chains where (a) demonstrates the $C_1 = S_z\sigma_0$ chiral symmetry and (b) shows the $C_2 = S_z\sigma_z$ chiral symmetry form. The sites labeled as A and B are what we consider the natural sublattice basis. Those sites labeled with A' and B' are those defined by the C_2 chiral operator. Projectors between sublattices are given by Eq. (3.1).

combined operator is given as $C_2 = S_z\sigma_z$. The total winding number will always be 0 for this case. In figure 4.1 we illustrate these two sublattice forms, i.e. A/B and A′/B′.

It is interesting that the winding number can not be uniquely defined in the uncoupled chains model. The block diagonal structure indicates there is an additional symmetry present that we haven't accounted for, in this case the charge is being conserved in each chain. This extra symmetry is subsequently causing the winding number to be ambiguious. We will break this symmetry by coupling the chains together which in turn causes the winding number to be defined explicitly (up to a sign). Note there are other additional symmetries in the system such as discrete translational symmetry that may affect the matrix structure however since the winding number is defined for the coupled chains case we don't worry about them.

With no other constraints other than chiral symmetry on the interchain coupling then the model in either case ($C_{1,2}$) belongs to the AIII class but are inequivalent. By applying further symmetry constraints on the interchain coupling we can force the model to fall with in one of the other four chiral classes, i.e. BDI, CII, DIII, or CI.

We will describe the derivation of the time-reversal operator for the BDI configuration here and leave the remaining derivations to the appendix (Appendix B) as they all follow the same logical procedure. Since we have constructed our AIII chains to be time-reversal

partners of each other, if we interpret the operation physically one needs to "swap" the chains in the matrix. This means the operator will be proportional to σ_x or σ_y.

This raises the question, why are there two distinct operators for TRS that are both symmetries of the decoupled system? The ambiguity of this choice of operators, much like the ambiguity in the chiral operator, exists because of the block diagonal structure and an additional unitary symmetry the uncoupled model exhibits. This additional symmetry is broken when the inter-chain rung coupling is added, which in turn lifts this ambiguity and the time-reversal operator is fixed to σ_x or σ_y. The interchain rung couplings fix the ambiguity in the operators. Recall the equation for time-reversal symmetry, Eq. (2.19a), and note that the time-reversal symmetry operator is a unitary operator times the complex conjugate operator, $T = U_T K$, which commutes with the Hamiltonian (4.4).

$$\hat{H}(k) = \begin{pmatrix} \hat{h}_+ & \hat{\Delta}(k) \\ \hat{\Delta}^\dagger(k) & \hat{h}_- \end{pmatrix} \qquad \hat{H}^*(-k) = \begin{pmatrix} \hat{h}_- & \hat{\Delta}^*(-k) \\ \hat{\Delta}^T(-k) & \hat{h}_+ \end{pmatrix} \tag{4.5}$$

As we don't know the internal structures of $\hat{\Delta}(k)$ we will revisit them in the next section. Comparing $\hat{H}(k)$ and $\hat{H}^*(-k)$, Eq. (4.5), we need an operator that will flip $\hat{h}_+$ and the $\hat{h}_-$ elements. As the internal components of these matrices are unchanged we need the identity operator to act on the sublattice basis, so we use S_0. Additionally the σ_x Pauli matrix performs the necessary flipping of the matrix elements. The BDI class requires the time-reversal symmetry operator to have the property $T^2 = +1$, which $S_0\sigma_x$ satisfies. Therefore the time-reversal symmetry operator for the BDI class,

$$T = U_T^+ K = S_0\sigma_x K \tag{4.6}$$

which satisfies the necessary symmetry equations,

$$TH^*(-k)T^\dagger = H(k) \tag{4.7a}$$

$$S_0\sigma_x H^*(-k)\sigma_x^\dagger S_0^\dagger = H(k) \tag{4.7b}$$

where we use the identity $(AB)^\dagger = B^\dagger A^\dagger$.

The particle-hole symmetry operator is derived in the same logical manner as above and is $S_z\sigma_x$ for the BDI class. The chiral symmetry operator can be derived from either the symmetry equation or by combining the time-reversal and particle-hole symmetry operators. Both methods yield the same result,

$$\begin{aligned} C &= T \cdot P \\ &= U_T K U_C K \\ &= S_z\sigma_0 \end{aligned} \tag{4.8}$$

All the symmetry operators for all of the chiral classes are derived in a similar procedure, Table 4.1. We see that the choice of chiral symmetry affects the description of the time-reversal and particle-hole symmetry operators. It is also interesting to note that the decoupled system is class ambiguous, it can be in any of the four different universality classes - BDI, CII, CI,

AIII	$C_1 = U_{C_1} = S_z\sigma_0$ $C_2 = U_{C_2} = S_z\sigma_z$

BDI	$T_+ = U_T^+ K = S_0\sigma_x K$ $P_+ = U_P^- K = S_z\sigma_x K$ $C_1 = U_{C_1} = S_z\sigma_0$	DIII	$T_- = U_T^- K = iS_0\sigma_y K$ $P_+ = U_P^+ K = S_z\sigma_x K$ $C_2 = U_{C_2} = S_z\sigma_z$
CII	$T_- = U_T K = iS_0\sigma_y K$ $P_- = U_P K = -iS_z\sigma_y K$ $C_1 = U_{C_1} = S_z\sigma_0$	CI	$T_+ = U_T^+ K = S_0\sigma_x K$ $P_- = U_P^- K = -iS_z\sigma_y K$ $C_2 = U_{C_2} = S_z\sigma_z$

Table 4.1 Symmetry operators for chiral universality classes.

or DIII. There is an extra symmetry that the decoupled system has that is broken when the interchain coupling is added which collapses the model to a specific class. This is a very curious result because these classes are different topologically. The BDI and CII class models are topological insulators with $\mathbb{Z}$ topology index, the DIII class model is a topological insulator with $\mathbb{Z}_2$ index, and CI is topologically trivial.

In order to collapse the uncoupled model to a specific class we will make our model concrete by deriving and defining specifically the $\hat{\Delta}(k)$ matrix to form the coupled chain model. In the next section we will construct $\hat{\Delta}(k)$ so that it is compatible for chiral, time-reversal, and particle-hole symmetries.

4.2.2 Deriving the $\hat{\Delta}(k)$ matrix

In this section we will derive the structure and properties of the $\hat{\Delta}(k)$ matrix in each universality class in terms of generic even and odd functions, and Pauli matrices. To properly construct the chiral symmetric topological models we need to understand how the Hamiltonian (4.4) of coupled chains transforms when symmetry operators $T_\pm$ and $P_\pm$, Table 4.1, are applied. The symmetry operators impose constraints on the $\hat{\Delta}(k)$ matrices that we can exploit to understand their properties. We work in k-space for simplicity.

Starting with the time-reversal symmetry equation (2.19a) and the T_- operator (CII) we find (see Appendix B for details),

$$\begin{pmatrix} \hat{h}_+(k) & -\hat{\Delta}^T(-k) \\ -\hat{\Delta}^*(-k) & \hat{h}_-(k) \end{pmatrix} = \begin{pmatrix} \hat{h}_+(k) & \hat{\Delta}(k) \\ \hat{\Delta}^\dagger(k) & \hat{h}_-(k) \end{pmatrix} \tag{4.9}$$

In order to maintain the T_- symmetry then the following relation for $\hat{\Delta}(k)$ must be true,

$$\hat{\Delta}(k) = -\hat{\Delta}^T(-k) \tag{4.10}$$

The procedure for the remaining classes is trivial from here and we list simply the full set of relations here:

$$T_+ : \quad \hat{\Delta}(k) = \hat{\Delta}^T(-k) \tag{4.11a}$$

$$T_- : \quad \hat{\Delta}(k) = -\hat{\Delta}^T(-k) \tag{4.11b}$$

$$P_+ : \quad S_z\hat{\Delta}(k)S_z = -\hat{\Delta}^T(-k) \tag{4.11c}$$

$$P_- : \quad S_z\hat{\Delta}(k)S_z = \hat{\Delta}^T(-k) \tag{4.11d}$$

We proceed now to solving for $\hat{\Delta}(k)$ explicitly in each case and find the general form for $\hat{\Delta}(k)$ for the chiral classes. Again we will derive the solution for an example and list the full results at the end. We will show the derivation using the T_- operator, Eq. (4.11b),

$$T_- : \hat{\Delta}(k) = -\hat{\Delta}^T(-k) \tag{4.12}$$

We can examine the matrix elements as functions in two ways, as either an even function or an odd function. We find the most general solution is the linear combination of even and odd functions. The real space structure of this matrix will depend on the choices of even or odd functions, i.e. constant functions provide the intracell hoppings while sinusoidal and exponentials provide intercell and longer range hoppings. From Figure 4.1 we know the $\hat{\Delta}(k)$ for the BDI and CII model will be a linear combination of S_x and S_y, since our basis is A_1, B_1, A_2, B_2. Equally, the DIII and CI class lattice will need a $\hat{\Delta}(k)$ consisting of S_0 and S_z. The full definitions of $\hat{\Delta}(k)$ in terms of even and odd functions for each class are listed at the end of this subsection, Eqs. (4.18).

For the odd functions ($f_o(k)$, $g_o(k)$) we only have $sin(k)$ as a choice. If we choose an odd function,

$$\hat{\Delta}_{odd}(k) = \hat{\Delta}^T_{odd}(k) \tag{4.13}$$

For the relation to hold true, as the function is a 2x2 matrix, it must be a linear combination of the Pauli matrices $S_{0,x,z}$.

Alternatively if the function is even ($f_e(k)$, $g_e(k)$) in k, the relation becomes,

$$\hat{\Delta}_{even}(k) = -\hat{\Delta}^T_{even}(k) \tag{4.14}$$

In this case we have the choice of S_x or iS_y. To preserve the U_T^- symmetry, $\hat{\Delta}(k)$ is a linear combination of the terms:

$$\sin(k)S_0,\ \sin(k)S_x,\ \sin(k)S_z,\ S_y,\ iS_y \tag{4.15}$$

Any even or odd function would work here, the ones shown here are merely examples of possible functions. However the choice of function must adhere to the physical lattice model we are analyzing, e.g. $sin(k)$, will add an extra factor of k so the hopping connects further separated sites, e.g. next-nearest neighbor and etc. Listing all of the terms for each symmetry

case:

$$U_T^-: \quad \sin(k)S_0,\ \sin(k)S_x,\ \sin(k)S_z,\ S_y,\ iS_y \tag{4.16a}$$
$$U_P^-: \quad S_0,\ \sin(k)S_x,\ S_z,\ \sin(k)S_z,\ iS_y \tag{4.16b}$$
$$U_T^+: \quad S_0,\ S_x,\ S_z,\ \sin(k)S_y,\ \sin(k)iS_y \tag{4.16c}$$
$$U_P^+: \quad \sin(k)S_0,\ S_x,\ \sin(k)S_z,\ S_y,\ \sin(k)S_y,\ \sin(k)iS_y \tag{4.16d}$$

It is now possible to construct the Hamiltonian for BDI, CII, DIII, and CI universality class models. To create a Hamiltonian that obeys the BDI class, for example, we will need to select functions that appear in both the U_T^+ and U_C^+ catergories. Doing this for all 4 classes, we get the following possible representations:

$$\begin{aligned}
BDI| \qquad & T^2 = P^2 = 1 \ \ (U_T^+, U_P^+) \\
& \hat{\Delta}(k) = aS_x + b\sin(k)(iS_y) \\
CII| \qquad & T^2 = P^2 = -1 \ \ (U_T^-, U_P^-) \\
& \hat{\Delta}(k) = a\sin(k)S_x + b(iS_y) \\
DIII| \quad & T^2 = -1 \ \ P^2 = 1 \ \ (U_T^-, U_P^+) \\
& \hat{\Delta}(k) = \sin(k)[aS_0 + bS_z] \\
CI| \quad & T^2 = 1 \ \ P^2 = -1 \ \ (U_T^+, U_P^-) \\
& \hat{\Delta}(k) = \sin(k)[aS_0 + bS_z]
\end{aligned} \tag{4.17}$$

These conditions are completely general and we could have chosen functions other than a constant for the even function and $\sin(k)$ for the odd function. From the equation set (4.17) it is easy to see that due to the presence of S_x and S_y matrices, which are off-diagonal, the BDI and CII models will have $A-B$ and $B-A$ interchain (rung) couplings, Fig. 4.1. Similary, the DIII and CI classes exclusively have the S_0 and S_z matrices which are diagonal resulting in $A-A$ and $B-B$ interchain rung couplings. The choice of even and odd functions in $\hat{\Delta}(k)$ determine how these sites are connected, same cell, nearest neighbor cells, etc. The $\hat{h}_+$ and $\hat{h}_-$ parts of the ladder Hamiltonian matrix, Eq. (4.4), describe how the sites along each chain are connected.

Let's be more general with our equations from (4.17) by noticing the even and odd function structure of each equation such that we can say:

$$BDI: \ \hat{\Delta}(k) = f_e(k)S_x + f_o(k)(iS_y) \tag{4.18a}$$
$$CII: \ \hat{\Delta}(k) = f_o(k)S_x + f_e(k)(iS_y) \tag{4.18b}$$
$$DIII: \ \hat{\Delta}(k) = f_o(k)S_0 + g_o(k)S_z \tag{4.18c}$$
$$CI: \ \hat{\Delta}(k) = f_e(k)S_0 + g_e(k)S_z \tag{4.18d}$$

where e and o subscripts denote even or odd, respectively. The goal from here is to build the coupling $\hat{\Delta}(k)$ that is compatible with chiral, time-reversal, and particle-hole symmetries in order to construct our models in the above four different chiral classes. In the next sections

we will investigate the dispersion spectrum properties of 4-band models and zero energy modes of each class model.

4.2.3 BDI and CII class models

In the previous section we derived the general function structures for the $\hat{\Delta}(k)$ matrices that couple the chains together. In this section we will present the general dispersion features of 4-band models, which will help us understand model specific band structures presented in a later section. We will make approximations about the $\hat{\Delta}(k)$ functions in order to plot the dispersions. The band structure is an important characteristic of a model as it shows the allowed and forbidden quantum mechanical wave functions of the electron in the system and in our case the degeneracies and zero energy modes of a topological insulator phase. The band structure will also give us insight into the winding number of the models.

We group BDI and CII together because their Hamiltonian matrix is similar, same with the DIII and CI classes. The BDI and CII model spectrums will be different. One reason is CII has Kramers degeneracy via the T_- time-reversal symmetry so there has to be degenerate points in the spectrum however this won't in general be the case for a BDI class model. We should be able to show that BDI can host degeneracies but also show that it doesn't and it only depends on the parameters and the degeneracy is fixed by some symmetry. Typical BDI models might have a degeneracy in the spectrum because an additional symmetry like inversion might be present. For CII there will always be degenerate points in the spectra so there should be some ambiguity in something like the winding number but BDI there should no ambiguity given no degeneracies in the spectra.

Let's first consider the case with the chiral symmetry operator $C_1 = S_0\sigma_z$. This case corresponds to the BDI and CII classes. The lattice model specific to this configuration has couplings according to figure 4.1(a). Starting from the general Hamiltonian using the basis $c_k^T = \{c_{A,1,k}, c_{B,1,k}, c_{A,2,k}, c_{B,2,k}\}$,

$$\hat{H}(k) = \begin{pmatrix} \hat{h}_+(k) & \hat{\Delta}(k) \\ \hat{\Delta}^\dagger(k) & \hat{h}_-(k) \end{pmatrix} \tag{4.19}$$

For the BDI and CII classes this gives the following 4x4 matrix,

$$\hat{H}_{BDI/CII}(k) = \begin{pmatrix} 0 & v + we^{ik} & 0 & A + B \\ v^* + w^*e^{-ik} & 0 & A - B & 0 \\ 0 & (A-B)^* & 0 & v^* + w^*e^{ik} \\ (A+B)^* & 0 & v + we^{-ik} & 0 \end{pmatrix} \tag{4.20}$$

Rearranging the basis set $c_n^T = \{c_{A,1,k}, c_{A,2,k}, c_{B,1,k}, c_{B,2,k}\}$ brings the Hamiltonian to full off-diagonal block form,

$$\hat{H}_{BDI/CII}(k) = \begin{pmatrix} 0 & 0 & x & \tau \\ 0 & 0 & \omega^* & y \\ x^* & \omega & 0 & 0 \\ \tau^* & y^* & 0 & 0 \end{pmatrix} \tag{4.21}$$

where,

$$x = v + we^{ik} \tag{4.22a}$$
$$y = v^* + w^* e^{ik} \tag{4.22b}$$
$$\tau = A + b \tag{4.22c}$$
$$\omega = A - B \tag{4.22d}$$
$$BDI: \ A = f_e(k), \ B = f_o(k) \tag{4.22e}$$
$$CII: \ A = f_o(k), \ B = f_e(k) \tag{4.22f}$$

Solving the matrix gives the dispersion,

$$\lambda^2 = \frac{1}{2}\Big[|\tau|^2 + |\omega|^2 + |x|^2 + |y|^2 \pm \sqrt{(|\tau|^2 + |\omega|^2 + |x|^2 + |y|^2)^2 - 4(|\tau|^2|\omega|^2 + |x|^2|y|^2 - \tau^*\omega x y - \tau\omega^* x^* y^*)}\Big] \tag{4.23}$$

It is trivial to see that equation (4.23) will give a 4-band dispersion plot. Any Hamiltonian constructed in this way will have four bands. The ± for the λ^2 sets the magnitude of the positive (upper) subbands and negative (lower) energy subbands while the ± on the inner square root dictates the splitting of the two positive bands and the two negative bands.

The terms under the square root open a gap between the two upper subbands and between the two lower subbands i.e. the degeneracy of the two time-reversed AIII models is lifted. Since chiral symmetry is an anti-unitary symmetry, its anticommutation results in a negative sign when the chiral symmetry operator is applied. The chiral symmetry ensures a mirroring effect of the bands over the zero energy ($\epsilon = 0$) axis. Such a feature is present in all chiral classes. The different symmetry properties of each class will show up in the spectra, which will be demonstrated in the next sections.

BDI

For the sake of simplicity to understand the basic features of these classed dispersion band structures we have set the odd function $f_o = 0$ and the even function will be some (small valued) real constant, Eq. (4.18a), such that it acts as a perturbation on the uncoupled chain system. As described in the previous section, any even and odd function would be permissible to use, however the choice would affect the real lattice hoppings and the band structures.

As we expect for an insulator state the valence and conduction bands are fully gapped, at half filling, through the entirety of the Brillouin zone, Fig. 4.2. We will see in the next chapter that our BDI model has degeneracies at $k = [-\pi, \pi)$. The difference arises in how we have

defined the interchain couplings in momentum space, here we have chosen a real constant while our model has exponentials due to the cell hoppings.

The magnitude of the interchain constant controls the size of the subband gaps. As expected, the band spectrum represents an insulator, i.e. the Fermi level is surrounded by gaps to the valence bands at lower energies and conduction bands at higher energies. Recalling the band features caused by symmetries, Eqs. (2.19), the bands have mirror symmetries across both axes resulting from the presence of all three symmetries.

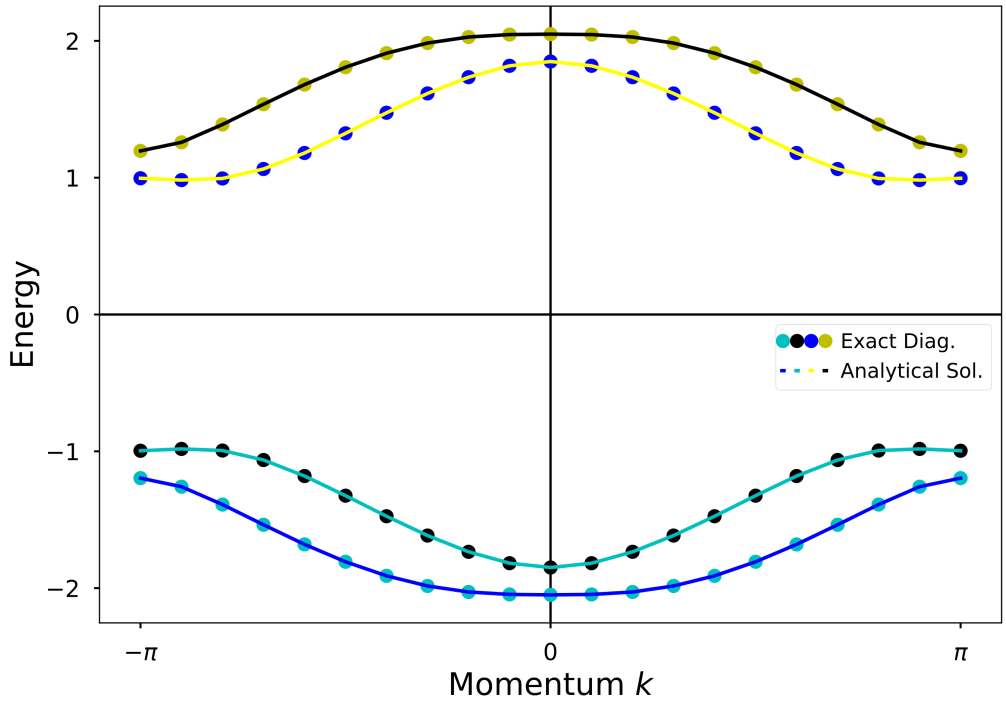

Fig. 4.2 BDI class model band structure with $v = 0.5$ $w = 1.5$ $f_e = 0.1$ $g_o = 0$. This plot uses a real constant for the even function f_e and sets the odd function $g_o = 0$. Analytically calculated dispersion matches the numerical calculations.

CII

In the CII model, where again the odd function is set as $f_o = 0$, and the even function is set to a constant imaginary value, Eq. (4.18b), that is small as not to close the gap. Due to the present Kramers degeneracy ($T^2 = -1$) there are multiple degenerate points where the subbands meet. These high symmetry points are fixed by time-reversal symmetry and not dependent on the parameters, Fig. 4.3. Examining the terms in the inner square root of equation (4.23) we see trivially these go to 0 in the high symmetry points of $k = \{0, \pm\pi\}$. For this model these degeneracies appear as a consequence of symmetries and the gap can not be opened via tuning of parameters.

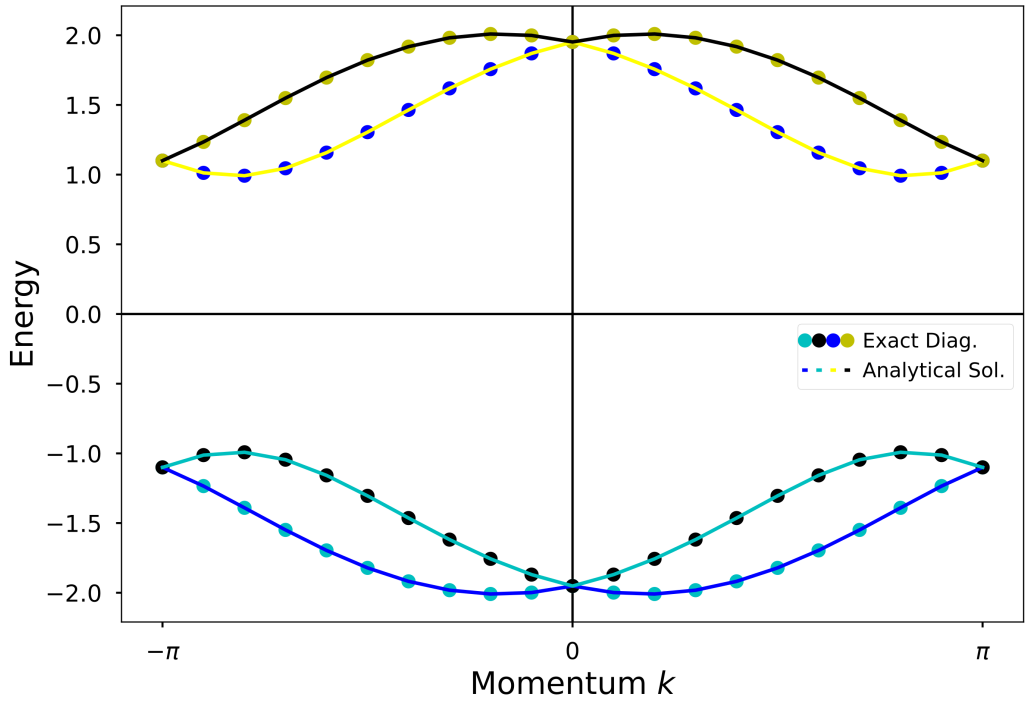

Fig. 4.3 CII class model band structure with $v = 0.5$ $w = 1.5$ $f_e = 0.1i$ $g_o = 0$. This plot uses a imaginary constant for the even function f_e and sets the odd function $g_o = 0$. Analytically calculated dispersion matches the numerical calculations.

4.2.4 DIII and CI class models

Next we build the lattices and Hamiltonians for the CI and DIII classes which have the second form of the chiral operator $C_2 = S_z\sigma_z$. For the CI class $\hat{\Delta}(k)$ consists of two even functions in momentum space Eq. (4.18d), alternatively for the DIII class these functions are odd, Eq. (4.18c). To reiterate the defining aspect that makes the lattices in these classes different from the BDI/CII lattices is that the rungs connect A sites to A sites and B sites to B sites. Therefore depending on the functions we choose the rungs could connect the same cells together (standard ladder) or next neighbor cells on the same site (cross hatched ladder similar to the previous lattices), see Fig. 4.1(b). However we will see that a square ladder lattice doesn't give the CI class model.

Any more complicated function, such as cosine, connect nearest neighbor cells together, as seen in the BDI and CII lattices. For the DIII and CI lattice type, A-sites are connected to the A'-site in the next unit cell, similarly for the B-sites. Additionally the rung couplings have an imaginary prefactor in order to make them odd. However the CI class is not topological in 1D so we shouldn't see any protected edge states.

Reiterating the CI/DIII momentum space Hamiltonian as,

$$\hat{H}_{DIII/CI}(k) = \begin{pmatrix} 0 & v + we^{ik} & f_n(k) - g_n(k) & 0 \\ v^* + w^* e^{-ik} & 0 & 0 & f_n(k) + g_n(k) \\ (f_n(k) - g_n(k))^* & 0 & 0 & v^* + w^* e^{ik} \\ 0 & (f_n(k) + g_n(k))^* & v + we^{-ik} & 0 \end{pmatrix} \tag{4.24}$$

where we have $n = even$ for the CI class and $n = odd$ for the DIII class representing even and odd functions in momentum/wavenumber k. Following the same abbreviation scheme as the previous subsection we get the matrix,

$$\hat{H}_{DIII/CI}(k) = \begin{pmatrix} 0 & x & \tau & 0 \\ x^* & 0 & 0 & \omega \\ \tau^* & 0 & 0 & y \\ 0 & \omega^* & y^* & 0 \end{pmatrix} \tag{4.25}$$

where x and y are defined the same as the BDI and CII case, and $\tau = f_n - g_n$ and $\omega = f_n + g_n$. This matrix cannot be brought into a block off-diagonal form in a convenient way. Solving the dispersion relation gives,

$$\lambda^2 = \frac{1}{2}\Big[|\tau|^2 + |\omega|^2 + |x|^2 + |y|^2 \pm \sqrt{(|\tau|^2 + |\omega|^2 + |x|^2 + |y|^2)^2 - 4(|\tau|^2|\omega|^2 + |x|^2|y|^2 - \tau\omega^* x^* y - \tau^* \omega x y^*)}\Big] \tag{4.26}$$

The relation is slightly different than the BDI/CII relation in the last two terms. The spectrums will be four bands and have similar features to the previous cases.

DIII

The model in the DIII class presents with the summation of two odd functions in the $\hat{\Delta}(k)$ matrix. Similar to the previous models of BDI and CII we will set one of these odd functions to 0 to simplify the calculations. We further restrict the nonzero function to be $f_o = -x$, which is a simple odd function. The characteristics of the spectrum will be invariant to whichever function is set to zero, as can be seen in figure 4.4.

Based on the symmetry properties of DIII (T_- and P_+) we can predict that the spectrum should have features common to both BDI and CII. Figure 4.4 shows there is a degenerate point at $k = 0$ which presents in the CII case and gaps at the $k = \{-\pi, \pi\}$ points which show up in the BDI case. The shape of the bands is determined by the function $f(k)$. Any odd function will work but they will all present a degenerate point at $k = 0$.

CI

The CI universality class is not topological in 1D, Table 2.1. However it is instructive to do some analysis for this class to compare the results of the other chiral classes. The simplest

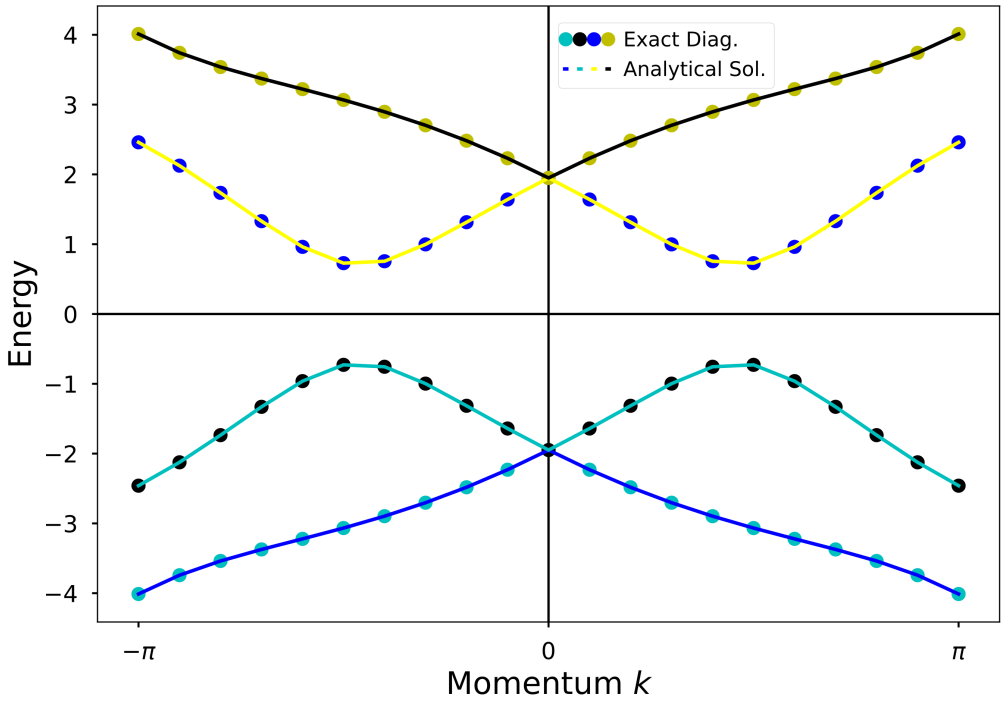

Fig. 4.4 DIII class model band structure with $v = 0.5$ $w = 1.5$ $f_o = 0.1i$ $g_o = 0$. This plot sets one odd function $f_o = 0.1i$ and sets the other odd function $g_o = 0$. Analytically calculated dispersion matches the numerical calculations.

model is to set f_e or g_e to zero and the remaining function to a small constant. A constant is the most trivial even function. As with the DIII model there is no difference to the characteristics of the spectrum which function we choose to set to zero.

Setting the functions in τ and ω to a constant will result in a fully gapped state, Fig. 4.5, notably at $k = 0$ which is degenerate in the previous models. The gap size will be some proportion of the value of the constant these functions are set to. We notice the subbands are gapped through the full regime of the Brillouin zone similar to the BDI model which is due to matrix elements of $\hat{\Delta}(k)$ being real constants in both models. We will see in the next chapter when we develop specific models that the band structures will be different.

In the next chapter we will use the general expressions derived here to construct the real lattice models in each chiral class and analyze the specific band structures as well as the energy spectra.

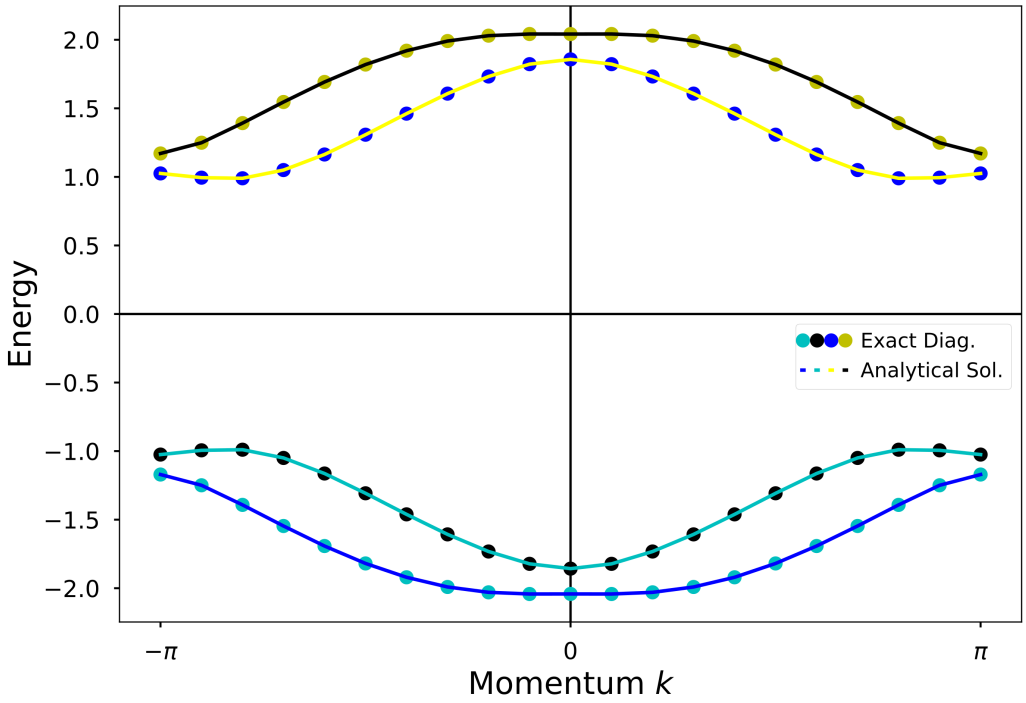

Fig. 4.5 CI class model band structure with $v = 0.5$ $w = 1.5$ $f_e = 0.1$ $g_e = 0$. This plot sets one odd function $f_o = 0.1$ and sets the other odd function $g_o = 0$. Analytically calculated dispersion matches the numerical calculations.

Chapter 5

Realizing real space 1D Topological Insulators

In this section we will build the real space realizations of our classed models and examine the eigenvalue and eigenvector spectrums for the hallmark characteristics of topological insulator states, notably zero energy modes and symmetry protected edge states. We will also take the opportunity to derive the specific band structures for each model. We will see that by coupling two chains together we expand the unit cell from two sites to four sites which has implications for the band structures, energy spectra, and edge states. The four topological classes will have degenerate points in the spectra at two or three of the high symmetry points, the CI class model will not.

We will demonstrate that our combined models maintain the characteristics of the topological insulator phase similar to the prototypical SSH model, i.e. zero energy edge modes. The topological and trivial phases still emerge as a function of the intra- (v) and intercell couplings (w). To reiterate, the fully gapped trivial phase emerges with intercell coupling being less than the intracell coupling, i.e. $|v| > |w|$. The topological phase arises in the opposing sector with the intracell coupling being less than the intercell coupling, $|v| < |w|$. In such a state the ends of the chains become increasingly isolated from the bulk of the system, given that the interchain rung coupling (α,β) remains small relative to the chain couplings, i.e. $\alpha,\beta < |w| - |v|$.

One of the defining characteristics of the topological insulator phase is the emergence of zero energy edge state modes in the topological sector protected by symmetries. These modes will be degenerate due to the chiral symmetry. We will first consider the chiral symmetry classes AIII, BDI and CII, and then look at the BdG classes DIII and CI. We will examine the energy spectrum, using exact diagonalization techniques, of each class to see these zero energy modes emerge in the topological phase.

5.0.1 AIII, BDI, and CII class models

In this section we will examine the energy spectrums for the C_1 chiral classes AIII, BDI, and CII, Fig. 4.1(a). These classes have similar characteristics in terms of their topological index ($\mathbb{Z}$) and winding number.

The minimal Hamiltonian $\hat{H}_1$ for these models is given by,

$$\hat{H}_1 = \hat{H}_0 + \hat{V}_1 \tag{5.1}$$

where $\hat{H}_0$ represents the Hamiltonians (Eq. (4.3)) for the uncoupled AIII chains (SSH model with complex hoppings). We reiterate it here for clarity,

$$\hat{H}_0 = v \sum_{n=1}^{N} c^{\dagger}_{An} c_{Bn} + w \sum_{n=1}^{N-1} c^{\dagger}_{Bn} c_{An+1} + h.c. \tag{5.2}$$

The interchain Hamiltonian, $\hat{V}_1$, are given as,

$$\hat{V}_1 = \alpha \sum_{n}^{N-1} (c^{\dagger}_{A,1,n} c_{B,2,n} + c^{\dagger}_{A,2,n} c_{B,1,n} + c^{\dagger}_{B,1,n} c_{A,2,n+1} + c^{\dagger}_{B,2,n} c_{A,1,n+1}) + h.c. \tag{5.3}$$

Note that $\hat{H}_1$ is not the most general Hamiltonian that could be written here and adiditional symmetry compatible terms could be added. For convenience we parameterize the chain couplings by defining $v = (1+\epsilon)e^{i\delta_1}$ and $w = (1-\epsilon)e^{i\delta_2}$, where ϵ is the variable parameterization factor that causes the phase to change and $\delta_{1,2}$ is valued so v and w are complex.

Due to the BDI, CII, and AIII class models having the same Hamiltonian structure we can trivially parameterize the value of the interchain rung couplings which distinguish each class from the others, such that $\alpha \rightarrow |\alpha| e^{i\theta}$. The parameter θ is adjusted to give the necessary value for each class model. In this way we can move between the classes in an easy manner. It is trivial to show that if α is real ($\theta = 0, \pi$) the Hamiltonian is T_+ and P_+ symmetric and is therefore within the BDI universality class. If α is imaginary ($\theta = \pi/2$) the Hamiltonian conforms to the T_- and P_- compliant and thus is CII classed. Lastly if α is complex (i.e. $\theta \neq \{0, \pi, \pi/2\}$) the Hamiltonian is in the AIII class with just chiral symmetry.

We will see that the spectrums for these classes are very similar, all showing the same features including fully gapped trivial states ($\epsilon > 0$, $|v| > |w|$) and zero modes in the topological phase ($\epsilon < 0$, $|v| < |w|$).

The transformation of $\hat{H}_1$ to momentum space gives the matrix,

$$\hat{H}_1(k) = \begin{pmatrix} 0 & 0 & x & a \\ 0 & 0 & b^* & y \\ x^* & b & 0 & 0 \\ a^* & y^* & 0 & 0 \end{pmatrix} \tag{5.4}$$

where,

$$x = v + we^{ik} \tag{5.5a}$$
$$y = v^* + w^* e^{ik} \tag{5.5b}$$
$$a = \alpha + \alpha^* e^{-ik} \tag{5.5c}$$
$$b = \alpha^* + \alpha e^{ik} \tag{5.5d}$$

The dispersion relation is then given by the general form equation (4.23), where $\tau = \alpha + \alpha^* e^{-ik}$ and $\omega = \alpha^* + \alpha e^{ik}$.

We will show the specific band structures of each of our models and demonstrate the properties pointed out in the previous chapter. As we have parameterized the interchain coupling in such a way moving through the complex plane, we will examine the BDI (real) model first, followed by the AIII (complex) model, and lastly the CII (imaginary) model. We present the band spectra for topological phase of each model. We will also show the energy spectrums, demonstrating the trivial and topological phases arising as the relative strengths of the chain hoppings are varied.

BDI class model

From the Hamiltonian matrix (5.4), we can calculate the dispersion relation numerically using exact diagonalization and analytically for this specific BDI model, Eq. (5.1). Unlike the band spectrum of the generic model, Fig. 4.2, our specific model hosts degeneracies in the subbands. These bands are gapped with crossings occur at the Brillouin zone terminal points $k = \pm\pi$.

As stated previously one of the indicative features of topological insulators is zero energy edge states in the topological phase. The lower and upper bands are fully gapped in the trivial phase and there are zero energy modes (in the middle of the gap) hosted in the topological phase ($|v| < |w|$). We will see these zero energy modes are 4-fold degenerate, and correspond to the four possible edge states, just as we saw in the SSH model. We will derive the symmetry properties of these edge states in the next chapter. Figure 5.2 shows a BDI classed system with isotropic real valued interchain couplings. The zero energy states are clearly visible in the $\epsilon < 0$ regime. The closing of the gap at $\epsilon = 0$ indicates the system undergoes a quantum phase transition between the trivial and nontrivial phases. This further indicates the gaps in the band structure would close, similar to the SSH case, for some expression of the hopping parameters at $E = 0$.

In the case $\alpha \sim 1$ the zero energy modes are maintained however the band gap closes in both phase sectors, Fig. 5.3. In the strong coupling case that α is large the system transitions to a full dimer state where the zero energy modes exist through the range of the calculated spectrum, Fig. 5.4. Once the gap closes in both phases the system transitions to a phase where the dimers exist on the rungs instead of the chains, explaining why the zero modes exist throughout the spectrum. This state will be broken (i.e. fully gapped) when the chain couplings are sufficiently large and are the dominant couplings again. All this amounts to

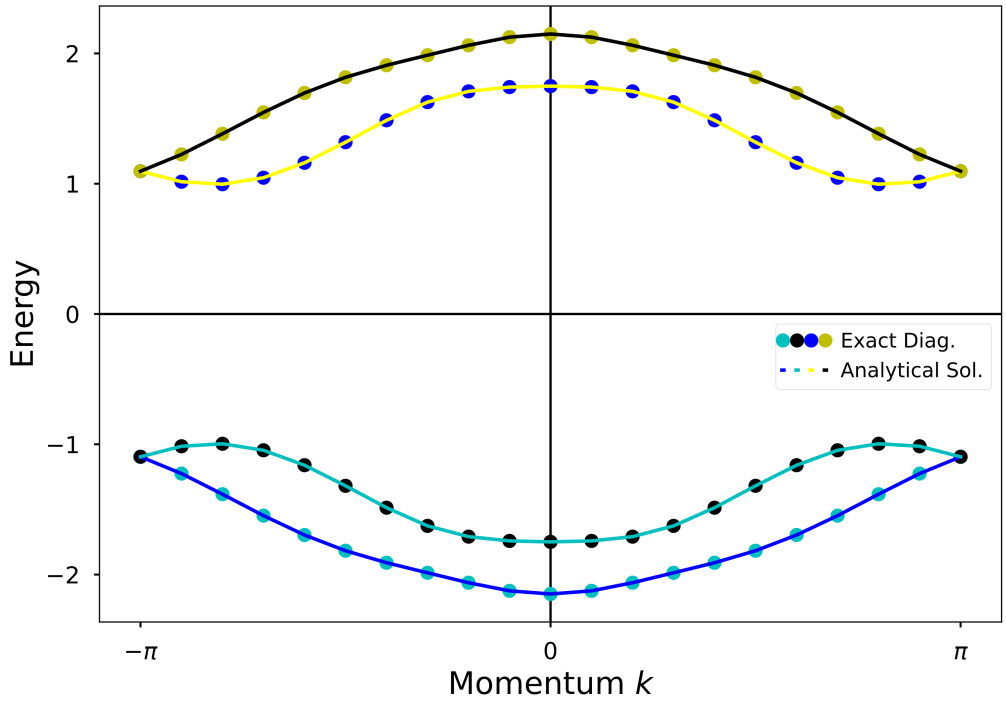

Fig. 5.1 Band structure for the BDI class model with isotropic real valued rung couplings $\alpha = 0.1$ with $v = 0.5$ $w = 1.5$ where the system is in the topological phase. Analytically calculated dispersion matches the numerical calculations.

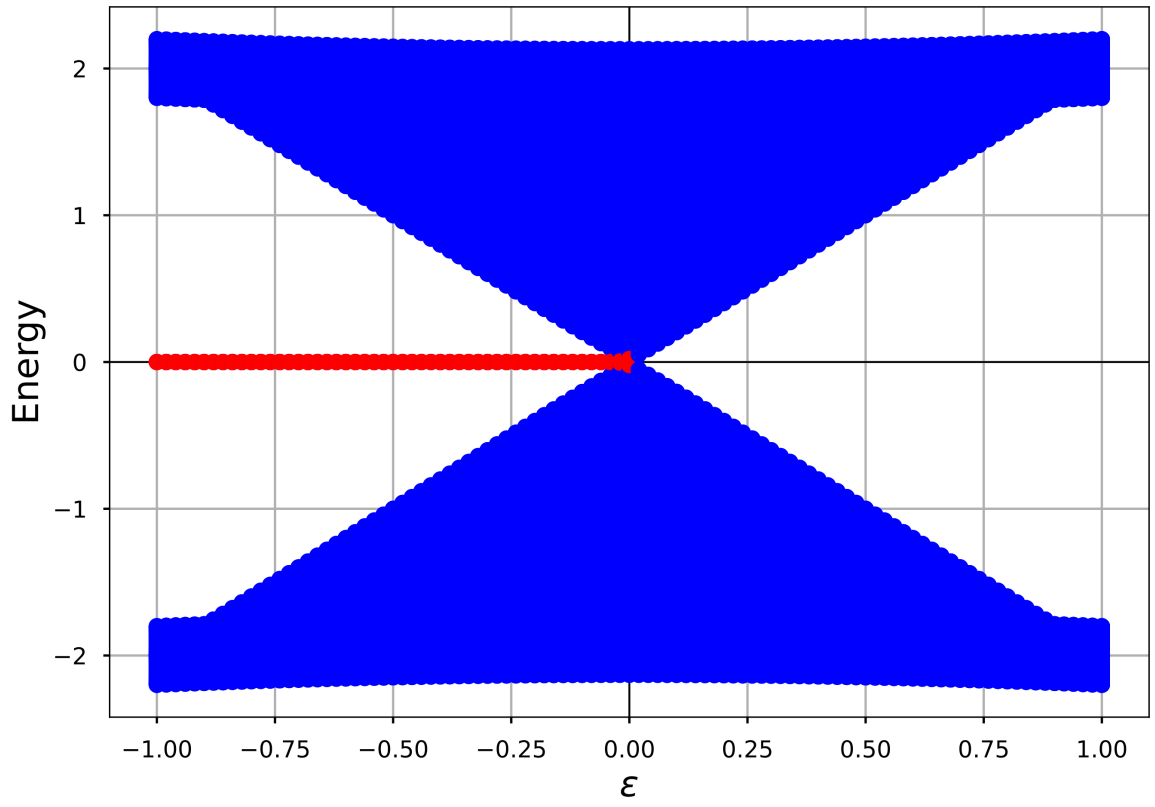

Fig. 5.2 Energy eigenvalue spectrum as a function of dimer parameter ϵ for the BDI model with real valued interchain couplings $\alpha = 0.1$ with 75 unit cells per chain.

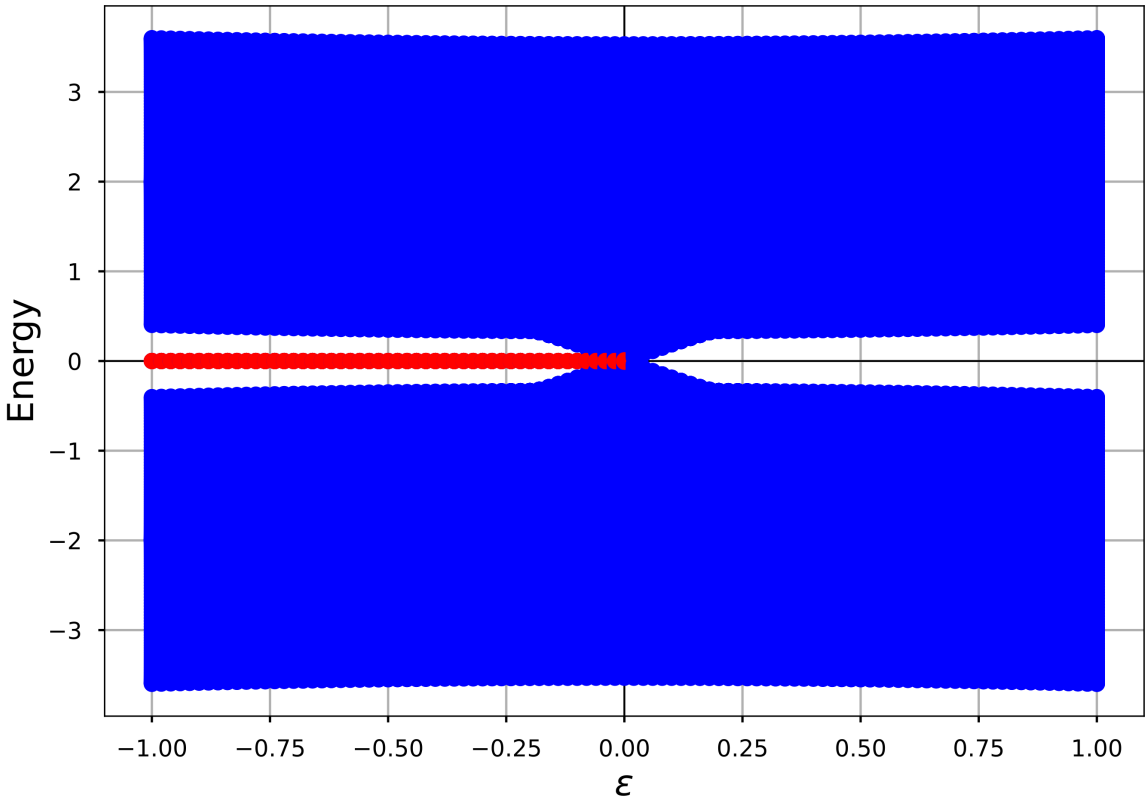

Fig. 5.3 Energy eigenvalue spectrum as a function of dimer parameter ϵ for the BDI model with real valued interchain couplings $\alpha = 0.8$ with 75 unit cells per chain.

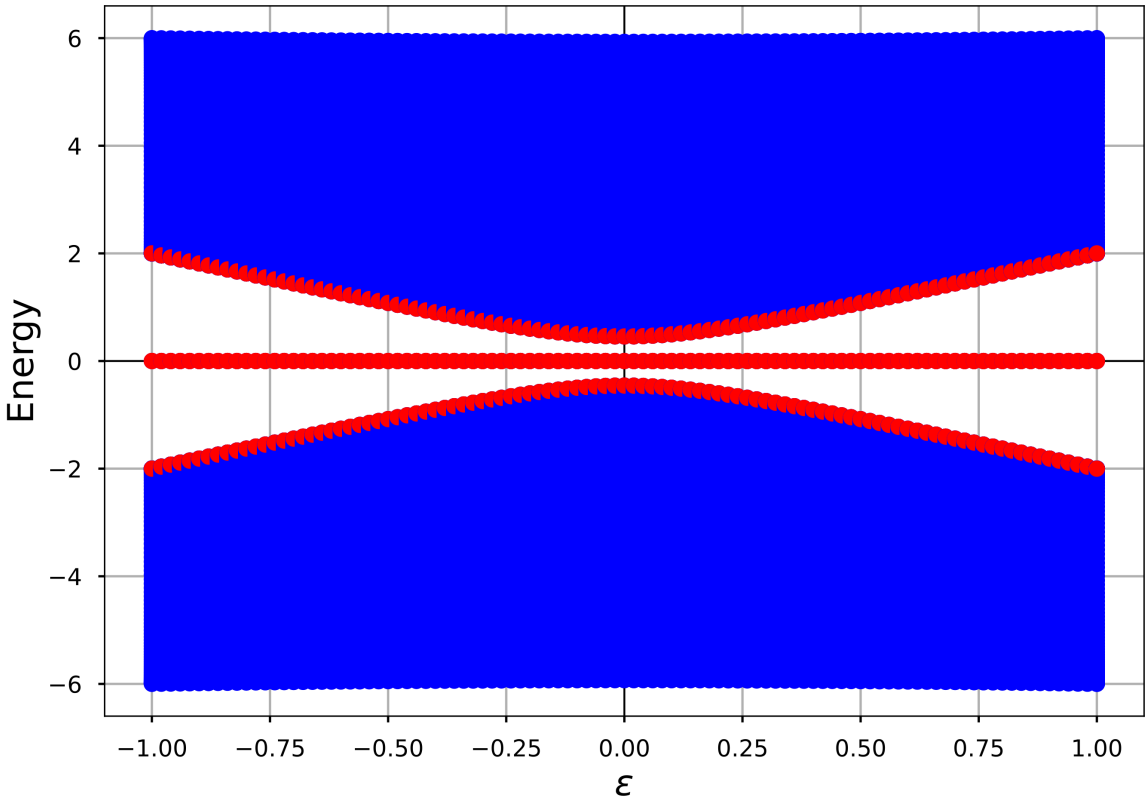

Fig. 5.4 Energy eigenvalue spectrum as a function of dimer parameter ϵ for the BDI model with real valued interchain couplings $\alpha = 2.0$ with 75 unit cells per chain.

shifting the phase transition point. At this interchain coupling strength, the 4-fold degeneracy is lifted to just a double degeneracy at zero energy throughout the spectrum. These results sufficiently demonstrate the strong interchain coupling regime forces a phase transition which may or not be topological. The basis for calculating the combined winding number is no longer valid. We have presented these results for completeness and clarity but will refrain in the remaining classes as they would return the same physics.

We note that the complex phase of v and w has little effect on the energy spectrum. The significant and defining factor, as we have definitively shown, is the relative strengths of these couplings.

AIII class model

Setting the interchain rung coupling to a complex value brings the model into the AIII class, we choose to $\theta = \pi/4$. The dispersion spectra, Fig. 5.5, indicates an insulator state as there is a gap separating the upper and lower bands. The upper bands and lower bands have degenerate points for $k = \pm\pi$. We will see that all of the dispersion spectra share this property,

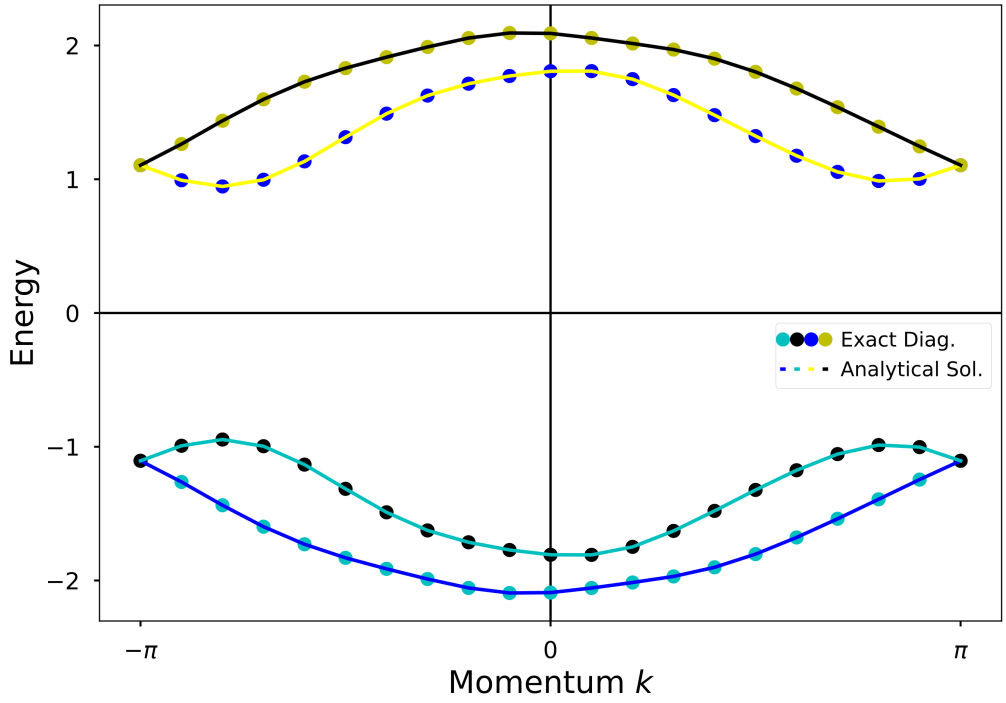

Fig. 5.5 Band structure for the AIII model with isotropic complex valued rung couplings $\alpha = 0.1$ with $v = 0.5$, $w = 1.5$. Deep in the topological phase $v < w$. Analytically calculated dispersion matches the numerical calculations.

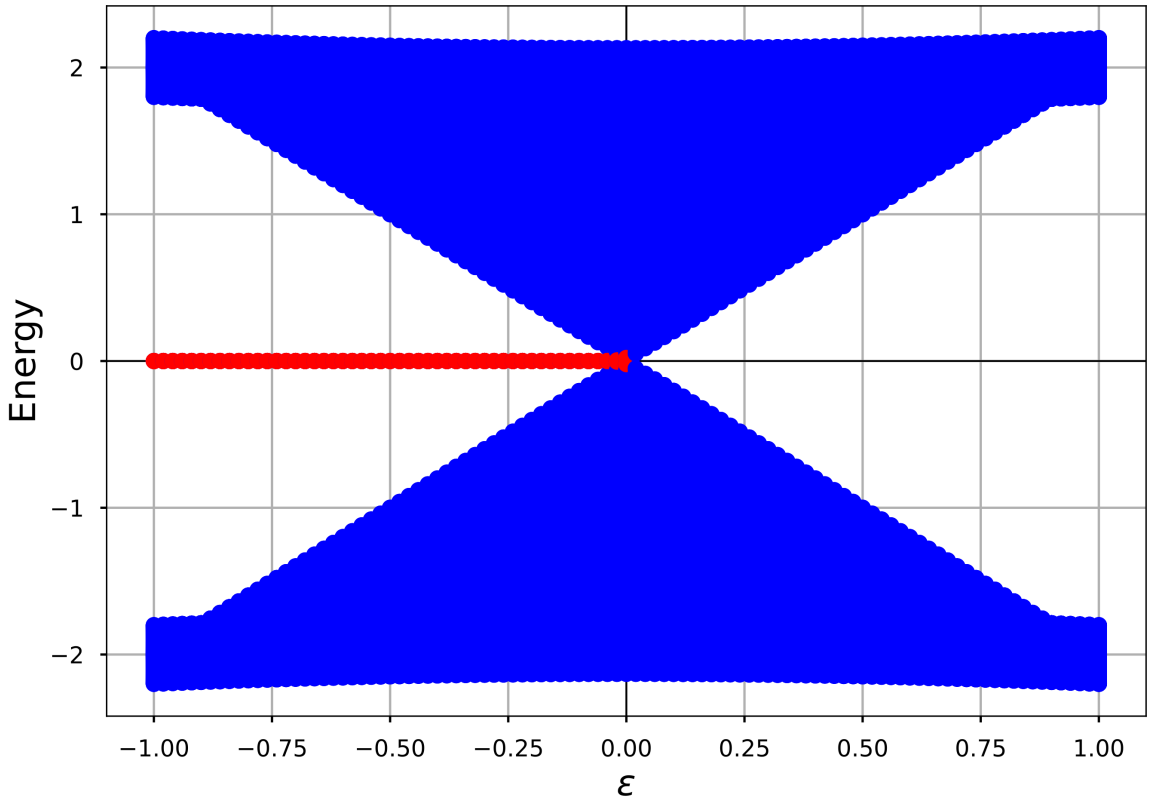

Fig. 5.6 Energy eigenvalue spectrum as a function of dimer parameter ϵ for the AIII model with complex valued interchain couplings $\alpha = 0.1 + 0.1j$ with 75 unit cells per chain.

The spectrum, Fig. 5.6, clearly shows the upper and lower energy bands separated by a gap and the phase transition point at $\epsilon = 0$. The trivial phase ($|v| > |w|$) is characterized by a full gap with no zero energy states in the gap. As the anistropy parameter ϵ becomes negative ($|v| < |w|$) the system undergoes a quantum phase transition to the topological phase, which is symmetry protected in this case. We will cover these topological characteristics in later sections. This same spectrum profile should appear the BDI and CII classed models.

CII class model

The dispersion plot for the specific CII model, Fig. 5.7, which has imaginary interchain couplings α, features multiple degeneracies at the high symmetry points $k = \{0, \pm\pi\}$ as a result of Kramers degeneracy. These characteristics are exactly as described in the generic CII model from section 4.2.3. The analytical calculations exactly match the numerical results from exact diagonalization. The degeneracies suggest that there is some nontrivial structure to the stationary states at these points.

The CII classed model shows similar results to the AIII and BDI classed models in the previous sections, with the only difference is the imaginary valued rung couplings. Just as in the BDI case zero energy states appear in the topological phase of $\epsilon < 0$ ($|v| < |w|$) and

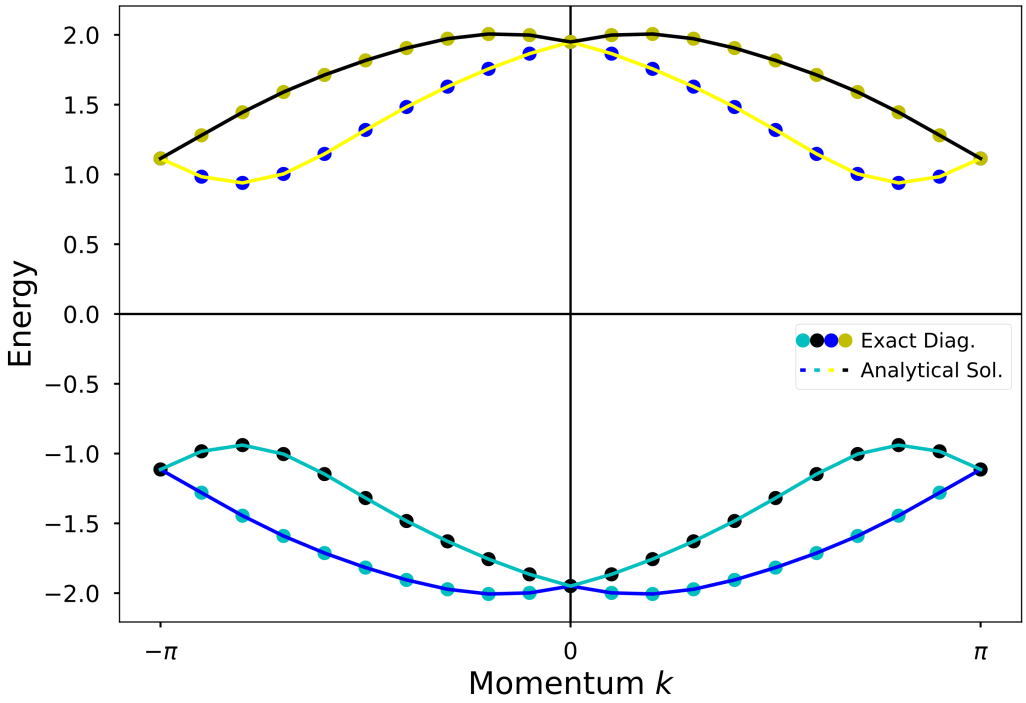

Fig. 5.7 Band structure for the CII model with isotropic imaginary valued rung couplings $\alpha = 0.1j$ with $v = 0.5$ and $w = 1.5$. Analytically calculated dispersion matches the numerical calculations.

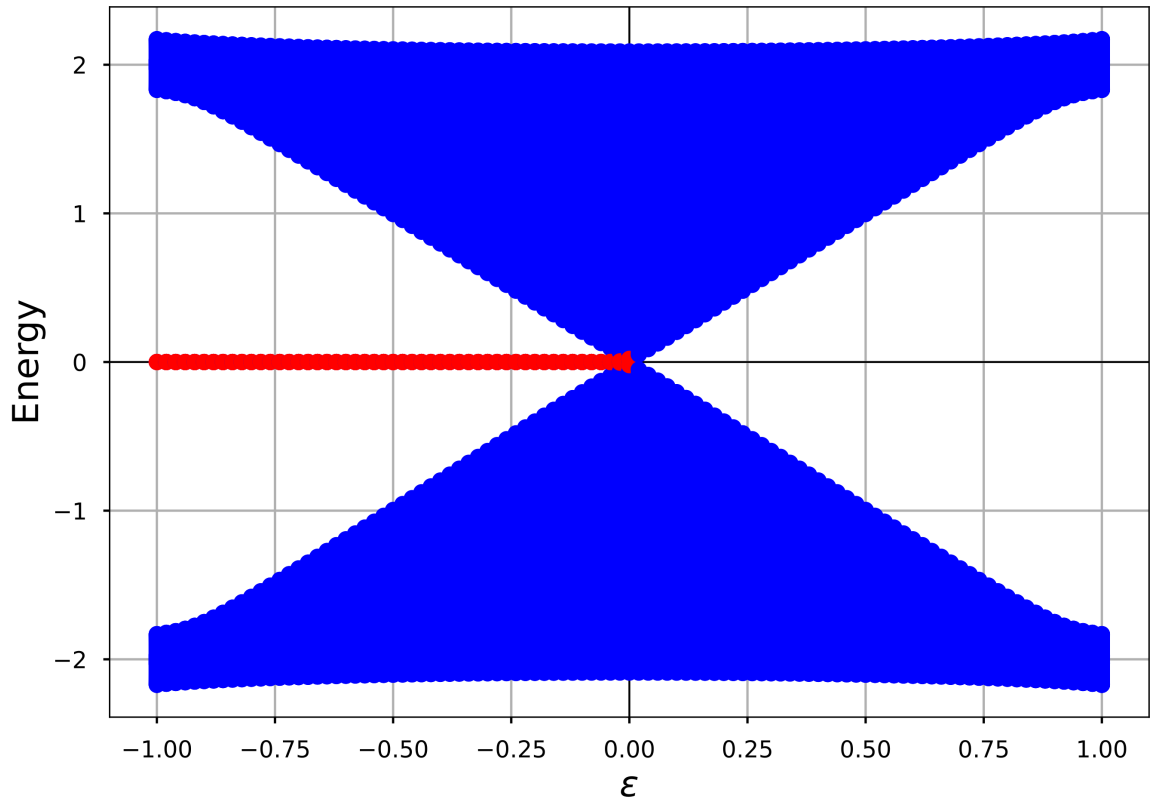

Fig. 5.8 Energy eigenvalue spectrum as a function of dimer parameter ϵ for the CII model with imaginary valued interchain couplings $\alpha = 0.1j$ with 75 unit cells per chain.

are 4-fold degenerate. As stated previously these four modes correspond to the four zero energy edge states present in the topological phase of the real space system. Due to Kramers degeneracy these states a two sets of paired eigenstates.

It is quite apparent that the energy eigenvalue spectrums for the AIII, BDI, and CII class models all look very similar. Given the similarity of these spectra we will show in a later section that these models are in essence topologically the same, to some degree it is possible to transition between these models without closing the gap, i.e. without a phase transition.

5.0.2 DIII and CI class models

In this section we will examine the energy and eigenvector spectrums for the BdG chiral classes DIII and CI which represent the C_2 form of the chiral operator, Fig 4.1(b).

For the DIII and CI models the chiral symmetry operator has the form $C_2 = S_z\sigma_z$ as shown in the previous sections, that couples $A-A$ and $B-B$. It is interesting to note that the simplest lattice configuration would be a regular square ladder however it is more useful to disregard (i.e. set to zero) this coupling and instead turn on the next-nearest neighbor interchain couplings. We label these couplings β, which are isotropic along the length of the ladder giving the Hamiltonian,

$$\hat{H}_2 = \hat{H}_0 + \hat{V}_2 \tag{5.6}$$

where the interchain coupling is given by,

$$\hat{V}_2 = \beta \sum_{n}^{n-1} (c^{\dagger}_{A,1,n} c_{A,2,n+1} + c^{\dagger}_{A,2,n} c_{A,1,n+1} + c^{\dagger}_{B,1,n} c_{B,2,n+1} + c^{\dagger}_{B,2,n} c_{B,1,n+1}) + h.c. \tag{5.7}$$

Note that $\hat{H}_2$ is not the most general Hamiltonian that could be written here and more symmetry compatible terms could be added.

If β is imaginary valued the Hamiltonian conforms to the T_- and P_+ symmetries making it DIII class. Conversely if β is real this complies with the CI class adhering to the T_+ and P_- symmetries. If β is any complex number the model is in the AIII class as shown previously. We refer the reader to the previous section on the AIII model for these results.

The momentum space transformation for this set of classes is given by,

$$\hat{H}_2(k) = \begin{pmatrix} 0 & x & a & 0 \\ x^* & 0 & 0 & b \\ a & 0 & 0 & y \\ 0 & b & y^* & 0 \end{pmatrix} \tag{5.8}$$

Where the equations for the abbreviations are the same as (5.4), with $a^* = a$ and $b^* = b$, and,

$$a = b = \beta e^{ik} + \beta^* e^{-ik} \tag{5.9}$$

This matrix is not easily rearranged into convenient blocks in the current basis. We will show that the properties of the band structures of our specific models are the same as those of the generic models in section 4.2.4, however the DIII model spectrum is quite different. The dispersion relation is identical to the general case, Eq. (4.26), where $\tau = \omega = a$.

DIII class model

From equation (5.8) we calculate and show the dispersion relation for our specific DIII model, Fig. 5.9. The dispersion shows degeneracies at $k = \{0, \pm\pi\}$. This is slightly inconsistent with the observations made in section 4.2.4. The spectrum shown here is similar to the CII case above with three degenerate points, which is expected since both classes have T_- time-reversal symmetry, i.e. Kramers pairing.

Similar to the previous models, the DIII classed model exhibits gapped bands in the trivial phase ($\epsilon > 0$) and zero energy modes in the topological sector ($\epsilon < 0$), Fig. 5.10. The fully gapped dispersion spectrum indicates an insulator state. As we will show later, CII has a winding number of 2 and DIII is always 0, which suggests again the band structure doesn't say much about the topological index of these models.

These zero energy modes can be gapped by adding a term that respects chiral symmetry but not time-reversal or particle hole symmetries. This fact suggests these modes are not protected by chiral symmetry, a fact we will prove in a later section. The previous models are robust against such chiral perturbations.

CI class model

We can make some interesting observations about the CI class model. A quick glance at a universality Class and Topology table, Table 2.1, in the lens of topological insulators would make one think that the CI class wouldn't host any edge states because it is not topological in 1D. We will find here that this is not the case. This particular model does in fact host edge states but they are not pinned to zero energy and are not robust against perturbations. One would think it was only able to host extended states, which turns out not to be the case.

The band spectrum for this model, Fig. 5.11, indicates fully gapped bands. Unlike all the previous models there are no degenerate points for the upper or lower subbands. This suggests that symmetric degenerate points are an indicator of some topological features in the model, as the previous models have.

The CI class which has the same lattice geometry, Fig. 4.1(b), as DIII however with real valued interchain rung couplings β. Figure 5.12 shows that energy spectrum of the model doesn't host states at zero energy. We know that CI is not topological in 1D so we cannot expect to see gapless states in what we have been referring to as the topological regime ($\epsilon < 0$).

There is still a zero energy point at the dimer limit $\epsilon = -1.0$. While there may be a zero energy state in this limit is it is the dimer limit, this state is not topologically protected and merely a consequence of the parameter sets. Looking at the spectrum we do see that the

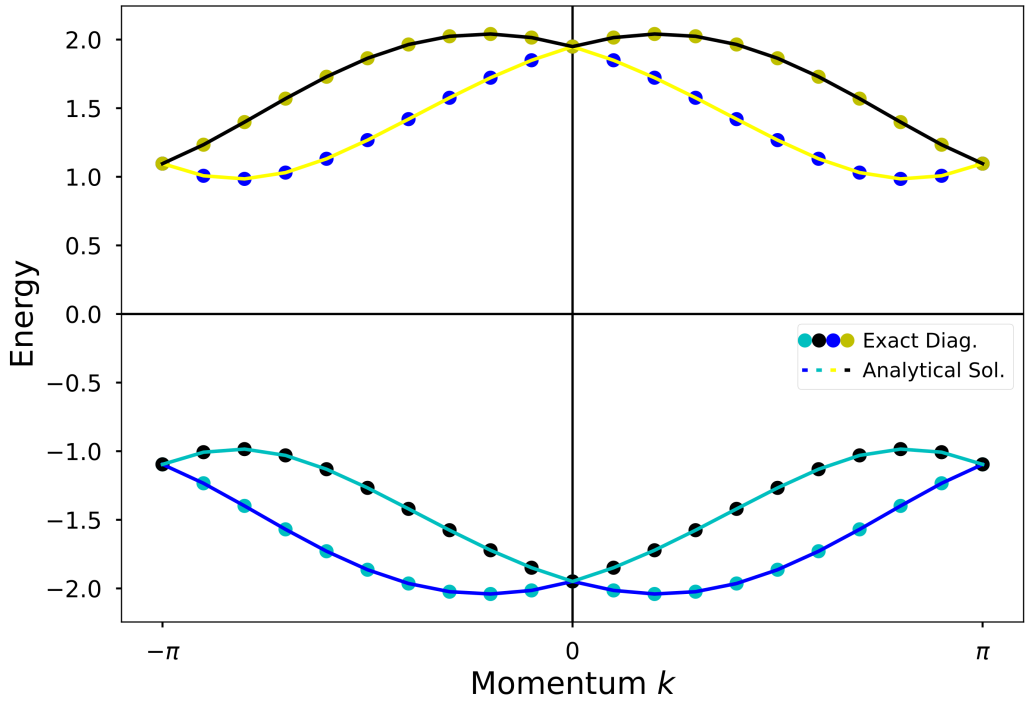

Fig. 5.9 Band structure for the DIII model with isotropic imaginary valued rung couplings $\beta = 0.1j$ with $v = 0.5$ and $w = 1.5$, i.e. the topological nontrivial phase. Analytically calculated dispersion matches the numerical calculations.

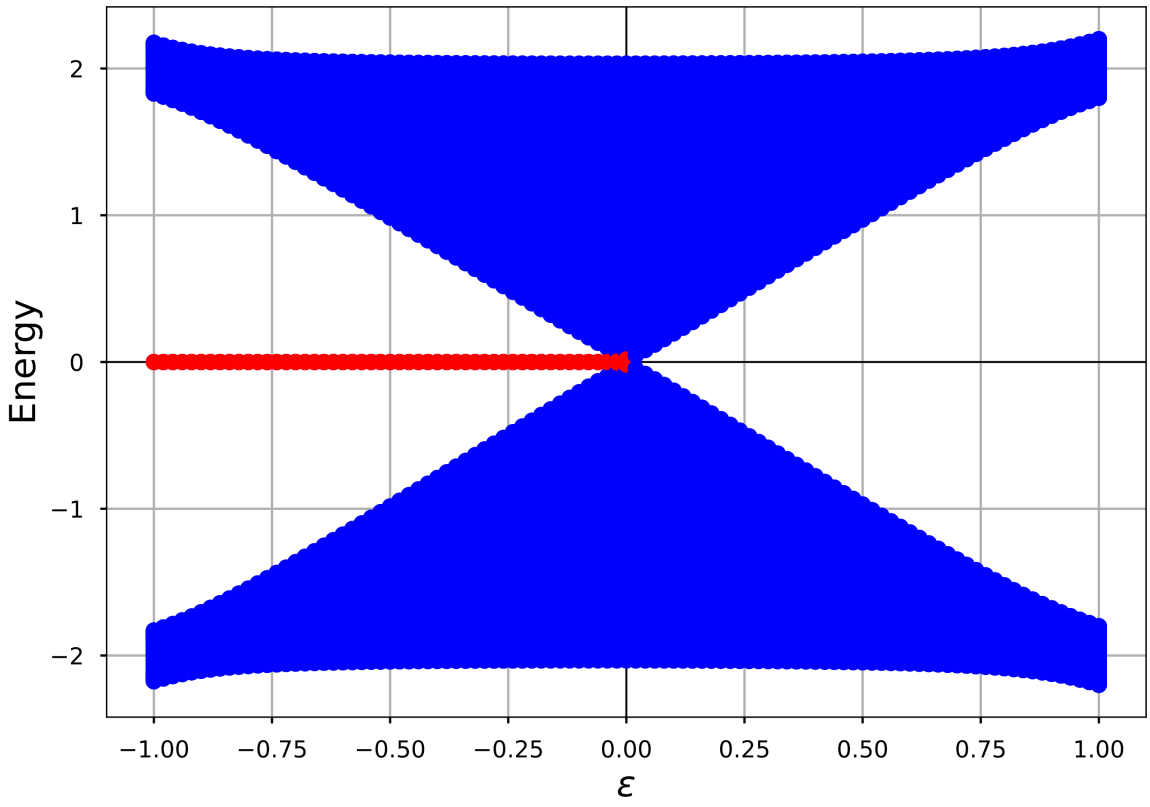

Fig. 5.10 Energy eigenvalue spectrum as a function of dimer parameter ϵ for the DIII model with imaginary valued interchain couplings $\beta = 0.1j$ with 75 unit cells per chain.

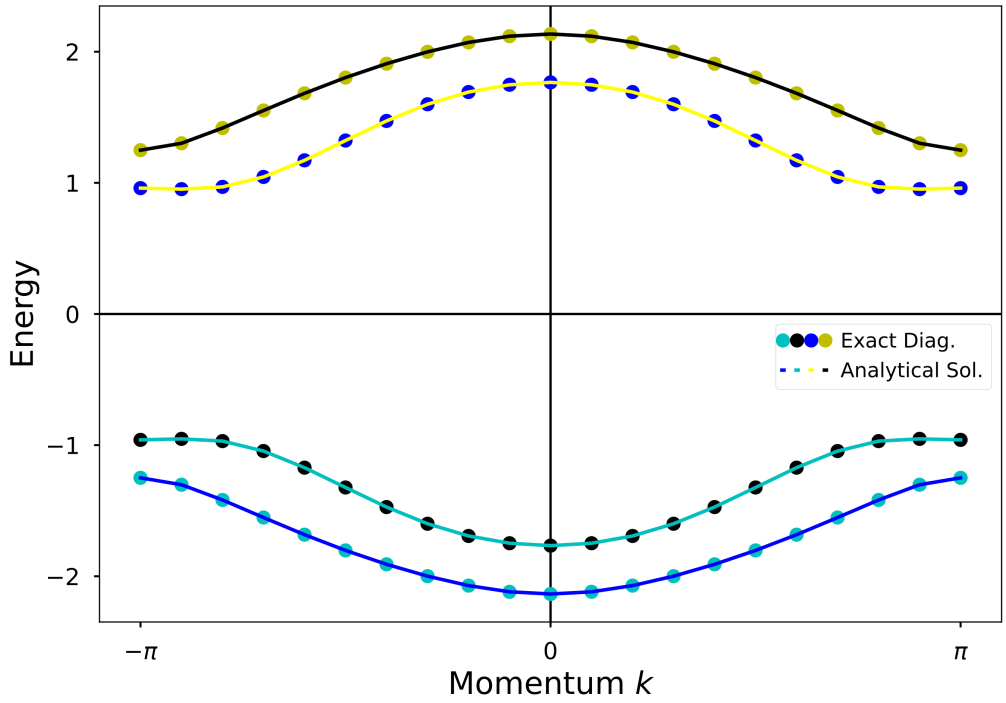

Fig. 5.11 Band structure for the CI model with imaginary valued interchain couplings $\beta = 0.1$ with $v = 0.5$ and $w = 1.5$.

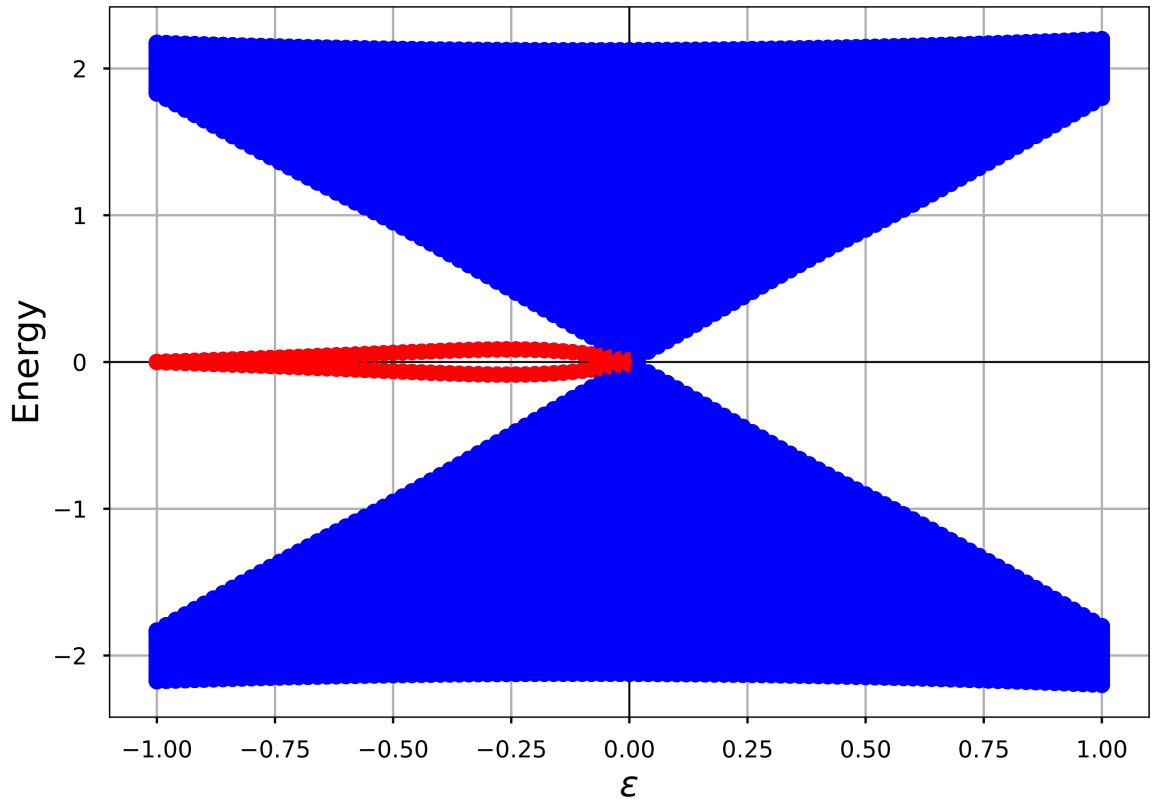

Fig. 5.12 Energy eigenvalue spectrum as a function of dimer parameter ϵ for the CI model with real valued interchain couplings $\beta = 0.1$ with 75 unit cells per chain.

states previously pinned to zero energy have now acquired a gap. Interestingly this gap is not consistent but changes, greater at some points and smaller at other values of ϵ.

5.1 Winding numbers revisited

In this section we will discuss the role of the winding number in the combined model. We consider the model in the topological phase when the interchain rung couplings are smaller than the gap. We can treat the topological properties of the combined model by considering the chains as separate such that the total winding number is the sum or difference of the individual chain indices, i.e. $\nu_{tot} = \nu_1 \pm \nu_2$.

We will examine how this is done for both possible cases, governed by the chiral operator descriptions C_1 and C_2.

5.1.1 BDI and CII class models

In this subsection we will consider the BDI and CII class models which are characterized by the chiral operator C_1 which couple $A-B$ sites between the chains, Fig. 4.1(a). These classes, along with AIII, have $\mathbb{Z}$ topology categories such that by adding chains the topological index increases.

In order to maintain the invariant properties of the individual chains the coupling between the chains α is small, compared to the difference between the chain couplings specifically $|v|-|w|$. If the rung coupling is too large it could close the gap, disrupting the insulator phase of the model possibly leading to conductive bulk states. Since α is small we can take the total winding number of the coupled system to be the sum of the individual (decoupled) chains, ie $\nu_{tot} = \nu_1 + \nu_2$. Since the chains can be considered as separate then the winding numbers can also be considered as such, from both a mathematical and physical stance. As we have shown in previous sections a decoupled chain can take the winding number of 0 for the topologically trivial phase or +1 for the topologically nontrivial phase, for this chiral operator case. The coupled system is characterized by the phases,

$$\nu_{tot} = \begin{cases} 2, & \text{if } |w/v| > 1 \\ 0, & \text{if } |w/v| < 1 \end{cases} \tag{5.10}$$

This result can be calculated directly from the winding number formula (3.5), and by reading off the matrix elements in the $\hat{h}(k)$ blocks in the momentum space Hamiltonians. It is also significant to note that this result is independent of the complex phase of the rung coupling α, and therefore the AIII, BDI, and CII models will have a winding number of 2 in the topological phase and an index of 0 in the trivial phase, see Figs. 5.13a, 5.13b, and 5.13c, respectively.

Equally as important is the implication that these gapped topological phases are equivalent across classes. We can show that one can take a smooth connected path through the complex phase space of $\alpha = |\alpha|e^{i\theta}$ from real α (BDI) at $\theta = 0$ to imaginary α at $\theta = \pi/2$ (CII) and complex (AIII) inbetween, and the state will remain topological along the whole path. The

zero energy edge modes will remain intact as well. We will demonstrate this graphically in the next chapter.

It is prudent to address a subtlety here about the CII class. The T_- symmetry leads to Kramers pairs for all states and this doubling causes the winding number to always be even, so the topological classification becomes $2\mathbb{Z}$ rather than $\mathbb{Z}$, as can be seen in the band structure. We can therefore say that any odd winding number can never be in the CII class and any model with an even winding number can be adiabatically deformed to the CII class without closing the gap.

5.1.2 DIII and CI class models

Turning to the second set of classes characterized by the chiral operator $C_2 = S_z\sigma_z$. In the natural basis like sites ($A-A$, $B-B$) are coupled across the chains and we do this in a next-nearest neighbor manner, Fig. 4.1(b).

When the interchain coupling $|\beta|$ is small, as shown in the previous section, we can define a total winding number as $\nu_{tot} = \nu_1 - \nu_2 = 0$ and can be calculated directly. In the DIII model, similar to the CII model, there is a present T_- symmetry resulting in Kramers pairs. Despite the winding number always being 0 owing from the different winding numbers on the top and bottom chains, we can actually define another invariant based on the parity of the winding number of one of the Kramers pairs [85]. The eigenstates of these weakly coupled chains are Kramers partners so a $\mathbb{Z}_2$ index can be determined by the winding number of one of the chains alone as follows,

$$p = (-1)^{\nu_{SSH}} \tag{5.11}$$

$$\nu_{SSH} = \begin{cases} 1, & \text{if } |w/v| > 1 \\ 0, & \text{if } |w/v| < 1 \end{cases} \tag{5.12}$$

The case with $p = -1$ hosts edge states and therefore can be considered a topological phase. The opposing case of $p = 1$ does not host edge states and is a trivial phase. The existence of the edge states is not protected by the chiral symmetry in the DIII model, which is in contrast to the chiral classes AIII, BDI, and CII. We will discuss this result further in a later section and simply note here that additional symmetries are necessary for this protection. An interesting property does appear that if the system is in the topological phase, tuning β can close the gap resulting in a phase transition to the trivial phase. However the opposite driving can not take the system from the trivial phase to the topological one. CI is not topological and therefore there is nothing to say or present about the properties of its topological invariant.

In the next chapter we will take the models we have built here and examine the wavefunction spectra for these zero energy modes. The wavefunctions will show the edge states indicative of topological insulator states, thus completing the picture of these nontrivial states in ladder models.

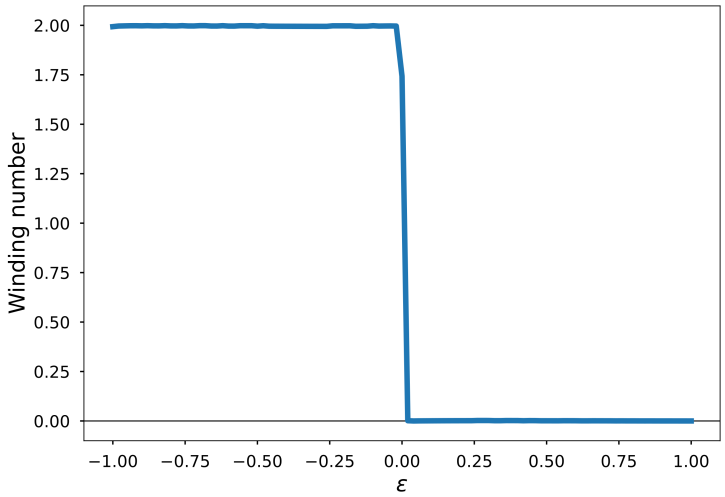

(a) Winding number as a function of the dimer parameter ϵ for the BDI combined ladder model with $\alpha = 0.1$. Winding number $\nu = 2$ for topological phase $\epsilon < 0$ and $\nu = 0$ for trivial phase $\epsilon > 0$.

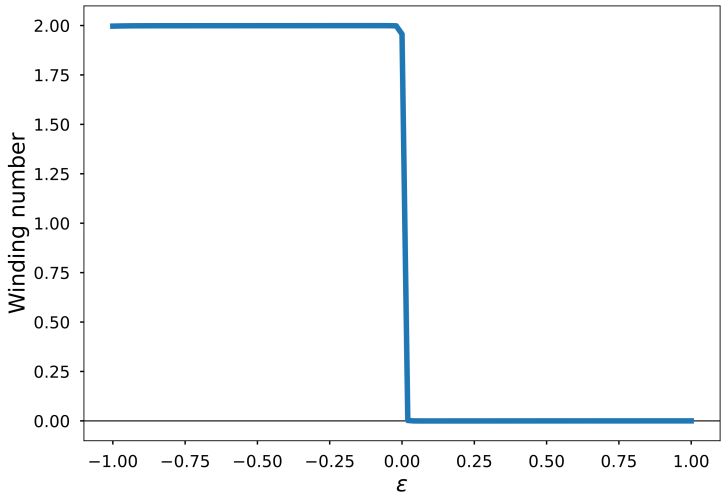

(b) Winding number as a function of the dimer parameter ϵ for the AIII combined ladder model with $\alpha = 0.1e^{i\pi/4}$. Winding number $\nu = 2$ for topological phase $\epsilon < 0$ and $\nu = 0$ for trivial phase $\epsilon > 0$.

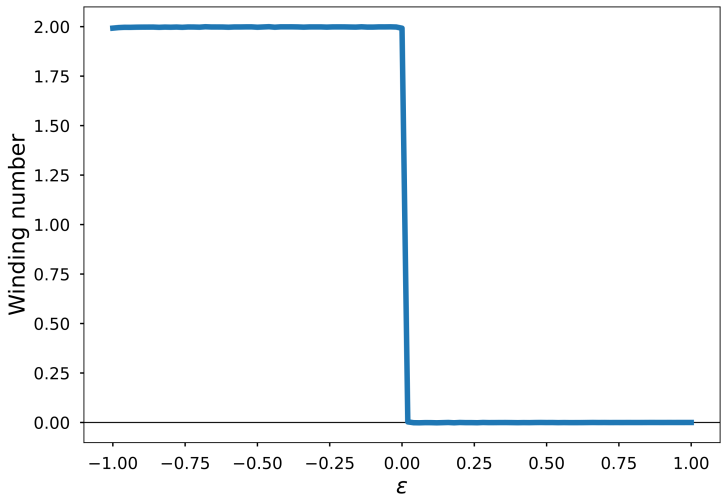

(c) Winding number as a function of the dimer parameter ϵ for the CII combined ladder model with $\alpha = 0.1j$. Winding number $\nu = 2$ for topological phase $\epsilon < 0$ and $\nu = 0$ for trivial phase $\epsilon > 0$.

Fig. 5.13 Winding numbers for chiral classes BDI (a), AIII (b), and CII (c).

Chapter 6

Edge states

In this chapter we will examine the zero energy edge states of the combined model and show the specific properties of the edge states, demonstrating the model symmetries are encoded in the properties of these states. It can also be shown that the edge states of the chiral classes (BDI, AIII, CII) can be connected along a continuous path without closing the gap. We will look at the numerical results and follow up with the analytical calculations, and discuss important general properties of these edge states as they pertain to our model. The literature typically only discusses these properties in reference to the SSH model, it is pertinent that we present and extend these considerations to our multi-chain models in a general way.

6.1 Edge states and their properties

We have shown our models in the classes AIII, BDI, and CII display zero energy modes and we will show that these correspond to exponentially localized edge states associated with the topological insulator phase. The BdG classes DIII and CI also host exponentially localized edge states however only the DIII class model has symmetry protected edge states. The edge states of the SSH model are localized on the A-sublattice on the left edge and B-sublattice on the right edge. We will show that this property continues to be true in the combined model. This fact is obvious for the C_1 cases where both end sites are A-sublattice on the left and B on the right. However the C_2 case is more subtle since the 'chiral' sublattice has A' and B' end sites on each edge.

6.1.1 BDI class models

In this section we present and examine the zero energy edge state wavefunctions of the BDI class model. We recall the BDI Hamiltonian Eq. (5.1) where the interchain coupling α is real and utilize exact diagonalization routines to calculate the eigenvalues and eigenvectors for an $N = 10$ size chain.

For clarity we select the four degenerate eigensets that corresponds to one of these zero energy states and plot the eigenvector wavefunctions as a function of the unit cell and sublattice. This tells us the coefficient probabilities associated with each sublattice (A and B).

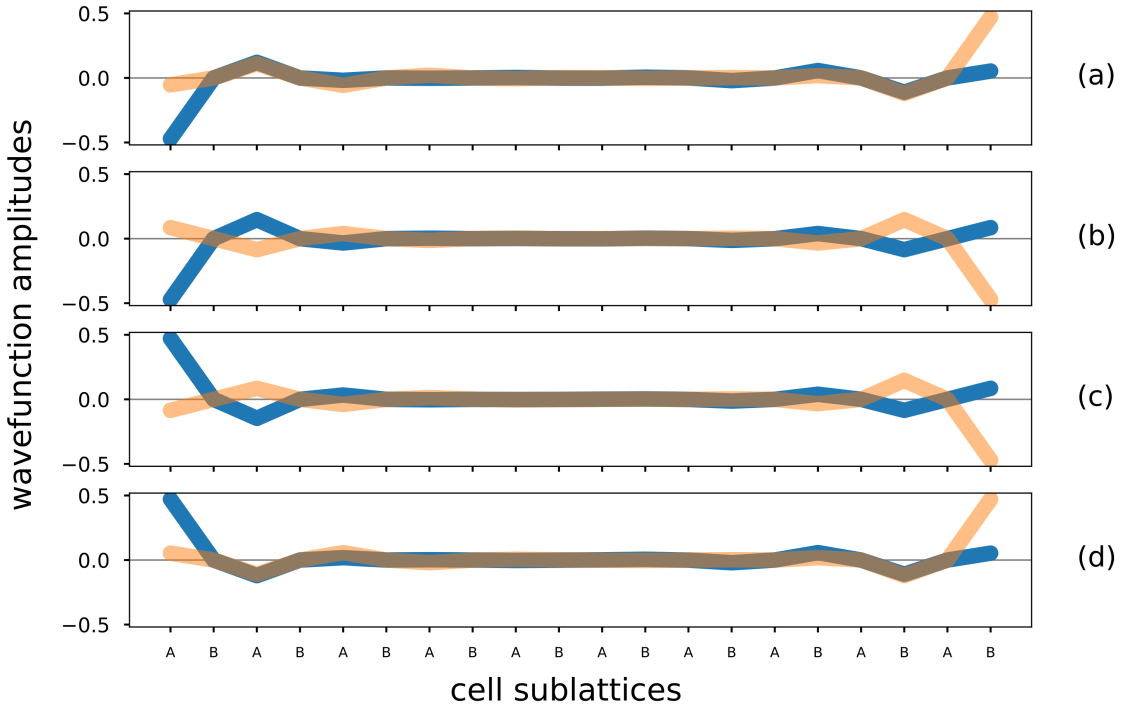

Fig. 6.1 Full eigenvector wavefunctions as a function of lattice site for BDI system for all four zero energy modes. Parameters are $v = 0.5$, $w = 1.5$, $\alpha = 0.1$, 10 cells are represented on this graph, with data for both the top (blue) and bottom (orange) legs.

The wavefunctions, Fig. 6.1, show clearly exponentially localized states at the edges of the system in all four states. We have chosen a parameter set slightly perturbed away from the dimer limit in order to demonstrate the full wavefunction decaying into the bulk. As stated previously, the Numpy routines return linear combinations of the eigenstates such that we see mixtures of several states in each wavefunction. An isolated edge state can be observed by taking linear combinations of these four states such that only a state on the end of one chain is present. However we find it more visually instructive to present the near dimerized chain limits to see the edges decay into the bulk, similar to the SSH model (Figs. 2.5(a),(b)). Along with the previous evidence of quantized winding number, zero energy modes, and these edge states we can conclude definitively this is a topological insulator phase.

The eigenvectors of a Hamiltonian matrix are orthogonal as long as their eigenvalues are distinct. However even if they are degenerate one can always find an orthogonal basis. In the case of our models the calculations done here are for a finite size system which experience finite size effects resulting in the eigenvalues not being exactly degenerate. The finite size of the system results in hybridization of the left and right edge states which lifts the degeneracies. The Numpy eigendecomposition routines give orthogonal eigenvectors

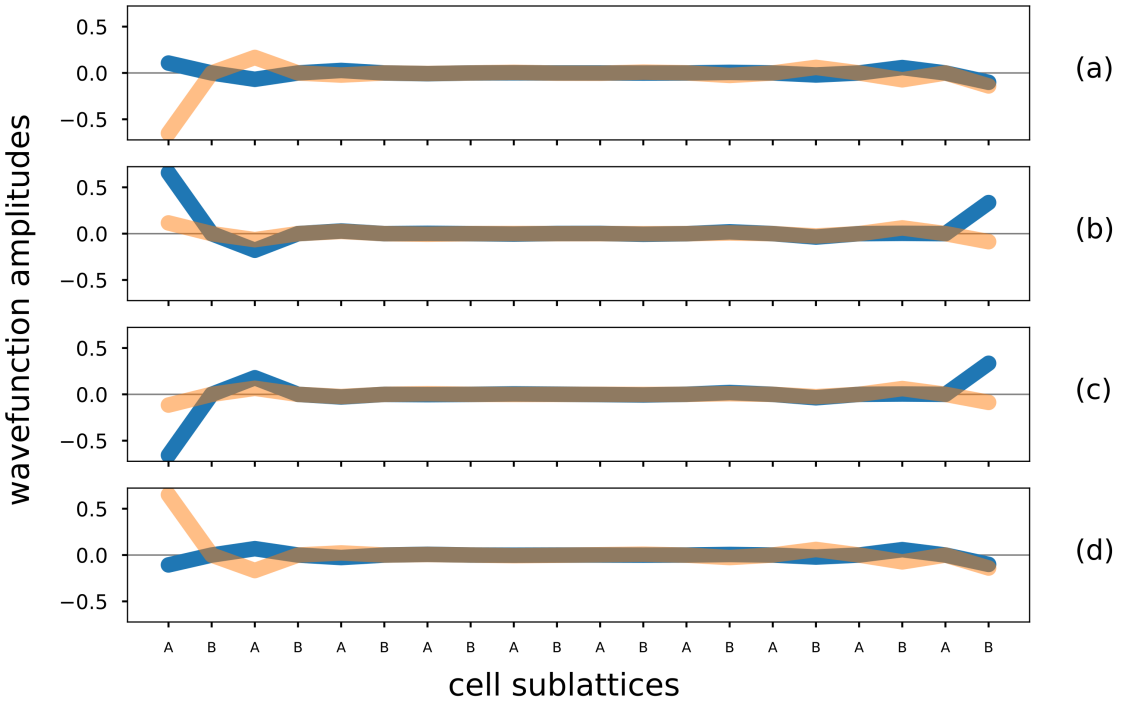

Fig. 6.2 Full eigenvector wavefunctions as a function of lattice site for CII system for all four zero energy modes. Parameters are $v = 0.5$, $w = 1.5$, $\alpha = 0.1j$, 10 cells are represented on this graph, with data for both the top (blue) and bottom (orange) chains.

anyway. One can find combinations of eigenvectors that aren't as well however one would typically not do such a thing. The wavefunctions presented are orthogonal to each other.

We note the system size (10 cells) is very small and thus the wavefunction suffers from finite size effects, notably hybridization of the edge states. While larger systems would be possible, using the correct numerical routines, we believe the characteristic details (exponentially decaying edge states) would be obscured in the larger size limit.

The wavefunction shows the transition between amplitudes hosted exclusively on the A-sublattices on the left edge and the B-sublattices hosted on the right edge. We use the same parameters for all of the eigenvalue wavefunctions and eigenvector wavefunctions for consistency but more importantly to do a comparative analysis of each chiral class. In the full chain dimer limit ($v = 0$), we would have near isolated ends on each chain.

6.1.2 CII class models

For this model class the edge states are clearly visible in the topological phase. The wavefunctions, Fig. 6.2, are remarkably similar to the BDI class model. It is easy to see the symmetric nature of the edge states in all cases, whether symmetric or antisymmetric combinations of the hybridized edge states, (a) and (d), (b) and (c). We see the transition

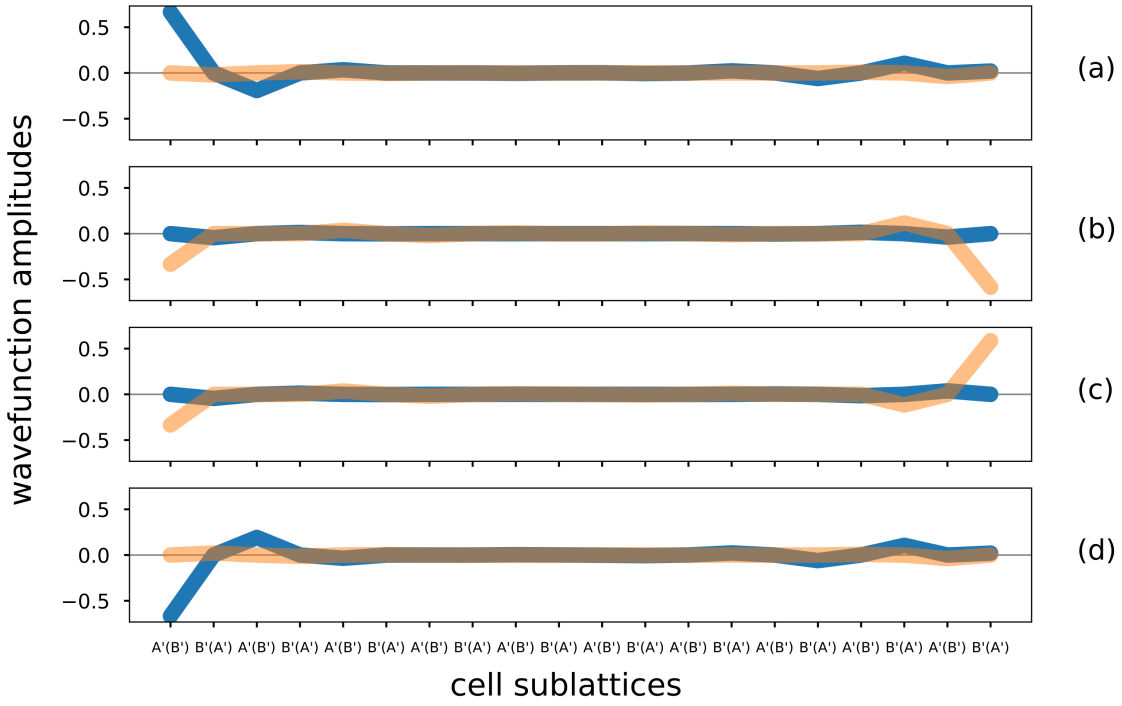

Fig. 6.3 Full eigenvector wavefunctions as a function of lattice site for DIII system for all four zero energy modes. Parameters are $v = 0.5$, $w = 1.5$, $\alpha = 0.1j$, 10 cells are represented on this graph, with data for both the top (blue) and bottom (orange) chains.

between the amplitudes present exclusively on the A-sites on the left edge and B-sites on the right edge. Unfortunately the time-reversal properties of the Kramers pairs doesn't appear in these plots because of how the Numpy routines calculate the eigensets, they are not pure eigenstates but linear combinations of left and right edge states due to hybridization, hence contributions on both chains.

6.1.3 DIII class models

Similar to the previous classes, the eigenvector wavefunctions, Figs. 6.3, shows states localized at the edges. The wavefunctions show symmetric and antisymmetric linear combinations from both edges, on both chains. The shift in amplitudes from the natural(chiral) sublattices $A(A',B')$ on the left edge to the $B(A',B')$ sublattices on the right edge is apparent.

Similar to the CII case the Kramers' pairs, although present are not visible in the wavefunctions due to the linear combinations of multiple eigenstates. The symmetry properties of the model do not come out in the spectra. The (a)-(d), (b)-(c) symmetric and antisymmetric state pairing is again present in these spectra.

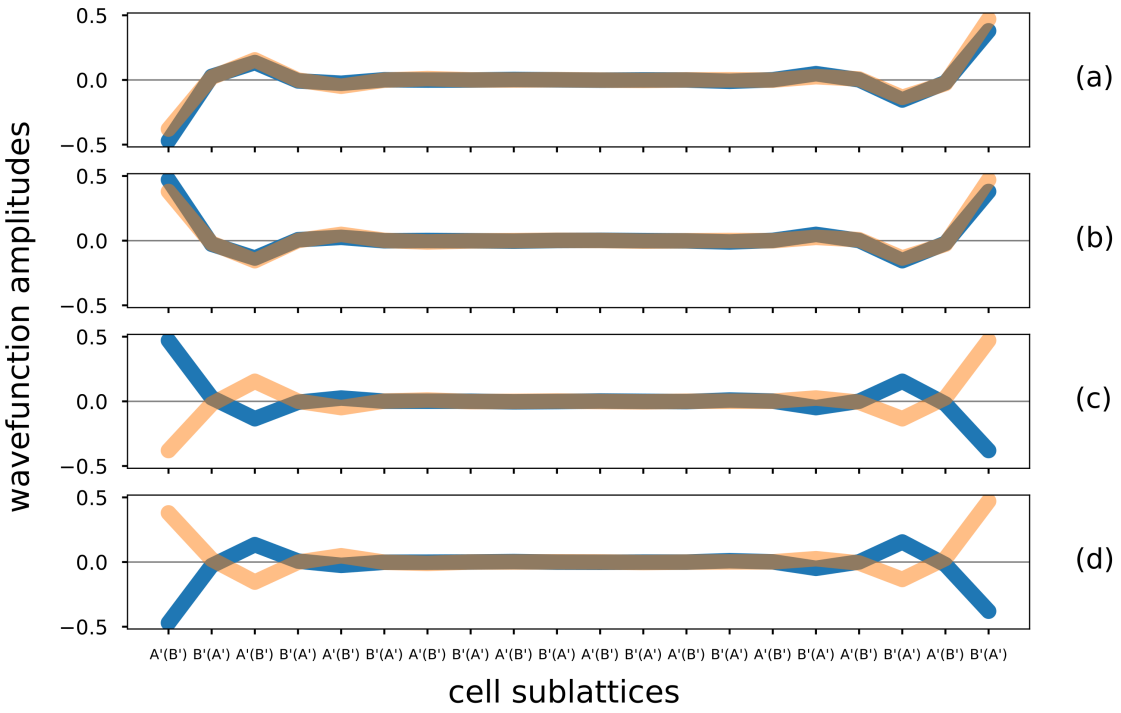

Fig. 6.4 Full eigenvector wavefunctions as a function of lattice site for CI system for all four zero energy modes. Parameters are $v = 0.5$, $w = 1.5$, $\alpha = 0.1$, 10 cells are represented on this graph, with data for both the top (blue) and bottom (orange) chains.

6.1.4 CI class models

Despite this class not being topological, exponentially localized edge states still arise in the 'topological' parameter regime, Fig. 6.4. However as we noted previously these states have no topological protection, they are merely a consequence of the parameters. Perturbing away from a purely real interchain coupling will destroy this state. We see the symmetric and antisymmetric pairing of states, (a) and (b), (c) and (d). The similarity of these spectra to the previous classes lends evidence to the fact the symmetry properties of the edge states cannot be seen in the spectra of the states.

6.1.5 Edge state calculation for AIII, BDI, and CII class models

In this subsection we will perform an analytical derivation to calculate the edge states in order to demonstrate the symmetry properties of these states and draw conclusions about the nature of these states. We will consider the chiral classes defined by the chiral symmetry operator $C_1 = S_z\sigma_0$, the chains are coupled in the BDI and CII configuration, Fig. 4.1(a). We will show that for this model the left edge states are localized on the A-sublattices (i.e. the amplitude is zero on the B-sublattices). We will also show that one can smoothly deform

through all three classes (AIII, BDI, CII) without closing the gap and the zero energy edge states will remain intact.

The minimal lattice model can be described by a Hamiltonian giving the chain components $\hat{H}_0$ and a Hamiltonian giving the rung components $\hat{V}_1$. Together this gives,

$$\hat{H}_1 = \hat{H}_0 + \hat{V}_1 \tag{6.1}$$

where $\hat{H}_0$ represents the chain terms and is given by,

$$\hat{H}_0 = \sum_{n\eta}^{N-1} (v c^\dagger_{An\eta} c_{Bn\eta} + w c^\dagger_{Bn\eta} c_{An+1\eta}) + h.c. \tag{6.2}$$

where $\eta = 1,2$ denotes the top and bottom chains, respectively, and n is the cell index. The intra- and intercell couplings along the chains v and w are generically complex. The general AIII Hamiltonian is written as,

$$\begin{aligned} \hat{V}_1 &= \sum_{n}^{N-1} c^\dagger_{An} [\vec{\alpha}\cdot\vec{\sigma}] c_{Bn} + c^\dagger_{Bn} [\vec{\omega}\cdot\vec{\sigma}] c_{A(n+1)} + h.c. \\ \vec{\alpha} &= \{\alpha_x, \alpha_y, 0\}, \quad \vec{\omega} = \{\omega_x, \omega_y, 0\} \end{aligned} \tag{6.3}$$

where $\vec{\alpha}$ represents the rung couplings and $\vec{\sigma}$ is the set of Pauli matrices. These act in the chain basis. Setting α couplings to be real gives the BDI topological class and imaginary couplings corresponds to the CII class.

The minimal model, Eq. (6.3), we are interested in can be obtained by setting $\alpha_x = \omega_x = \alpha$, $\alpha_y = \omega_y = 0$. In this case the interchain terms are given by,

$$\hat{V}_1 = \alpha \sum_{n\eta}^{N-1} (c^\dagger_{An\eta} c_{Bn-\eta} + c^\dagger_{Bn\eta} c_{A(n+1)-\eta}) + h.c. \tag{6.4}$$

where the strength of this interchain coupling is given by α and is uniform along the length of the ladder. As we have defined previously, when α is real this Hamiltonian is symmetric under T_+ and P_+ so it is in the BDI class. If α is purely imaginary it adheres to T_- and P_- the Hamiltonian is CII classed. For any case where α is complex the Hamiltonian only has chiral symmetry and is therefore AIII classed.

We derive the equations of motions, (see Appendix C for details), where the terms decouple nicely, as is expected, and can be handled separately. The equations of motion of these zero energy eigenstates are given by,

$$\begin{aligned} |nB1\rangle: &\quad a_{n1} v^* + a_{n+1,1} w + a_{n+1,2} \alpha + a_{n2} \alpha^* = 0 \\ |nB2\rangle: &\quad a_{n2} v + a_{n+1,2} w^* + a_{n+1,1} \alpha + a_{n1} \alpha^* = 0 \\ |nA1\rangle: &\quad b_{n1} v + b_{n-1,1} w^* + b_{n2} \alpha + b_{n-1,2} \alpha^* = 0 \\ |nA2\rangle: &\quad b_{n2} v^* + b_{n-1,2} w + b_{n1} \alpha + b_{n-1,1} \alpha^* = 0 \end{aligned} \tag{6.5}$$

To be concrete in this derivation we will consider only the left edge of a semi-infinite ladder. Determining the right edge would give an analogous calculation and conclusions. The general form of the wavefunction on a given site,

$$\psi_n = \sum_{n,i=1,2}^{N} \vartheta_i(-\lambda)^n \vec{u}_i \tag{6.6}$$

consists of the linear combination of the amplitudes on both chains. Here $\vartheta_{1,2} \in \mathbb{C}$ represent the prefactor of each component, λ is the eigenvalue of the recurrence matrix, Eq. (6.11), and $\vec{u}_i$ is the wavefunction component. The most general form would be a four component sum however as we have restricted the calculation to the left edge (two sites), the sum is only over two elements.

We will derive the eigenvalue and eigenvector components of the recurrence matrix to construct our analytical edge state wavefunction in the following paragraphs. For the left edge in the thermodynamic limit we expect states to be only on the A-sublattices such that all b_n coefficients should be 0 for all n. This gives us the boundary condition $b_0 = 0$. So we work with the $|nB,1\rangle$, $|nB,2\rangle$ sets. The A-site coefficients (a_n) need to decay into the bulk otherwise the state is unnormalizable. Here we will solve for only the A-site coefficients (i.e. amplitudes). The A-site coefficients should decay from the left edge to zero on the right edge. Equally the B-site amplitudes decay from the right edge to the left edge.

The solutions derived here, especially for the wavefunction of the A-sublattices, will have zero amplitudes for all B-sublattices since we are only solving for the A-sublattices using the assertion that in the thermodynamic limit all B-sublattices on the left side are 0. We could do this derivation for the B-sites for completeness but the wavefunction should be identical, just from the right edge.

The next steps are to solve the recurrence relation to gather the eigensets to build the wavefunctions. Collecting like cell terms and expressing as a matrix,

$$\begin{pmatrix} w & \alpha \\ \alpha & w^* \end{pmatrix} \begin{pmatrix} a_{n+1,1} \\ a_{n+1,2} \end{pmatrix} = -\begin{pmatrix} v^* & \alpha^* \\ \alpha^* & v \end{pmatrix} \begin{pmatrix} a_{n,1} \\ a_{n,2} \end{pmatrix} \tag{6.7}$$

Rearranging and simplifying, C represents the 2x2 matrix on the left side, D the same on the right side,

$$\vec{a}_{n+1} = -C^{-1} D \vec{a}_n \tag{6.8}$$

We can define the recurrence matrix T, by combining C and D matrices,

$$\vec{a}_{n+1} = -T\vec{a}_n \tag{6.9}$$

where,

$$T = \frac{1}{|w|^2 - \alpha^2} \begin{pmatrix} w^* v^* - |\alpha|^2 & w^*\alpha^* - \alpha v \\ w\alpha^* - v^*\alpha & wv - |\alpha|^2 \end{pmatrix} \tag{6.10}$$

Solving for the eigenvalues,

$$\lambda_{1,2} = \frac{-(2|\alpha|^2 - w^*v^* - wv) \pm i\sqrt{|\Omega|}}{2} \tag{6.11}$$

where Ω is defined,

$$\Omega = -4w^*v^*|\alpha|^2 - 4wv|\alpha|^2 + (w^*v^*)^2 + (wv)^2 - 2|w|^2|v|^2 + 4|w|^2\alpha^{*2} + 4|v|^2\alpha^2 \tag{6.12}$$

To be complete, we define the decay length and oscillating frequency of the edge state wavefunction by taking the real $Re(\delta)$ and imaginary $Im(\delta)$ parts, respectively, of the logarithm of the eigenvalue, $\delta = ln(\lambda_{1,2})$.

Additionally we make the assertion that $\lambda_1 = \lambda_2^*$ at the 'high symmetry points' (i.e. time-reversal symmetry points) where α is purely real or imaginary, such that the wavefunctions of these states carry symmetry properties. For this assertion to be true the sign of the square root term needs to change and as none of the terms under the square root change this is indicating that the sign of the square root must always be negative at the time-reversal symmetry points. The eigenvectors $\vec{u}_{1,2}$ of the transfer matrix are derived simply,

$$\vec{u}_{1,2} = \begin{pmatrix} 1 & \frac{wv - w^*v^* \pm \sqrt{|\Omega|}}{2(w^*\alpha^* - \alpha v)} \end{pmatrix} \tag{6.13}$$

Now that we have the necessary eigenvalues and eigenvectors we return to equation (6.6) and expand,

$$\psi_{A,n} = \begin{pmatrix} a_{n,1} \\ a_{n,2} \end{pmatrix} = \vartheta_1(-\lambda_1)^n\vec{u}_1 + \vartheta_2(-\lambda_2)^n\vec{u}_2 \tag{6.14}$$

These eigenvectors represent the edge states present on the left edge and as they are degenerate we can take any linear combination. However the choice of a symmetric and antisymmetric combination is useful to demonstrate the properties of the edge states.

In order to do that consider $\vartheta_1 = \pm\vartheta_2$ and have the following definitions,

$$\begin{aligned} \psi_+ &\Rightarrow \vartheta_1 = \vartheta_2 \\ \psi_- &\Rightarrow \vartheta_1 = -\vartheta_2 \end{aligned} \tag{6.15}$$

We refine the equation to a simpler notation where the sign prefactors have been incorporated into the eigenvalues (λ_i) and the eigenvectors $\vec{u}_{1,2}$ have the basis (A_1, A_2),

$$\vec{\Psi}_\pm = (\lambda_1)^n\vec{u}_1 \pm (\lambda_2)^n\vec{u}_2 \tag{6.16}$$

The edge states are normalizable if they decay (from the left in this case) into the bulk, i.e. $|\lambda_{1,2}| < 1$, which corresponds to the topological phase as demonstrated in the previous sections.

The symmetry properties of the model must be reflected in the properties of the edge states wave functions. We can demonstrate these properties analytically by studying how

they transform under the action of time-reversal symmetry. We propose the conjectures that for the BDI class, application of the time-reversal symmetry will transform the state back to itself, i.e. the wavefunctions is its own time-reversed partner. For the CII class, to comply with Kramers theorem, the state will transform to its counterpart with a ±1 prefactor. For some arbitrary state $\phi_\pm$,

$$BDI: \quad T_+\phi_\pm \propto \phi_\pm \quad T_+ = S_0\sigma_x K, \tag{6.17}$$

$$CII: \quad T_-\phi_\pm \propto \phi_\mp \quad T_- = iS_0\sigma_y K \tag{6.18}$$

From figure 6.1 we know these two edge states are degenerate one can take any linear combination, however our choice of $\Psi_\pm$ is useful to demonstrate the symmetry properties of these edge states.

So then if we have the state $\Psi = \begin{pmatrix} a \\ b \end{pmatrix}$,

$$T_+\Psi = \sigma_0 S_x K \begin{pmatrix} a \\ b \end{pmatrix} = \begin{pmatrix} b^* \\ a^* \end{pmatrix}, \quad T_-\Psi = i\sigma_0 S_y K \begin{pmatrix} a \\ b \end{pmatrix} = \begin{pmatrix} -b^* \\ a^* \end{pmatrix} \tag{6.19}$$

where σ_0 applies to the A, B-sublattice so nothing changes there. In the T_+ (BDI) case we would need $a = b^*$. In the T_- case then we need $a = -b$. Let us demonstrate these expressions explicitly using the eigenvectors $\vec{u}_{1,2}$,

$$T_+\vec{u}_1 = S_0\sigma_x K \begin{pmatrix} 1 \\ \frac{w^*v^* - wv + i\sqrt{|\Omega|}}{2(v^*a^* - wa)} \end{pmatrix} \tag{6.20}$$

$$= \begin{pmatrix} \frac{wv - w^*v^* - i\sqrt{|\Omega|}}{2(va - w^*a^*)} \\ 1 \end{pmatrix} = \vec{u}_2 \tag{6.21}$$

It is trivial to check that $T_+\phi_- = -\phi_-$. Thusly $T_+\phi_\pm = \pm\phi_\pm$ which is consistent with the aforementioned BDI conjectures. By acting with T_- on the eigenstates $\vec{u}_1$ and $\vec{u}_2$ we get,

$$T_-\vec{u}_1 = iS_0\sigma_y K \begin{pmatrix} 1 \\ \frac{w^*v^* - wv + i\sqrt{|\Omega|}}{2(v^*a^* - wa)} \end{pmatrix} \tag{6.22}$$

$$= \begin{pmatrix} \frac{wv - w^*v^* - i\sqrt{|\Omega|}}{2(va - w^*a^*)} \\ -1 \end{pmatrix} = -\vec{u}_2 \tag{6.23}$$

Thus our conjectures hold for the CII model since operating on one of the eigenstates gives a minus sign needed to transform ϕ_+ to ϕ_-. This follows from the fact that operating twice on the state should return the negative of the original state. Therefore the characteristic feature of the CII class model is that the edge states can be chosen to form a Kramers doublet. If the time-reversal symmetry is broken the eigenvectors are not related to each other by any symmetry transformation.

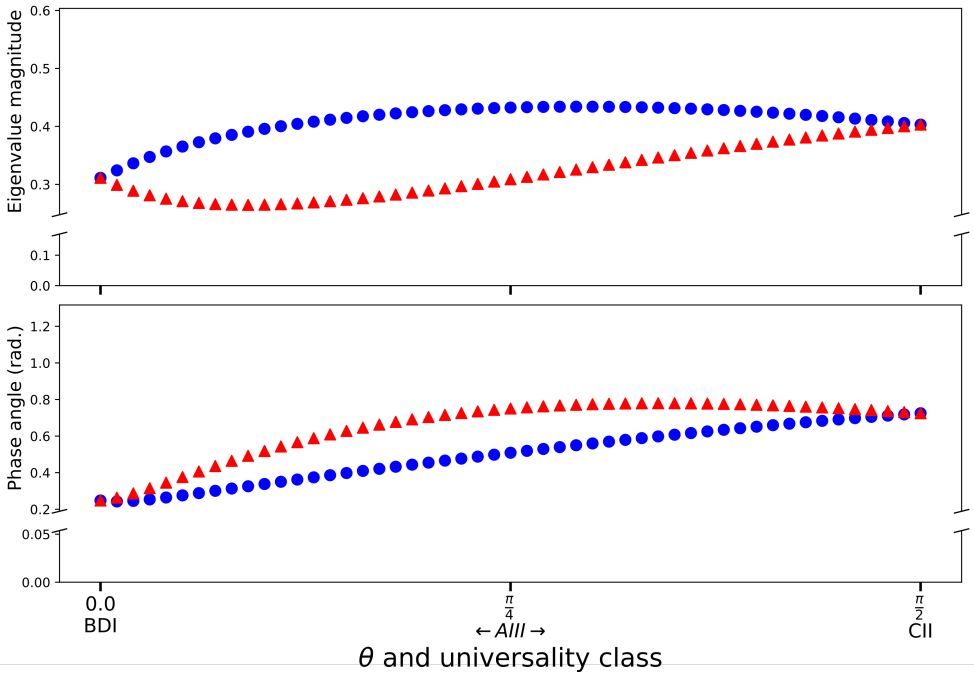

Fig. 6.5 Amplitude and absolute value of phase for the eigenvalues of transfer matrix λ_1 and λ_2 defined in equation (6.11) with $v = 0.2$, $w = 1.8$, and $\alpha = 0.1e^{i\theta}$. The phase θ of the interchain hopping parameterizes the path between two topological classes BDI and CII. Blue circles is λ_1 and red triangles is λ_2.

For generic complex α, which corresponds to the AIII universality class, there is no particular relationship between λ_1 and λ_2 - meaning the amplitude and the phase will be different. So there are two edge states with slightly different decay lengths and oscillation wavevectors. From here we can show that one can connect BDI and CII through AIII adiabatically via the eigenvalues of the transfer matrix, Fig. 6.5.

If one goes to one of the high symmetry points, i.e. α is real which is the BDI class or α is imaginary which corresponds to the CII class we see that $\lambda_1 = \lambda_2^*$. The relationship between the values of the λ_1 and λ_2 highlights the importance of time-reversal symmetry. For BDI each edge state is its own time-reversal partner,

$$T_+\phi_\pm = \pm\phi_\pm \tag{6.24}$$

For CII we see the inherent Kramers doublet,

$$T_-\phi_\pm = \pm\phi_\mp \tag{6.25}$$

The linear combination of these edge states is a general result that is valid for any complex α. One can take a continuous path from BDI to CII through AIII. The only change is the

properties of the edge states. The conclusion is that if the universality class has time-reversal symmetry, the edge will demonstrate this.

Strong rung coupling limit

Let us now briefly examine the strong interchain (rung) coupling limit. Increasing the strength of this coupling may close the gap which causes the system to undergo a phase transition to a different topological phase where the winding number may be different. In the BDI case, where α is real the gap closes when $a = \pm(|w| - |v|)/2$, i.e. when the coupling becomes of the order of the gap of the uncoupled chain. The winding number changes by 1 at this transition point, as was seen in the previous chapter, since one set of edge states is lost. When α is imaginary, the CII case, the winding number is only determined by the ratio $|v/w|$. So the strongly coupled physics matches that of the weakly coupled chains, i.e. $|v/w| < 1$ the winding number $\nu = 2$ and when $|v/w| > 1$ then $\nu = 0$.

6.1.6 Edge state calculation for DIII and CI class models

We will now turn to the second form of the chiral symmetry operator $C_2 = S_z\sigma_z$. This case gives couplings between A' and B'. The easiest lattice to make would be a standard ladder however we found it more useful to have next-nearest neighbor connections and consider the direct cell couplings between the chains to be zero, See Fig. 4.1(b).

A minimal model can be written,

$$\hat{H}_2 = \hat{H}_0 + \hat{V}_2 \tag{6.26}$$

where $\hat{H}_0$ is the Hamiltonian for the AIII chains given by equation (5.2) and $\hat{V}_2$ represents the rung couplings given by equation (5.7). We restate it in its general form here for clarity,

$$\begin{gathered}\hat{V}_2 = \sum_n^N c^\dagger_{A,n}[\beta_A \cdot \sigma]c_{A,n+1} + c^\dagger_{B,n}[\beta_B \cdot \sigma]c_{B,n+1} + c^\dagger_{A,n}[\delta_A \cdot \sigma]c_{A,n} + c^\dagger_{B,n}[\delta_B \dot{\sigma}]c_{B,n} + h.c. \\ \beta = \{\beta_{A/B,x}, \beta_{A/B,y}, 0\}, \quad \delta = \{\delta_{A/B,x}, \delta_{A/B,y}, 0\}\end{gathered} \tag{6.27}$$

We can obtain the minimal model, Eq. (6.27), by setting $\delta_{A/B} = 0$. The case of imaginary couplings in $\beta_{A/B}$ corresponds to the DIII class and real couplings gives a Hamiltonian in the CI class.

As stated previously, when the interchain coupling β is imaginary the model is symmetric under T_- and P_+ operators which leads to the DIII universality class; if β is real the model has T_+ and P_- symmetry and therefore falls in the CI class. If β is complex the model is in the AIII class, as shown in the previous sections. We clarify again here that this Hamiltonian is not the most general one could write, additional symmetrically compatible terms could be added. The existence of zero energy edge states of the DIII model are not protected by chiral symmetry and additional symmetries are needed, as will show in the following derivation. See [83] for a more rigorous and elegant calculation of this derivation. We will

find the recurrence relation and edge states using the same method as the previous section. From equation (6.26) and a general wavefunction ansatz we obtain the equations of motion, Eqs. (6.28), for the C_2 model types, i.e. DIII and CI class models. We leave the details of the derivation in Appendix C.

$$\begin{aligned}
|nA,1\rangle: &\quad b_{n,1}v + b_{n-1,1}w^* + a_{n+1,2}\beta + a_{n-1,2}\beta^* = \epsilon\,|nA,1\rangle \\
|nA,2\rangle: &\quad b_{n,2}v^* + b_{n-1,2}w + a_{n+1,1}\beta + a_{n-1,1}\beta^* = \epsilon\,|nA,2\rangle \\
|nB,1\rangle: &\quad a_{n,1}v^* + a_{n+1,1}w + b_{n+1,2}\beta + b_{n-1,2}\beta^* = \epsilon\,|nB,1\rangle \\
|nB,2\rangle: &\quad a_{n,2}v + a_{n+1,2}w^* + b_{n+1,1}\beta + b_{n-1,1}\beta^* = \epsilon\,|nB,2\rangle
\end{aligned} \tag{6.28}$$

Unlike the previous BDI/CII case, these equations do not decouple nicely if we focus on the natural A-B-sublattice and zero energy. However they decouple in the C_2 basis, i.e. in the chiral basis where $A \to A^{'}$, $B \to B^{'}$ on the top chain and on the bottom chain $A \to B^{'}$, $B \to A^{'}$, see Fig. 4.1b. We convert the prefactors in equations (6.28) accordingly and we come to a set of decoupled equations at zero energy,

$$\begin{aligned}
a'_{n,1}v^* + a'_{n+1,1}w + a'_{n+1,2}\beta + a'_{n-1,2}\beta^* = 0 \\
a'_{n,2}v^* + a'_{n-1,2}w + a'_{n+1,1}\beta + a'_{n-1,1}\beta^* = 0
\end{aligned} \tag{6.29}$$

$$\begin{aligned}
b'_{n,2}v + b'_{n+1,2}w^* + b'_{n+1,1}\beta + b'_{n-1,1}\beta^* = 0 \\
b'_{n,1}v + b'_{n-1,1}w^* + b'_{n+1,2}\beta + b'_{n-1,2}\beta^* = 0
\end{aligned} \tag{6.30}$$

If we think about the state vector on cell n being of the form $\Psi_n^T = \begin{pmatrix} a'_{n,1} & a'_{n,2} & b'_{n,1} & b'_{n,2} \end{pmatrix}$ and if we expect the solution to be in the form of plane waves then we can take the state at cell 0 and then apply an 'evolution' parameter that will give us the amplitude at any cell in the system.

Thus we can define the following ansatz,

$$\Psi_n = \Psi_0 e^{i\lambda n} \quad \Psi_n = \begin{pmatrix} a'_{n,1} \\ a'_{n,2} \\ b'_{n,1} \\ b'_{n,2} \end{pmatrix} \quad \Psi_0 = \begin{pmatrix} a'_{0,1} \\ a'_{0,2} \\ b'_{0,1} \\ b'_{0,2} \end{pmatrix} \tag{6.31}$$

where the exponential $e^{i\lambda n}$ is the decay factor and λ is the decay rate which is essentially the eigenvalues of the transfer matrix. If we break the vectors down further into the component sets we are interested in,

$$\Psi_n \to \Psi_n^{(1)} = \begin{pmatrix} a'_{n,1} \\ a'_{n,2} \end{pmatrix} \quad \Psi_n^{(2)} = \begin{pmatrix} b'_{n,2} \\ b'_{n,1} \end{pmatrix} \tag{6.32}$$

We can analyze two components of the edge state wavefunction rather than four as these properties will be mimiced in the other Ψ vector.

If we define $Z = e^{i\lambda}$ then we can propogate our equations as above. We take the first set of equations (6.29) and derive the recurrence relation,

$$\begin{pmatrix} (v^* + wZ) & (\beta Z + \beta^*/Z) \\ (\beta Z + \beta^*/Z) & (v^* + w/Z) \end{pmatrix} \begin{pmatrix} a'_{n,1} \\ a'_{n,2} \end{pmatrix} = \begin{pmatrix} 0 \\ 0 \end{pmatrix} \tag{6.33}$$

which we can write in the compact form,

$$M_1 \Psi^1 = 0 \tag{6.34}$$

Solving for the determinant with the condition $detM_1 = 0$ we can obtain the allowed values for Z,

$$v^{*2} + \frac{wv^*}{Z} + wv^*Z - (\beta Z)^2 - 2|\beta|^2 - \frac{\beta^{*2}}{Z^2} = 0 \tag{6.35}$$

With some working the values for Z are,

$$Z_{1,2,\pm} = \frac{-x_{1,2} \pm \sqrt{x_{1,2}^2 - 4}}{2} \tag{6.36}$$

where,

$$\begin{aligned} x_1 &= \frac{wv^* + \sqrt{(wv^*)^2 + 4(v^*\beta)^2 - 8|\beta|^2\beta^2 + 4(w\beta)^2 + 8\beta^2}}{2\beta^2} \\ x_2 &= \frac{wv^* - \sqrt{(wv^*)^2 + 4(v^*\beta)^2 - 8|\beta|^2\beta^2 + 4(w\beta)^2 + 8\beta^2}}{2\beta^2} \end{aligned} \tag{6.37}$$

This gives four solutions for Z where these solutions have the relations $Z_{1+} = 1/Z_{1-}$ and $Z_{2+} = 1/Z_{2-}$.

Previously we found in the BDI, CII, and AIII class models that the a's and b's decoupled and the left edge only had solutions with the a's, or there were none. For DIII we'll find a set of solutions with a_1 and b_2 and another set for a_2 and b_1. The general solutions have nonzero elements everywhere - contributions on A- and B-sublattices on both chains but that can be decomposed into the two solutions localized on a_1/b_2 or a_2/b_1 sites. These two solutions will be time-reversed partners.

Using these definitions of Z we calculate the eigenvectors of the recurrence matrix (6.33),

$$\begin{pmatrix} a'_1 \\ a'_2 \end{pmatrix}_1 = \begin{pmatrix} 1 \\ \frac{-(v^* + wZ)}{\beta Z + \beta^*/Z} \end{pmatrix} \quad \begin{pmatrix} a'_1 \\ a'_2 \end{pmatrix}_2 = \begin{pmatrix} 1 \\ \frac{-(v^* + w/Z)}{\beta Z + \beta^*/Z} \end{pmatrix} \tag{6.38}$$

where the correct solutions for the left side will have $|Z| < 1$ which correspond to Z_{1+} and Z_{2+}. Thus the general solution for the left edge,

$$\Psi_n^L = c\Psi_0^{(1)} Z_1^n + d\Psi_0^{(2)} Z_2^n \tag{6.39}$$

is a linear combination of the eigenfunctions $\Psi_{1,2}$ and solutions for $Z_{1,2}$ where n is the cell index of a system with L cells. The full solution of equation (6.26) will include terms for the

right side (i.e. b' factors) and be four terms. We identify the relationship between c and d by looking at the left edge boundary condition $a_{-1,1} = b_{-1,2} = 0$,

$$\Psi^L_{-1} = c\Psi^{(1)}_0 Z_1^{-1} + d\Psi^{(2)}_0 Z_2^{-1} = 0 \tag{6.40}$$

Multiplying the vectors by Z_i will make the calculation easier down the line,

$$\Psi^i_0 = \begin{pmatrix} Z_i \\ A_i \end{pmatrix} \quad A_i = \frac{-(v^* + wZ_i)Z_i}{\beta Z_i + {}^{\beta^*}/_{Z_i}} \tag{6.41}$$

We declare that the prefactors c and d will absorb the vector normalization. For cell -1 there should be zero amplitude such that,

$$\begin{pmatrix} 0 \\ 0 \end{pmatrix} = c\Psi^1_0 Z_1^{-1} + d\Psi^2_0 Z_2^{-1} \tag{6.42}$$

Take the top components of Ψ,

$$\begin{aligned} 0 &= c(Z_1)Z_1^{-1} + d(Z_2)Z_2^{-1} \\ 0 &= c + d \quad d = -c \end{aligned} \tag{6.43}$$

Bottom components,

$$\begin{aligned} 0 &= c(A_1)Z_1^{-1} + d(A_2)Z_2^{-1} \\ 0 &= c((A_1)Z_1^{-1} - (A_2)Z_2^{-1}) \end{aligned} \tag{6.44}$$

For this to be true then either $c = 0$ (no solution) or the parenthesed term is 0 (in the topological phase, non-zero in the trivial phase). This would mean that $A_1 = A_2$. Or more precisely,

$$\frac{-(v^* + wZ_1)}{\beta Z_1 + {}^{\beta^*}/_{Z_1}} = \frac{-(v^* + {}^{w}/_{Z_2})}{\beta Z_2 + {}^{\beta^*}/_{Z_2}} \tag{6.45}$$

This equality holds true for the topological phase ($|v| < |w|$) but breaks in the trivial phase ($|w| < |v|$), as predicted. This gives the final left edge wavefunction of,

$$\Psi_n = c(\Psi^1_0 Z_1^n - \Psi^2_0 Z_2^n) \tag{6.46}$$

Then we have the general equation for the left edge,

$$\Psi_n = c(\Psi^1_0 Z_1^n - \Psi^2_0 Z_2^n) \tag{6.47}$$

The full general solution is,

$$\Psi_n = \gamma_1 \Psi^1_0 Z_1^n - \gamma_2 \Psi^2_0 Z_2^n + \gamma_3 \Psi^3_0 Z_3^n - \gamma_4 \Psi^4_0 Z_4^n \tag{6.48}$$

where the eigenvectors are,

$$\Psi^{(1,2)} = \begin{pmatrix} 1 \\ X_A \\ 0 \\ 0 \end{pmatrix}, \quad \Psi^{(3,4)} = \begin{pmatrix} 0 \\ 0 \\ 1 \\ X_B \end{pmatrix} \tag{6.49}$$

The components $X_{A,B}$ are given by,

$$X_A = -\frac{-\beta Z_i + \beta^*/Z_i}{v^* + wZ_i} \tag{6.50}$$

$$X_B = -\frac{-\beta Z_i + \beta^*/Z_i}{v + w^* Z_i} \tag{6.51}$$

The coefficients γ_i are chosen is such a way the wavefunction goes to 0 at the boundary, i.e. $\Psi_{n=0} = 0$. These boundary conditions are satisfied for $\gamma_1 = -\gamma_2$ and $\gamma_3 = -\gamma_4$. These relations imply $X_A(Z_1) = X_A(Z_2)$ and $X_B(Z_3) = X_B(Z_4)$. One can check the time-reversal conditions these states must obey for the above relations to be true. If time-reversal symmetry is broken the boundary conditions can not be satisfied. We can also show the Kramers pairs of these edge states by noticing $T_-\Psi_1 = \Psi_3$ and $T_-\Psi_3 = -\Psi_1$. Equally, $T_-\Psi_2 = \Psi_4$ and $T_-\Psi_4 = -\Psi_2$.

This gives the general equation for a Kramers pair of states on the left edge,

$$\Psi_\pm = (\Psi_0^1 Z_1^n - \Psi_0^2 Z_2^n) \pm (\Psi_0^3 Z_3^n - \Psi_0^4 Z_4^n) \tag{6.52}$$

Strong rung coupling limit

When the interchain coupling tends to the strong coupling limit, i.e. the order of the gap, the gap between the bands may close. When the system is in the topological phase $|v| < |w|$, increasing the interchain coupling β one can drive the system to the nontopological trivial phase. The reverse process doesn't drive the trivial phase to the topological one, i.e. the gap doesn't close by tuning β.

Here we would like to make some crucial comments about the edge states of the DIII model as compared to the AIII, BDI, and CII models detailed in the previous section. One important detail is that the zero energy edge states of the DIII model are not protected solely by chiral symmetry, other symmetries are needed. This is in contrast to the AIII,BDI, and CII models. We will discuss this further in a later section.

In the basis $(A_1^{'}\ A_2^{'})$ one of the edge states can be written in the general form,

$$\phi_\pm(n) = \lambda_1^n \phi_{0,1} - \lambda_2^n \phi_{0,2} \tag{6.53}$$

where $\lambda_{1,2} = e^{\delta_{1,2}}$ are complex eigenvalues with magnitudes less than 1, and $\phi_{0,1(2)}$ are the corresponding eigenvectors, where the first index denote the cell (0) and (1,2) are the eigenvectors of the recurrence matrix, see Appendix C. This edge state is defined and localized on the $A^{'}$ sublattice. The other edge state is the Kramers pair and is localized on the $B^{'}$ sublattice. Contrast this with the CII case in which both Kramers states are localized on the A-sublattice.

BDI	The edge states are time-reversal symmetric, i.e. the state returns itself when acted on by the time-reversal operator, there may be a ±1 phase factor to account for.
CII	Hosts Kramers pairs so one edge state transforms into its time-reversal partner.
AIII	While hosting zero energy edge states does not have any time-reversal properties
DIII	Will also have Kramers pairs but the sublattices change between the two states.
CI	Not topological

Table 6.1 Edge state wavefunction properties for each chiral universality class.

To be more concrete about this analysis if one perturbs slightly away from the DIII point in phase space, i.e. β becomes complex, there are no normalizable zero energy states satisfying the boundary conditions. In the previous case where the AIII model 'connected' the BDI and CII models the edge states remained intact via chiral symmetry, that doesn't seem to be the case with DIII and CI. The protected states require more symmetries than just chiral. It is possible to find solutions that exponentially decay into the bulk however they don't satisfy the boundary conditions of the chain without splitting a unit cell. While it is important to note the possibility of these states, we are not interested in them so we conclude this discussion here.

6.2 General properties of edge states in chiral models

Here we will consider the general properties of edge states in chiral symmetric models because they can be applied in a general manner. It is a very well known fact that the edge states in the topological phase of the SSH model are localized on the A sublattice at one end of the chain and on the B sublattice at the opposing end. This characteristic, as we will show, continues to be true in the combined C_1 type models (BDI, CII) which have nonzero winding numbers. However when considering the C_2 type models (DIII, CI) where the winding number is zero, the edge states are slightly different. Going by the 'natural' sublattice the left edge will host one state on the A'-sublattice and one on the B'-sublattice. Table 6.1 gives a summary of the properties of edge states of each universality class.

We analyze the symmetry properties of the edge states via projection operators. It is a property of chiral symmetric models in 1D that the edge state is localized on a single sublattice, which can be demonstrated by defining the chiral symmetry operator using sublattice projection operators (recall Eqs. (3.1)),

$$U_C = P_A - P_B \tag{6.54}$$

It is well known that the anticommutation properties of these projectors [69] will return the negative energy state when acting on an eigenstate of the Hamiltonian, this follows from

$U_C^{-1}H(k)U_C = -H(k)$. As such if this state is in the zero energy subspace (this includes the space of edge states) then the projection operation will remain in this subspace. From the structure of equation (6.54), acting on a left edge state must create another edge state on the left edge, similarly for the right edge. This is because if all the probability weight is on the A-sublattice edge then the projection will return the A-sublattice and get rid of the rest, so to speak. Therefore if all the weight is on an A-sublattice (left edge) going in then that's what is going to be come out after projection, i.e. another left edge.

Let's take a model with a single edge state, and such a state is an eigenstate of the U_C operator. This can only be true if $P_A|\phi\rangle = 0$ or $P_B|\phi\rangle = 0$. This indicates that this eigenstate must be localized on one of the sublattices. For the edge state to be fully localized on the edge site then the above must be true, otherwise the state is spread across the unit cell and wouldn't necessarily then be a zero energy edge state.

For models with more than one edge state per edge we can find linear combinations of these states that are eigenstates of U_C. This is possible because, as stated above, these states all exist within the same subspace. Thus using the same logic as above, each one must be localized on either the A- or B-sublattice.

It is necessary for completeness to show that the edge states protected by chiral symmetry are localized on the same sublattice. Let's consider two edge states $|\psi_1\rangle$ and $|\psi_2\rangle$ (on the same edge) which are both eigenstates of the chiral symmetry operator such that,

$$C|\psi_{1,2}\rangle = \alpha_{1,2}|\psi_{1,2}\rangle \tag{6.55}$$

where $\alpha_{1,2}$ are the eigenvalues with value ± 1 because $U_C^2 = 1$. We can add a perturbation that preserves chiral symmetry $\{V, C\} = VC + CV = 0$ and acts within the same subspace as the eigenstates. We then have the matrix elements $\langle\psi_1|V|\psi_2\rangle = \alpha_1\alpha_2\langle\psi_1|C^\dagger VC|\psi_2\rangle = -\alpha_1\alpha_2\langle\psi_1|V|\psi_2\rangle$. The matrix elements vanish if the edge states are the eigenstates of the chiral operator with the same eigenvalue. Therefore, if the states are topologically protected they must be localized on the same sublattice. The topological protection arises because even when a (symmetry perserving) perturbation is added, like changing the edge of a sample, the phase remains the same.

This obviously won't be the case for DIII because the edge states are localized on different sublattices and therefore it can't be chiral symmetry alone that provides the topological protection. A weak perturbation that respects chiral but breaks time-reversal symmetry and particle-hole symmetry can hybridize the edge states, consistent with a zero winding number. The perturbation causes the zero energy modes to become gapped, i.e. they are not protected against a perturbation so not protected topologically.

In the single particle basis chiral symmetry is a unitary operator (no complex conjugate) while time-reversal symmetry and particle-hole symmetry are antiunitary operators (have complex conjugate terms). Particle-hole and chiral symmetries anticommute with the Hamiltonian. The difference between unitary and antiunitary shows up in the topology class if we focus on singular symmetry classes, for this case AIII (chiral symmetry only), D (P_+), and C (P_-). The D class is a $\mathbb{Z}_2$ topology while the C class is trivial.

Chiral symmetry alone topologically protects edge states only if they are on the same sublattice. Edge states on one edge localized on different sublattices (one on the A-sublattice, one on the B-sublattice) can not be protected by chiral symmetry alone, additional symmetries are needed. In the case of different sublattices a weak perturbation respecting chiral symmetry only can hybridize these edge states.

A system with P_+ symmetry alone protects a single zero-energy edge state. Similar to chiral symmetry, P_+ gives $P_+ |E\rangle \propto |-E\rangle$. So a zero energy edge mode remains pinned to zero energy as long as P_+ is intact. For two edge states, on the same edge, chiral symmetry will protect both states as long as they are on the same sublattice. The P_+ symmetry can't protect both, regardless of edge configuration. Additionally if there an odd number of edge states then P_+ alone will protect only one of those states. An even number of edge states (on one edge) will hybridize and not be protected. A chain, one edge state per end, with only P_+ symmetry will have protection with $\mathbb{Z}_2$ topology.

A system with only P_- can't topologically protect edge states. Using a similar argument to how Kramers pairs occur, then we can say for P_- the states come in pairs with energies, $|\pm E\rangle$. One can always write a perturbation that can hybridize these states, even at $E = 0$ so this symmetry alone can't topologically protect edge states.

With the DIII class model we can see what these symmetries look like when we put them together (P_+, T_-, C_2). The pair of edge states, localized on different sublattices, requires all symmetries to keep the states pinned to zero energy and unhybridized. Introducing a generic perturbation that is chiral symmetry only respecting (breaking time-reversal and particle-hole symmetries) will hybridize the edge states. The P_+ symmetry alone will only protect one of the two edge states. The T_- symmetry enforces the Kramers pairs with same energy and the P_+ symmetry enforces states to come in pairs with $\pm E$. The only way this can happen is with $E = 0$. (Obviously having both time-reversal and particle-hole symmetries gives chiral symmetry).

The symmetry properties we have outlined here for edge states are completely general and can be applied any 1D chiral symmetric models.

Chapter 7

Interacting SSH model at $\upsilon = 1/4$ filling

The previous chapters have dealt heavily with 4-band models, at integer filling (half-filling in the band picture), and their topological properties in the context of topological insulator states. We can extend this line of research by asking questions about the effects of density-density interactions and fractional fillings on similar models. These broad questions give rise to more specific ones about the characterization of the Zak phase [86], the mean-field effects, and nontrivial ground states. Work by Barbarino et al [34] demonstrated topological phases stabilized by interactions and reduced particle fraction in a BDI classed ladder model. We build on these results here by connecting it to the SSH model and by constructing a noninteracting version of this model via mean field theory.

The mean field theory leads nicely to the SSH4 model which we show has quantized Zak phases in a given parameter regime. In this chapter we will show that the model presented by Barbarino et al is easily rotated to an SSH-like chain and in doing so we construct a simple chain model to investigate the topological properties using mean field theory and Zak phase calculations. The ground state of this model is a $\mathbb{Z}_2$ classification for which the mean field effect causes a symmetry breaking, akin to that of the original conclusions of Su, Schrieffer, and Heeger on their model of polyacetylene. This paper investigates the physical properties of a symmetry breaking soliton (phonon) between two possible dimerization states of a linear chain. We use this model as motivation for replacing the soliton and investigating the topological phases that arise when nearest neighbor interactions are added to the linear chain model.

We will give a brief summary of the results that motivated this work then perform a unitary transformation of the Barbarino model to a chain which is very similar to the SSH model. The SSH model has not been studied at reduced filling fractions with interactions and we will present compelling results to this effect. Unlike the topological insulators previously studied, in this case we will be interested in the lowest energy states rather than the mid-gap zero energy ones connected to the edge modes.

The Barbarino model is similar to the SSH model in that it is a series of connected unit cells with two internal spin states, with an interaction term acting within the unit cells. In the single particle basis at integer filling this model is a 1D ladder in the BDI universality class that supports a topological phase. Typically interactions destabilize a topological

phase however they showed that at fractional fillings this one-dimensional model had stable topological phases. These states are described by density wave ground states, quantized Wilczek-Zee phases, and degenerate entanglement spectra. Interacting models do not have a comprehensive symmetry classification system like the universality classes such that in the interacting regime this model is no longer classified BDI.

If we consider the single particle Hamiltonian at integer filling the model has two gapped energy bands in the band spectrum in the topological insulator phase. In the band spectrum perspective, reducing the particle filling fraction only partially fills the lower band permitting conductive states to exist and the system is no longer in an insulating phase. Adding an interaction will gap this lower band into two subbands at some critical interaction strength, turning the system back to an insulator. This gap can be seen in the spin and charge sectors, and in this regime the model is basically the XXZ chain [87, 88] with two degenerate ground states. We can then think about it in terms of this, breaking the Néel ground state symmetry with some applied field. With only the lowest band filled this amounts to a $\upsilon = 1/4$ model and a four-site unit cell, where we can think about the cells being occupied or not. This symmetry broken state is characterized by a quantized Wilczek-Zee phase equal to 1. Additionally there is some unconventional edge physics, however unlike many other topological insulator states these are gapped and not hosted at zero energy.

From here we will rotate the Barbarino model to a more convenient chiral symmetric basis and describe how the interactions create a bond density ground state in this basis. Our goal in this chapter is then to show that these previously described topological effects arise as a result of mean field rather than strong correlation effects.

7.1 4-band models

Similar to the procedure in the previous sections we will begin with an SSH-like chain model, in this case with onsite potentials and density-density interactions. At a reduced filling fraction this becomes a 4-band model, which we now have experience dealing with. While interactions in topological insulators are still being researched we will apply a mean field theory to take this model to the noninteracting regime and show the inherent topological features.

These sections are motivated by the work of Barbarino et al so we start with the model presented there, Fig. 7.1, by bringing it into a more convenient chain form. The advantage of this form is we can utilize our understanding of the SSH model making this a more intuitive model to work with. This method amounts to reducing the integer filling to $\upsilon = 1/4$ such that the lower band is half-filled now, then projecting onto the lower band. A gap is opened in the bands via a density-density interaction, bringing the system to a 4-band model with interest only in the lowest band turning it back to an insulator.

We can show that in a certain regime this rotated single particle Hamiltonian is equivalent to the SSH model with longer range hoppings and an intracell interaction. The interaction acts as a symmetry breaking term so the logical thing to do is perform a mean field transformation

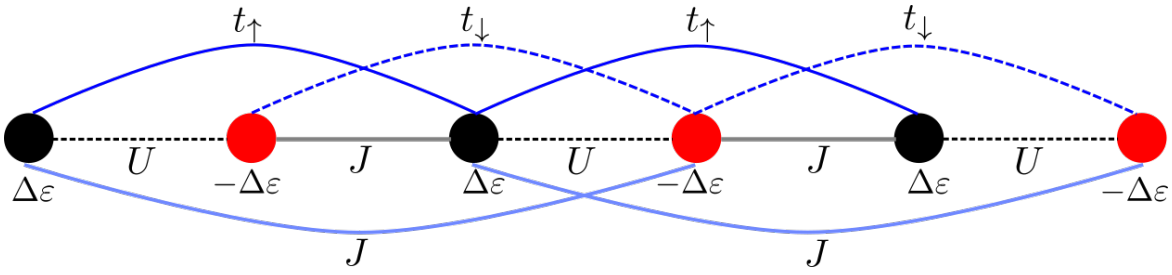

Fig. 7.1 Barbarino ladder model rearranged into chain form. The model has couplings $t_{\uparrow(\downarrow)}$ between like sites and J between different sites. The interaction U acts within the cell. There exists an alternating onsite potential $\pm\Delta\epsilon$.

to make it noninteracting. This mean field version of the chain is in essence the SSH model with an alternating 'field'.

7.1.1 Rotation to SSH-like basis

We begin by rotating the noninteracting terms in the Hamiltonian, Eq. (7.1), unitarily to a more convenient chain form, i.e. where the chiral operator is diagonal, forcing the Hamiltonian to be off-diagonal. We use the Pauli matrices to show the relations between the internal states of the unit cell ($\uparrow, \downarrow$) and institute our own coupling notation for consistency.

The model is described by kinetic (noninteracting), $\hat{H}_{kin}$, and interacting, $\hat{H}_{int}$, terms. Start with the single particle Hamiltonian,

$$\hat{H} = \hat{H}_{kin} + \hat{H}_{int} \tag{7.1}$$

where,

$$\hat{H}_{kin} = \Delta\epsilon \sum_j^N c_j^\dagger \sigma_z c_j + \sum_j^{N-1} c_j^\dagger (t_0\sigma_0 + \delta t\sigma_z + J\sigma_x)c_{j+1} + c_{j+1}^\dagger (t_0^*\sigma_0 + \delta t^*\sigma_z + J^*\sigma_x)c_j \tag{7.2a}$$

$$\hat{H}_{int} = U \sum_j^N n_{j\uparrow} n_{j\downarrow} \tag{7.2b}$$

where the sums are taken over each unit cell j and coupling t is parameterized to $t_0 \pm \delta t$. The kinetic Hamiltonian terms, Eq. (7.2a), account for the noninteracting coupling terms t, J, and $\delta\epsilon$. The interacting Hamiltonian, Eq. (7.2b), handles the intracell density-density interaction U. We will drop the interacting term and focus on the noninteracting kinetic terms since the SSH model is a noninteracting model. Transforming the kinetic Hamiltonian to momentum space using the standard Fourier operators, Eq. (2.6),

$$\hat{H}_{kin}(k) = \Delta\epsilon \sum_k^{BZ} c_k^\dagger \sigma_z c_k + \sum_k^{BZ} c_k^\dagger (t_0\sigma_0 + \delta t\sigma_z + J\sigma_x)c_k e^{-ik} + c_k^\dagger (t_0^*\sigma_0 + \delta t^*\sigma_z + J^*\sigma_x)c_k e^{ik} \tag{7.3}$$

Condensing into a more compact matrix form gives,

$$\hat{H}_{kin}(k) = \sum_{k}^{BZ} C_k^\dagger \begin{pmatrix} \Delta\epsilon + t_0 e^{-ik} + \delta t e^{-ik} + t_0^* e^{ik} + \delta t^* e^{ik} & Je^{-ik} + J^* e^{ik} \\ Je^{-ik} + J^* e^{ik} & -\Delta\epsilon + t_0 e^{-ik} - \delta t e^{-ik} + t_0^* e^{ik} - \delta t^* e^{ik} \end{pmatrix} C_k \tag{7.4}$$

where $C_k^\dagger = \{c_\uparrow^\dagger \, c_\downarrow^\dagger\}$ and $C_k = \{c_\uparrow \, c_\downarrow\}$ are the vector of creation (annihilation) operators. This transformation will consist of two rotations. While it would be more mathematically rigorous to use the standard axes rotation matrices, we find it more intuitive to use this method to show that many 2x2 Hamiltonians can be transformed to SSH(-like) forms. Firstly, passively rotate the Hamiltonian by $\pi/2$ about the x-axis so that nothing becomes σ_z, i.e. so there are no diagonal terms. The axes transform to,

$$\sigma_x \longrightarrow \sigma_x \tag{7.5a}$$
$$\sigma_y \longrightarrow \sigma_z \tag{7.5b}$$
$$\sigma_z \longrightarrow -\sigma_y \tag{7.5c}$$
$$\sigma_0 \longrightarrow \sigma_0 \tag{7.5d}$$

Such that the Hamiltonian reads,

$$\hat{H}_{kin}(k) = -\Delta\epsilon \sum_{k}^{BZ} c_k^\dagger \sigma_y c_k + \sum_{k}^{BZ} c_k^\dagger (t_0\sigma_0 + \delta t \sigma_y + J\sigma_x) c_k e^{-ik} + c_k^\dagger (t_0^*\sigma_0 + \delta t^* \sigma_y + J^*\sigma_x) c_k e^{ik} \tag{7.6}$$

And the matrix form,

$$\hat{h}_{kin}(k) = \begin{pmatrix} t_0 e^{-ik} + t_0^* e^{ik} & i\Delta\epsilon + i\delta t e^{-ik} + Je^{-ik} + i\delta t e^{ik} + J^* e^{ik} \\ -i\Delta\epsilon - i\delta t e^{-ik} - Je^{-ik} - i\delta t e^{ik} + J^* e^{ik} & t_0 e^{-ik} + t_0^* e^{ik} \end{pmatrix} \tag{7.7}$$

The second rotation is $\pi/2$ about z-axis,

$$\sigma_x \longrightarrow -\sigma_y \tag{7.8a}$$
$$\sigma_y \longrightarrow \sigma_x \tag{7.8b}$$
$$\sigma_z \longrightarrow \sigma_z \tag{7.8c}$$
$$\sigma_0 \longrightarrow \sigma_0 \tag{7.8d}$$

Which gives the Hamiltonian,

$$\hat{H}_{kin}(k) = -\Delta\epsilon \sum_{k}^{BZ} c_k^\dagger \sigma_x c_k + \sum_{k}^{BZ} c_k^\dagger (t_0\sigma_0 - \delta t \sigma_x - J\sigma_y) c_k e^{-ik} + c_k^\dagger (t_0^*\sigma_0 - \delta t^* \sigma_x - J^*\sigma_x) c_k e^{ik} \tag{7.9}$$

Where the matrix version is,

$$\hat{h}_{kin}(k) = \begin{pmatrix} t_0 e^{-ik} + t_0^* e^{ik} & -\Delta\epsilon - \delta t e^{-ik} + iJe^{-ik} - \delta t^{ik} + iJ^* e^{ik} \\ -\Delta\epsilon - \delta t e^{-ik} - iJe^{-ik} - \delta t^{ik} - iJ^* e^{ik} & t_0 e^{-ik} + t_0^* e^{ik} \end{pmatrix} \tag{7.10}$$

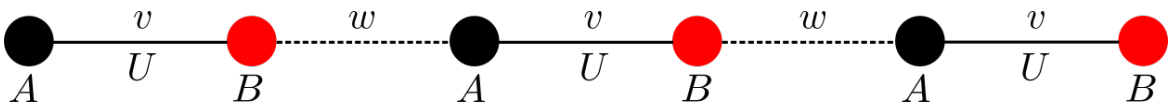

Fig. 7.2 Barbarino ladder rotated into SSH-like chain form in BDI regime. The intracell coupling is given by v and the intercell coupling is w where $v = \delta\epsilon$ and $w = 2\delta t$. An interaction U acts within the unit cell.

To get full off-diagonal chiral structure set $t_0 = 0$,

$$\hat{h}_{kin}(k) = \begin{pmatrix} 0 & -\Delta\epsilon - \delta t e^{-ik} + iJe^{-ik} - \delta t e^{ik} + iJ^* e^{ik} \\ -\Delta\epsilon - \delta t e^{-ik} - iJe^{-ik} - \delta t e^{ik} - iJ^* e^{ik} & 0 \end{pmatrix} \tag{7.11}$$

Following the rotations the operators, now in diagonal form, look like,

$$c_{A(B)} = \frac{1}{\sqrt{2}}(c_\uparrow \pm c_\downarrow) \tag{7.12}$$

In the BDI regime $J = i\delta t$ and δt is real, reducing the Hamiltonian to,

$$\hat{h}_{kin}(k) = \begin{pmatrix} 0 & -\Delta\epsilon - 2\delta t e^{-ik} \\ -\Delta\epsilon - 2\delta t e^{ik} & 0 \end{pmatrix} \tag{7.13}$$

Further, to get the full SSH model we go to the regime where $v = \Delta\epsilon$ and $w = 2\delta t$ which is easily compared to the SSH Hamiltonian equation (2.8).

$$\hat{h}_{kin}(k) = -\begin{pmatrix} 0 & v + 2\delta t e^{-ik} \\ v + 2\delta t e^{ik} & 0 \end{pmatrix} \tag{7.14}$$

We can redefine the unit cell in terms of an A-site and a B-site like the SSH model, see Figure 7.2 for the lattice of the rotated chain. In the $\uparrow\downarrow$ basis the interaction acted within the cell and is therefore a σ_0 component. We saw from the rotation derivation this axis remains constant and is not rotated in any way such that U acts within the rotated unit cell ($A - B$).

As we showed in a previous section the SSH model hosts two phases, a topological phase with winding number $\nu = 1$ and symmetry protected edge states, and a trivial phase of winding number $\nu = 0$ with no edge states. This rotated Barbarino (noninteracting) chain will behave similarly, having a two band dispersion structure in the single particle Hamiltonian. We see that it is an SSH chain with an interaction within the cell.

With this form we will reduce the particle fraction to $\upsilon = 1/4$ and study the strong coupling properties. We then turn to the interaction term and take a mean field approach to get rid of this interaction in favor of an effective noninteracting Hamiltonian. This leads to an alternating 'field' term.

7.1.2 Strong coupling at $v = 1/4$ filling

In the previous chapters we have been working with half-filled models, i.e. both negative energy bands are full. These models were four-site unit cell ladders acting as gapped band insulators with topological properties. In this section we will diagrammatically examine the lattice and energy levels, Figs 7.3, in the strong coupling limit ($v << w$) at $v = 1/4$ filling fraction of our SSH-like chain model from the previous section. The objective of this section is to understand the ground states in the topological phase of this model, interpret how the interaction acts on the system and can be modelled in a noninteracting way.

Let us briefly look at the half filled case, $v = 1/2$, where there would be 1 particle per unit cell, Fig. 7.2. In the strong coupling limit there will be two states, one with energy $+w$ and the other with energy $-w$, we are only interested in the lowest energy states. It is energetically favorable for the particles to sit on the bonds rather than the sites. Unlike the charge and spin density waves in which the particles sit on the sites, this is a bond density wave as the particle wavefunctions are spread across the bond Figure 7.3a. There is a single ground state in this strong coupling picture.

In this strong coupling picture we neglect the end sites as they are higher energy and in a macroscopic system we are interested in the bulk. In this half-filled state the particles interact with each other via U. Turning off U, this model reverts to the SSH model. It is trivial to see that the ground state is all the lowest energy states filled in these 'bonds' and the interaction doesn't act as a symmetry breaking term. In the band spectrum picture this would look like the SSH model. Given these characteristics we now look at the quarter filled picture ($v = 1/4$).

The noninteracting part of the model gives a two band spectrum with the lower band being half filled when the model is quarter filled. The lowest energy configuration would have every other bond filled, which leads to two possible ground state configurations. Adding the interaction term opens a gap in the subbands taking the spectrum from two bands to four bands, Fig. 7.3b. This interaction acts as a ground state symmetry breaking mechanism. In the strong coupling picture the particle could sit on the inner bond in the unit cell or the bond between cells i.e. a $\mathbb{Z}_2$, that depend on the sign of the interaction. For repulsive interactions the particles would want to sit as far apart from each other as possible, such a configuration leaves no interactions between the particles, Fig. 7.3b. In order to make this configuration energetically favorable we need to lower the energy on the occupied bonds and increase them for the sites we want to be unoccupied. This is achieved by adding a 'field' modulation term to w, i.e. δw.

We can think about this in terms of the XXZ chain, where there are two degenerate ground states. At some critical field strength the $\mathbb{Z}_2$ symmetry breaks and a gap opens between the ground states. In the same manner, we want to make one of these configurations lower energy so we attach a dimerization field factors such that $w \rightarrow w \pm \delta w$, and $v \rightarrow v \pm \delta v$. A nonzero dimer value breaks the $\mathbb{Z}_2$ symmetry, opening a gap in the spin and charge sectors. The field causes the energy to lower on the $w + \delta w$ bonds and increase on the $w - \delta w$ bonds. Thus the energy favorability is for the particles to sit on alternating bonds resulting in a ground state with no interactions.

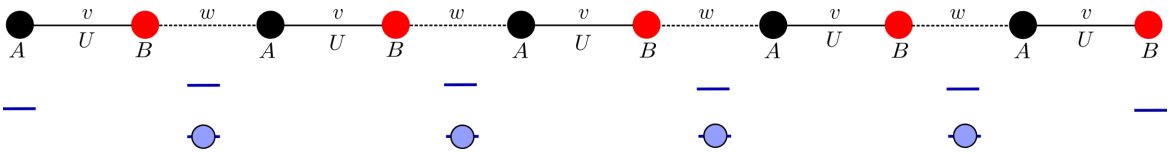

(a) SSH-like chain with repulsive interactions U with particle picture. The ground state at half-filling has the lowest energy states filled (solid blue circles).

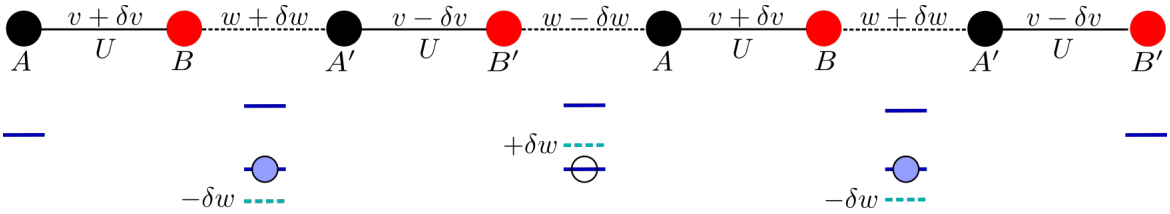

(b) SSH-like chain at $v = \frac{1}{4}$ filling with repulsive interactions U with particle picture. In this model the energy levels are modified by $\pm\delta w$ with every second bond being filled (solid blue dots).

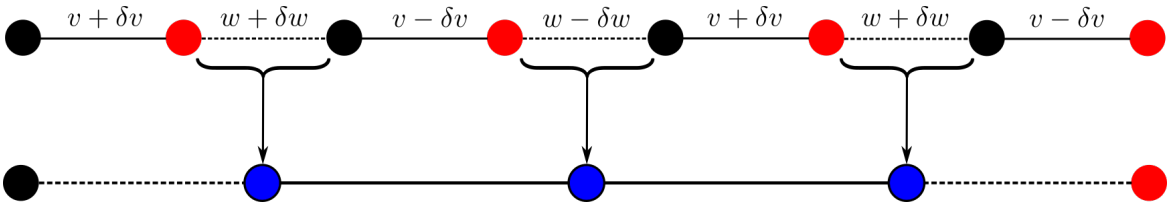

(c) Reduced SSH-like chain at $v = \frac{1}{4}$ filling.

Fig. 7.3 Schematic evolution of the lattice and energy levels at (a) half-filling, (b) quarter-filling, and (c) the 'bond' picture.

Adding in the dimerization factors doubles the size of the unit cell, extending the model to four bands. We further simplify the lattice picture by thinking about these bonds as 'sites' creating an effective site chain, Fig. 7.3c. This gives a more intuitive image of the particle picture in terms of occupied and unoccupied sites.

7.1.3 Mean field theory

In this section we will utilize mean field theory to reduce the interacting density-density terms in equation (7.1) to a noninteracting average field 'felt' by each particle. We will show that the results presented by Barbarino et al can be produced via mean field effects. The mean field calculations will verify our schematic derivations from the previous section. In the context of quantum many-body physics, we will interpret the mean field approximation as a method of replacing pairs of operators with averages [89]. The idea is that we develop a mean field theory and then insert a given model and calculate the energy for a given field strength. The goal is to find the model that minimizes the energy the most. The motivation

here is we know there is some symmetry breaking action in this model so the first stop is mean field theory to determine if the breaking is due to strong correlations or the collective action of the interactions.

The Barbarino model has density-density interactions and for the sake of time we will just say the mean field version of the intracell interaction term U looks like,

$$U \sum_j n_j n_{j+1} \rightarrow h_s \sum_j (-1)^j n_j \tag{7.15}$$

where this is a standard definition, [89]. We will make an educated guess as to what the operator looks like in terms of the original c fermion operators,

$$n_j = c^\dagger_{j\downarrow} c_{j+1\uparrow} + c^\dagger_{j+1\uparrow} c_{j\downarrow} \tag{7.16}$$

In the rotated basis this looks like,

$$h_s \sum_j (-1)^j (c^\dagger_{j\downarrow} c_{j+1\uparrow} + c^\dagger_{j+1\uparrow} c_{j\downarrow}) = -h_s \sum_j (-1)^j (c^\dagger_{j\downarrow} \sigma_y c_{j+1\uparrow} + c^\dagger_{j+1\uparrow} \sigma_y c_{j\downarrow}) \tag{7.17}$$

Equation (7.17) indicates an alternating 'applied' field term $\pm h$ which in essence extends the original 2-site unit cell to a 4-site cell. In the strong δw limit, the chain becomes dimerized with edge states, matching the findings in Barbarino. The Hamiltonian of which looks like,

$$\hat{H}^{MF} = v \sum_n^N (c^\dagger_{nA} c_{nB} + h.c.) + w \sum_n^N (c^\dagger_{nB} c_{n+1,A} + h.c.) + \delta w \sum_n^{N-1} (-1)^n (c^\dagger_{nB} c_{n+1,A} + h.c.) \tag{7.18}$$

which gives an effective noninteracting Hamiltonian for our diagrammatic derivation. From here we will perform a proper mean field calculation, firstly on an SSH-like chain then on a generic 4-band model.

7.1.4 Practical Mean field theory for 4-band models

We can do a quick mean field calculation to check that our guess was correct. We derive the mean field expectation value integrals for the 4x4 case using the interacting Barbarino chain then feed in the noninteracting mean field version and show that our guess was correct. Coincidently the model derived is known as the SSH4 model, in essence an SSH chain with a four site unit cell.

We will perform a mean field calculation on a two-site unit cell to understand the fundamentals of the process for the four-site case. If we have the two-site unit cell Hamiltonian, although it's not really a two-site unit cell because all the hoppings and interactions are the same on every bond but we write it as such because we know the symmetry is going to be broken. This is what happens in the exactly solved spin-1/2 XXZ model [90] when the symmetry gets broken in the Néel phase, in essence the unit cell doubles in size which

redefines the Brillouin zone. This particular two-site cell model is the XXZ model after a Jordan-Wigner transformation [89]. We give the essentials of the derivation here and leave the details to the appendix (D). Begin with a real space Hamiltonian with uniform hopping α and interaction U in the kinetic and interactions terms respectively,

$$\hat{H}_n = \alpha \sum_n^N (c_{nA}^\dagger c_{nB} + c_{nB}^\dagger c_{n+1A} + h.c.) + U \sum_n^{N-1} (c_{nA}^\dagger c_{nA} c_{nB}^\dagger c_{nB} + c_{n+1A}^\dagger c_{n+1A} c_{nB}^\dagger c_{nB}) \tag{7.19}$$

Converting to momentum space gives the Hamiltonian,

$$\hat{H}(k) = \alpha \sum_k^{BZ} (c_{kA}^\dagger c_{kB} + c_{kB}^\dagger c_{kA} e^{ik} + h.c.) + U \sum_{kpq}^{BZ} (c_{kA}^\dagger c_{k+qA} c_{pB}^\dagger c_{p-qB} (1 + e^{-iq})) \tag{7.20}$$

where we have parameterized $k_1 = k,\ k_2 = k+q,\ k_3 = p,\ k_4 = p-q$ in the interacting terms. Diagonalizing the Hamiltonian allows us to work in terms of the individual bands, such that, $H = C_k^\dagger \tilde{U} D \tilde{U}^{-1} C_k$ where $\tilde{U}^{-1} C_k = \{c_-\ c_+\}^T$ and $C^\dagger \tilde{U} = \{c_-^\dagger\ c_+^\dagger\}$ with $-$ and $+$ representing the lower and upper bands respectively. The $\tilde{U}$ matrices are the eigenvectors of equation (7.20),

$$\tilde{U} = \begin{pmatrix} u_{11} & u_{21} \\ u_{12} & u_{22} \end{pmatrix} \tag{7.21}$$

which are unitary such that $\tilde{U}^{-1} = \tilde{U}^\dagger$ and are all functions of the crystal momentum k. The first eigenvector is the first column $(u_{11}\ u_{12})$ and the second eigenvector is $(u_{21}\ u_{22})$. The operators in band space are given as,

$$\begin{aligned} c_{kA}^\dagger &= u_{11}^* c_-^\dagger + u_{21}^* c_+^\dagger \qquad & c_{kA} &= u_{11} c_- + u_{21} c_+ \\ c_{kB}^\dagger &= u_{12}^* c_-^\dagger + u_{22}^* c_+^\dagger \qquad & c_{kB} &= u_{12} c_- + u_{22} c_+ \end{aligned} \tag{7.22}$$

At half-filling the only nonzero terms are the (-,-) terms, and the remaining terms from each substitution are dropped. Calculating the expectation values of the kinetic operators gives,

$$\langle c_{kA}^\dagger c_{kB} \rangle = u_{11}^* u_{12} \langle c_-^\dagger c_- \rangle \tag{7.23}$$

And the $c_{kB}^\dagger c_{kA}$ term simply gives the complex conjugate of equation (7.23) with $\langle c_-^\dagger c_- \rangle = 1$ and all other expectation values are zero. To save ourselves calculating all of the components in the four operator interacting term we use the half-filling condition to know that the only nonzero terms are $\langle c_-^\dagger c_- c_-^\dagger c_- \rangle$ and $\langle c_-^\dagger c_+ c_+^\dagger c_- \rangle$ which occur when $q = 0$ and $q = p - k$, respectively. The interacting expectation values are given by,

$$\langle c_k^\dagger c_{k+q} c_p^\dagger c_{p-q} \rangle = \begin{cases} |u_{11}|^2 |u_{12}|^2 & if\ q = 0 \\ u_{11}^* u_{21} u_{22}^* u_{12} & if\ q = p - k \\ 0 & otherwise \end{cases} \tag{7.24}$$

where $\langle c_-^\dagger c_- c_-^\dagger c_c\rangle = \langle c_-^\dagger c_+ c_+^\dagger c_c\rangle = 1$ and all other operator combinations have an expectation value of zero. Assembling the mean field integrals, calculated over the Brillouin zone, for kinetic and interacting terms,

$$\langle \hat{H}_{kin}\rangle = \alpha \int_{BZ} [u_{11}^* u_{22}(1+e^{ik}) + u_{11}u_{22}^*(1+e^{-ik})]\frac{dk}{2\pi} \tag{7.25a}$$

$$\langle \hat{H}_{int}\rangle = U \int_{BZ}\int_{BZ} [2|u_{11}|^2|u_{12}|^2 + u_{11}^* u_{21} u_{22}^* u_{12}(1+e^{i(k-p)})]\frac{dk}{2\pi}\frac{dp}{2\pi} \tag{7.25b}$$

As this is a completely general set of equations for a uniform hopping and interaction term we can slot in the eigenvector components of any 2x2 Hamiltonian. We know that the mean field version of this model (i.e. noninteracting) has uniform hoppings with an alternating field vector within the cells which looks like $\delta w(-1)^n$,

$$\hat{h}_1^{MF} = \begin{pmatrix} \delta w & -t(1+e^{-ik}) \\ -t(1-e^{ik}) & -\delta w \end{pmatrix} \tag{7.26}$$

We use the eigenvector elements from the Hamiltonian, Eq. (7.26), to calculate the expectation value integrals. In general performing the integrals analytically is not advised so we stick to simple numerical integration using the trapezoidal rules in both one, Eq. (7.27), and two dimensions, Eq. (7.28), [91]. Obviously one could use one of the more accurate Simpsons rules but this one is accurate enough for our purposes.

$$\int_a^b f(x) = \frac{\Delta x}{2}[f(x_0) + 2f(x_1) + 2f(x_2) + \cdots + 2f(x_{N-1}) + f(x_N)] \tag{7.27}$$

$$\begin{aligned}\int_a^b \int_c^d f(x,y)dxdy = \frac{\Delta x \Delta y}{4}[&f(a,c) + f(b,c) + f(a,d) + f(b,d) + 2\sum_i f(x_i,c) + 2\sum_i f(x_i,d) \\ &+ 2\sum_j f(a,y_j) + 2\sum_j f(b,y_j) + 4\sum_j\sum_i f(x_i,y_j)]\end{aligned} \tag{7.28}$$

where $\Delta x = \Delta y = \frac{b-a}{N}$, since x and y span the Brillouin zone. We expect for the energy of the system as a function of the interaction to be minimized for repulsive interactions ($U < 0$) at zero field $\delta w = 0$. As expected the energy is minimized at zero field for $U < 0$ and not minimized for $U > 0$, Fig. 7.4.

We now turn to our 4-band model where the procedure is exactly the same as the 2x2 case simply with more terms. The kinetic and interacting terms are,

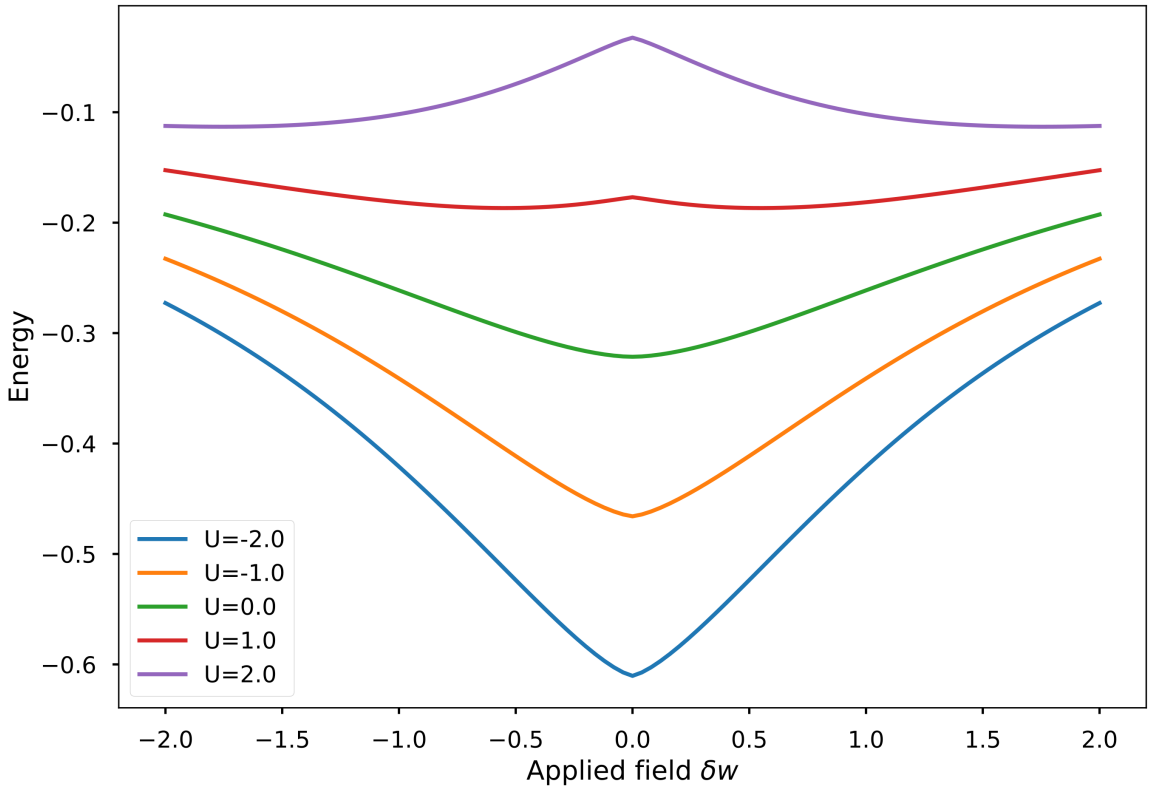

Fig. 7.4 Energy spectrum as a function of applied field δw for attractive $U < 0$ and repulsive $U > 0$ interactions for 2 site unit cell linear chain, Eq. (7.26), with $t = 1.0$.

$$\hat{H}_{kin} = \alpha \sum_{n}^{N} (c^{\dagger}_{nA} c_{nB} + c^{\dagger}_{nA'} c_{nB'} + h.c.) + \beta \sum_{n}^{N-1} (c^{\dagger}_{nB} c_{nA'} + c^{\dagger}_{nB'} c_{n+1A} + h.c.) \tag{7.29}$$

$$\hat{H}_{int} = U \sum_{n}^{N} (c^{\dagger}_{nA} c_{nA} c^{\dagger}_{nB} c_{nB} + c^{\dagger}_{nA'} c_{nA'} c^{\dagger}_{nB'} c_{nB'}) \tag{7.30}$$

where the unit cell basis is the set $\{A\ B\ A'\ B'\}$. The kinetic couplings constants α and β act in an alternating manner between sites, note they are unrelated to the interchain couplings from previous chapters. The interacting coupling U acts between sites A and B, and between A' and B', within the unit cell. There is no interacting term connecting adjacent unit cells. Converting this Hamiltonian to momentum space,

$$\hat{H}_{kin}(k) = \alpha \sum_{k}^{BZ} (c_{kA}^{\dagger} c_{kB} + c_{kA'}^{\dagger} c_{kB'} + h.c.) + \beta \sum_{k}^{BZ} (c_{kB}^{\dagger} c_{kA'} + c_{kB'}^{\dagger} c_{kA} e^{ik} + h.c.) \tag{7.31a}$$

$$\hat{H}_{int}(k) = U \sum_{k}^{BZ} (c_{kA}^{\dagger} c_{k+qA} c_{pB}^{\dagger} c_{p-qB} + c_{kA'}^{\dagger} c_{k+qA'} c_{pB'}^{\dagger} c_{p-qB'}) \tag{7.31b}$$

Using this representation we change to a band basis, as it will be easier to project onto and deal with just the lowest band terms. We label the four bands from lowest to highest as 1,2,3,4. We give the matrix of eigenvectors (columns),

$$\tilde{U} = \begin{pmatrix} u_{11} & u_{21} & u_{31} & u_{41} \\ u_{12} & u_{22} & u_{32} & u_{42} \\ u_{13} & u_{23} & u_{33} & u_{43} \\ u_{14} & u_{24} & u_{34} & u_{44} \end{pmatrix} \tag{7.32}$$

The band basis operators are given by,

$$c_{kA} = u_{11} c_1 + u_{21} c_2 + u_{31} c_3 + u_{41} c_4 \tag{7.33a}$$

$$c_{kB} = u_{12} c_1 + u_{22} c_2 + u_{32} c_3 + u_{42} c_4 \tag{7.33b}$$

$$c_{kA'} = u_{13} c_1 + u_{23} c_2 + u_{33} c_3 + u_{43} c_4 \tag{7.33c}$$

$$c_{kB'} = u_{14} c_1 + u_{24} c_2 + u_{34} c_3 + u_{44} c_4 \tag{7.33d}$$

On to calculating the expectation values of each term. Since we are working at quarter filling ($\upsilon = 1/4$) this cuts down the number of nonzero terms significantly. We will only write these nonzero terms to save time. The only nonzero expectation value terms from the kinetic Hamiltonian, Eq. (7.31a), involve $\langle c_1^{\dagger} c_1 \rangle$,

$$\langle c_{kA}^{\dagger} c_{kB} \rangle = u_{11}^{*} u_{12} \langle c_1^{\dagger} c_1 \rangle \tag{7.34a}$$

$$\langle c_{kA'}^{\dagger} c_{kB'} \rangle = u_{13}^{*} u_{14} \langle c_1^{\dagger} c_1 \rangle \tag{7.34b}$$

$$\langle c_{kB}^{\dagger} c_{kA'} \rangle = u_{12}^{*} u_{13} \langle c_1^{\dagger} c_1 \rangle \tag{7.34c}$$

$$\langle c_{kB'}^{\dagger} c_{kA} \rangle = u_{14}^{*} u_{11} \langle c_1^{\dagger} c_1 \rangle \tag{7.34d}$$

We have also parameterized the momentums in the same way as the 2x2 case which leads to the only nonzero interacting expectation value terms are those involving,

$$\langle c_1^{\dagger} c_1 c_1^{\dagger} c_1 \rangle \tag{7.35a}$$

$$\langle c_1^{\dagger} c_2 c_2^{\dagger} c_1 \rangle \tag{7.35b}$$

$$\langle c_1^{\dagger} c_3 c_3^{\dagger} c_1 \rangle \tag{7.35c}$$

$$\langle c_1^{\dagger} c_4 c_4^{\dagger} c_1 \rangle \tag{7.35d}$$

All other operator combinations are zero. For $q = 0$,

$$\langle c^\dagger_{kA} c_{kA} c^\dagger_{pB} c_{pB}\rangle = |u_{11k}|^2 |u_{12p}|^2 \langle c^\dagger_1 c_1 c^\dagger_1 c_1\rangle \tag{7.36}$$

and for $q = p - k$,

$$\langle c^\dagger_{kA'} c_{kA} c^\dagger_{pB'} c_{pB'}\rangle = |u_{13k}|^2 |u_{14p}|^2 \langle c^\dagger_1 c_1 c^\dagger_1 c_1\rangle \tag{7.37}$$

$$\langle c^\dagger_{kA} c_{pA} c^\dagger_{pB} c_{kB}\rangle = u^*_{11k} u_{21p} u^*_{22p} u_{12k} \langle c^\dagger_1 c_2 c^\dagger_2 c_1\rangle + u^*_{11k} u_{31p} u^*_{32p} u_{12k} \langle c^\dagger_1 c_3 c^\dagger_3 c_1\rangle + u^*_{11k} u_{41p} u^*_{42p} u_{12k} \langle c^\dagger_1 c_4 c^\dagger_4 c_1\rangle \tag{7.38}$$

$$\langle c^\dagger_{kA'} c_{pA'} c^\dagger_{pB'} c_{kB'}\rangle = u^*_{13k} u_{23p} u^*_{24p} u_{14k} \langle c^\dagger_1 c_2 c^\dagger_2 c_1\rangle + u^*_{13k} u_{33p} u^*_{34p} u_{14k} \langle c^\dagger_1 c_3 c^\dagger_3 c_1\rangle + u^*_{13k} u_{43p} u^*_{44p} u_{14k} \langle c^\dagger_1 c_4 c^\dagger_4 c_1\rangle \tag{7.39}$$

Then the mean field expectation value integrals are,

$$\langle \hat{H}_{kin}\rangle = \int_{BZ} [A(u^*_{11} u_{12} + u^*_{13} u_{14} + h.c.) + B(u^*_{12} u_{13} + u^*_{14} u_{11} e^{ik} + h.c.)] \frac{dk}{2\pi} \tag{7.40}$$

$$\begin{aligned}\langle \hat{H}_{int}\rangle = U \int_{BZ}\int_{BZ} [&|u_{11k}|^2 |u_{12p}|^2 + |u_{13k}|^2 |u_{14p}|^2 + u^*_{11k} u_{21p} u^*_{22p} u_{12k} + u^*_{11k} u_{31p} u^*_{32p} u_{12k} \\ &+ u^*_{11k} u_{41p} u^*_{42p} u_{12k} + u^*_{13k} u_{23p} u^*_{24p} u_{14k} + u^*_{13k} u_{33p} u^*_{34p} u_{14k} \\ &+ u^*_{13k} u_{43p} u^*_{44p} u_{14k}] \frac{dk}{2\pi} \frac{dp}{2\pi}\end{aligned} \tag{7.41}$$

We calculate the eigenvector components from the effective chain Hamiltonian, Eq. (7.18), we derived in the first section of this chapter,

$$\hat{h}(k) = \begin{pmatrix} 0 & (v+\delta v) & 0 & (w-\delta w)e^{-ik} \\ (v+\delta v) & 0 & (w+\delta w) & 0 \\ 0 & (w+\delta w) & 0 & (v-\delta v) \\ (w-\delta w)e^{ik} & 0 & (v-\delta v) & 0 \end{pmatrix} \tag{7.42}$$

and insert them into the mean field equations. The next step is to analyze the energy minimization. The kinetic term expectation value will always be minimized at zero field $\delta w = 0$ and symmetric about this point. The interaction term will also be symmetric but not necessarily always minimized at zero field.

We expect the energy to be minimized at zero field ($\delta w = 0$) for attractive interactions ($U < 0$) and the energy to be minimized at some finite field for repulsive interactions ($U > 0$) Similar to the 2x2 case, we observe that the $U < 0$ case the energy is minimized at zero field $\delta w = 0$ but is not minimized for $U > 0$ at zero field, Fig. 7.5a. It is energetically favorable for repulsive interactions, lowering the energy for increasing strength and the ground state is best approximated at this minimal energy. We can do another check by modulating v with δv, for $w > v$, Figure 7.5b. For this case the energy is always minimized at zero field, and therefore the ground state is best approximated at zero field. We will see later in this chapter that $\delta v = 0$ is important for calculating topological invariants.

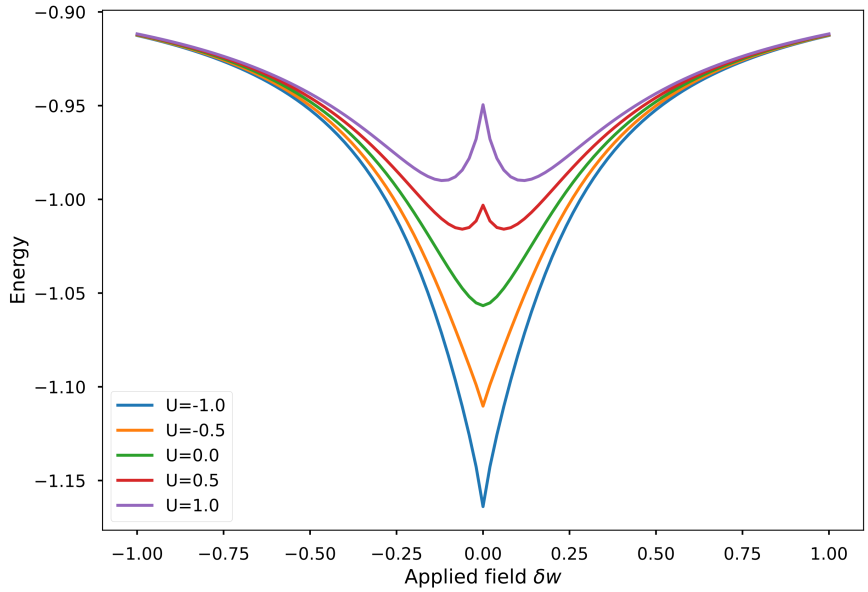

(a) Mean field energy as a function of the applied field δw for the case of modulated w, with $v = 0.3$ and $w = 1.7$. The energy is minimized at zero field $\delta w = 0$ for cases of attractive interaction $U < 0$. Repulsive interactions $U > 0$ cause the energy to be minimized at a finite field $\delta w \neq 0$.

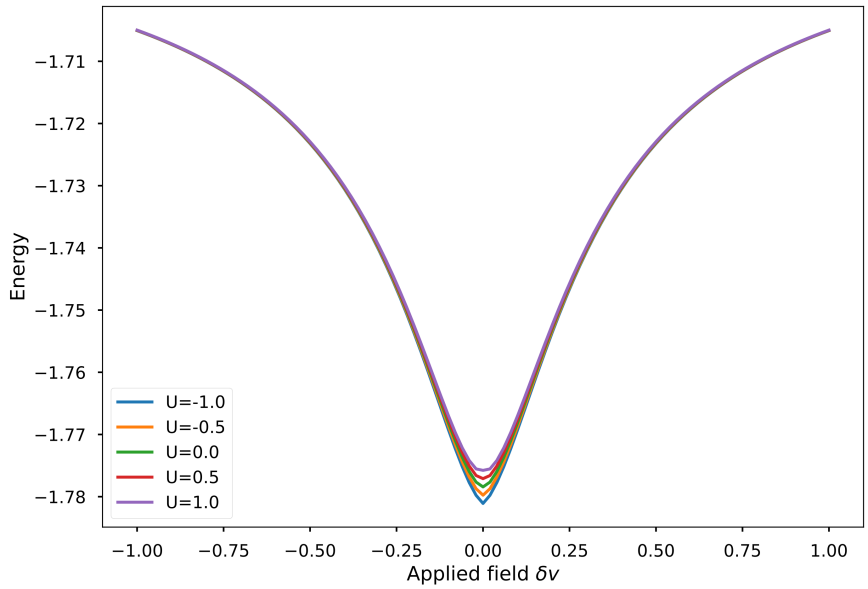

(b) Mean field energy as a function of the applied field $h = \delta v$ for the case of modulated v, with $v = 0.3$ and $w = 1.7$. The energy is minimized at zero field $\delta v = 0$ for all cases of interaction U.

Fig. 7.5 Mean field energy spectrums as a function of applied field for the four-site Hamiltonian (7.42).

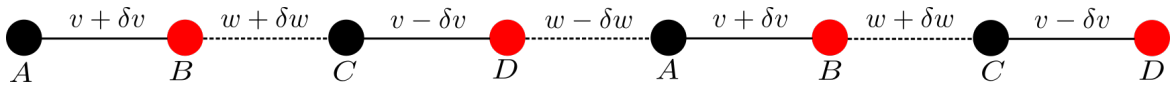

Fig. 7.6 Lattice diagram for the SSH4 model. All couplings are real valued.

7.2 SSH4 model

The mean field noninteracting chain model, Fig. 7.6, is in essence an SSH-like model with a four-site unit cell, known as the SSH4 model. The SSH4 model in the single particle regime is known to be in the BDI universality class with $\mathbb{Z}$ invariant. In the interacting picture the topological insulator phase transitions to a charge density wave state [92]. The topological properties have been studied via the long time dynamics [93] and in a non-Hermitian form [94]. These properties have also been exposed using cold atom set ups and mean chiral displacement measurements [68]. In this section we will examine this model in the reduced filling fraction regime. We will show that this mean field version of the SSH chain host topological states in some regime with bond density wave order and quantized Zak phase topological indexes.

The SSH4 Hamiltonian is,

$$\begin{aligned}\hat{H}_{SSH4} = &\sum_{j}^{N}((v+\delta v)c_{jA}^{\dagger}c_{jB} + (w+\delta w)c_{jB}^{\dagger}c_{jC} + (v-\delta v)c_{jC}^{\dagger}c_{jD}) + \sum_{j}^{N-1}((w-\delta w)c^{\dagger}c_{j+1,A} + (w-\delta w)c_{j+1,A}^{\dagger}c_{jD}) \\ &+ \sum_{j}^{N}((v+\delta v)c_{jB}^{\dagger}c_{jA} + (w+\delta w)c_{jC}^{\dagger}c_{jB} + (v-\delta v)c_{jD}^{\dagger}c_{jC})\end{aligned} \tag{7.43}$$

Convert to momentum space and block diagonalize,

$$\hat{h}_{SSH4}(k) = \begin{pmatrix} 0 & 0 & (v+\delta v) & (w-\delta w)e^{-ik} \\ 0 & 0 & (w+\delta w) & (v-\delta v) \\ (v+\delta v) & (w+\delta w) & 0 & 0 \\ (w-\delta w)e^{ik} & (v-\delta v) & 0 & 0 \end{pmatrix} \tag{7.44}$$

Where we have used the basis $\{A\ A'\ B\ B'\}$ which brings the Hamiltonian into block off-diagonal form. The block off-diagonal nature of the SSH4 Hamiltonian, Eq. (7.44), indicates some chiral symmetry properties of the model. We expect similar phases as the SSH model, i.e. a topological phase for $v < w$ and a trivial phase for $v > w$. In the limits that v or w approach 0 the bands become flat. In the limit $v = w$ the upper bands have degeneracies at the high symmetry points $k = 0, \pm\pi$, if the Brillouin zone is defined $[-\pi, \pi)$. The band structure for the $w > v$ and $v > w$ limits are identical, the upper band and lower band sets are gapless at the $k = \pm\pi$ points. Adding in the dimerizatiom opens a gap at these points.

SSH4 - Topological invariants

Since the model is at $v = 1/4$ filling we will proceed to calculate the Zak phase of the lower two subbands. We will show that the Zak phase is quantized in one of these bands for a given regime of the parameters. The calculations will show that the phase is not quantized for nonzero δv. Similar to the winding number, for the Zak phase [86] to be defined explicitly the model requires inversion symmetry,

$$IH(k)I^{\dagger} = H(-k) \tag{7.45}$$

Spatial inversion symmetry considers the effects of spatially 'flipping' the unit cell. In the band structure picture this symmetry gives a mirror effect over the energy (y) axis. One must be careful to define the inversion symmetry properly, boundaries permit gapless modes localized at these boundaries [95]. Zak showed that the Berry's phase can be used to label energy bands in solids. The Zak phase refers to the Berry's phase picked up by an electron in a periodic potential in the presence of an externally applied time-dependent vector potential. The Berry's phase [96] is a geometric phase a wavefunction picks up when it is taken through a slow adiabatic evolution in a given parameter space and is well-defined in the continuum limit of the space. This evolution needs to be slow otherwise you may introduce excitations, i.e. energy will be added into the system. The vector potential acts to change the Bloch quasimomentum k adiabatically such that the gradual change allows the Hamiltonian to start in an eigenstate and end in the corresponding eigenstate of the final Hamiltonian [97]. For a linear chain with no symmetries, the Berry's phase can take on any value. However in the presence of inversion symmetry, the Berry's phase becomes quantized to only 0 or π (modulo 2π) in this case. The Zak phase is a specific iteration of the Berry's phase using the Brillouin zone as the continuous parameter space. The Zak phase is calculated along a closed path in the Brillouin zone and is given by,

$$z = i \oint_{BZ} \langle u_k | \partial_k | u_k \rangle \, dk \tag{7.46}$$

where $|u_k\rangle$ are the eigenvectors of the state with momentum k and are assumed to be smooth and differentiable. The Zak phase is a gauge invariant quantity (modulo 2π) and can be thought of as the 'left over' phase following a parallel transport operation around a loop of an initial eigenstate. This formula can be connected to the band representations of space groups. The Zak phase gets picked up because of the toroidal (cyclic) nature of the Brillouin zone ($[-\pi/a, \pi/a)$) and the symmetry properties of the Bloch eigenfunctions. We can ask some interesting questions about the Zak phase of this model, notably can we calculate and define invariants for individual bands. It is important that there are no band-crossings or degeneracies (single-band approximation) in the spectrum otherwise there exists an arbitrariness about the definition of the phase for individual bands. The total phase, i.e. sum of occupied bands, will still be quantized [98].

In the regime that $w > v$ the lowest band is quantized to 1 for negative field ($\delta w < 0$) while the second band is 0, although we are looking exclusively at the lower band, Figure

7.7a. The lower band is no longer quantized for positive field strength ($\delta w > 0$) indicating a phase transition to a trivial phase. Turning on the δv parameter disrupts this phase, Fig. 7.7b. While the bands still appear quantized, they are not, and the system is in a topologically trivial phase. In the regime that v is modulated by δv, Figs. 7.7c and 7.7d, the Zak phase is no longer quantized in any bands. Thus we have the condition that $\delta v = 0$ for the Zak phase to be quantized in either of the lower two bands.

Taken as a whole these results tell us the mean field calculations were correct in indicating some topological features in certain regimes. The important point being that nontrivial topological phases are arising as a result of mean field effects rather than any strongly correlated effects.

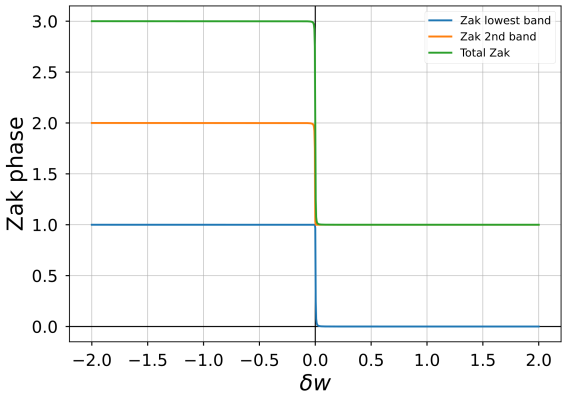

(a) Zak phase of the SSH4 model as a function of the dimer parameter δw (applied field). $v = 0.3$ $w = 3.0$ $\delta v = 0.0$.

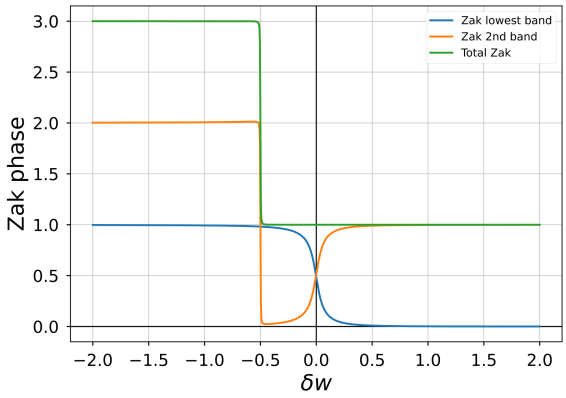

(b) Zak phase of the SSH4 model as a function of the dimer parameter δw (applied field). $v = 0.3$ $w = 3.0$ $\delta v = 0.05$.

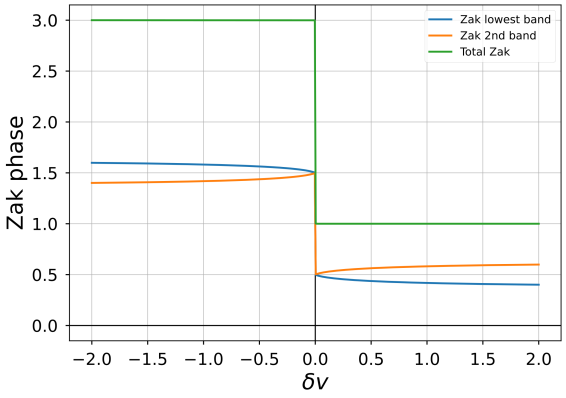

(c) Zak phase of the SSH4 model as a function of the dimer parameter δv. $v = 0.3$ $w = 3.0$ $\delta w = 0.0$.

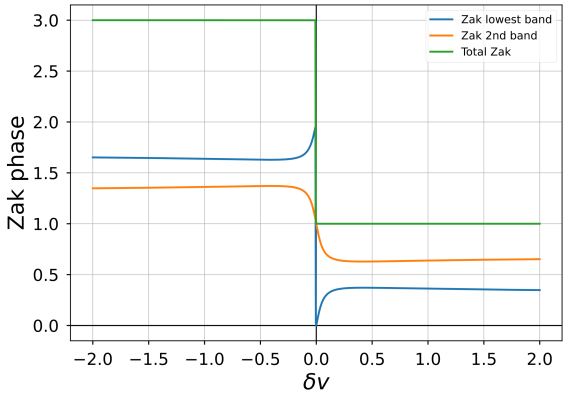

(d) Zak phase of the SSH4 model as a function of the dimer parameter δv. $v = 0.3$ $w = 3.0$ $\delta w = 0.05$.

Fig. 7.7 Zak phase results for SSH4 model with modulated δw (a),(b) and modulating δv (c),(d).

Chapter 8

Conclusions and outlook

In this thesis we have studied the nontrivial phases of chiral topological insulator states in coupled SSH-like chains. The topological insulator phase arises when the interior of a material acts as an insulator and the edges or surfaces act as an electrical conductor. The quantum Hall effects, in the various flavors it has are considered to be topological insulator states. The insulator part comes from the gap between the valence and conduction bands of a material. However these states host edge modes that exist in the gap. A topological insulator cannot be continuously transformed into a trivial one without closing this gap. These states are robust against local symmetry preserving perturbations, one must break one or more symmetries to alter these states. Topological insulators are an example of symmetry protected topological state as the state is protected by one or more symmetries. Topological insulators have been theorized since the 1980s in 1, 2 and 3-dimensions. The advantage of working in 1D is the ease of construction with the use of optical lattice traps.

In the first part of this thesis we constructed noninteracting topological insulator ladder models by coupling two SSH-like chains using symmetry and winding number arguments. The hypothesis being that the topological insulator phase presented in the SSH model can arise in a ladder model given properly designed couplings that adhere to one of the five of the chiral universality classes. Analysis of the winding number of the prototypical topological insulator the SSH model revealed an ambiguity in its sign. While probably known to experts, this nuance does not seem to be published. This ambiguity was found to arise when the individual sublattices in the unit cell are relabelled. When it comes to weakly coupling two SSH chains together we are offered two choices of how this coupling can be defined.

In the first case, coupling chains with the same sign winding number leads to one of the chiral classes BDI, AIII, or CII with topological index $\mathbb{Z}$. In the second case coupling chains with oppositely signed winding numbers leads to the BdG classes DIII and CI with topological indexes $\mathbb{Z}_2$ and 0, respectively. The energy spectrums for BDI, AIII, CII, and DIII all show zero energy modes in the topological phase of each model, with a phase transition to a trivial insulator for $v = w$. In the CI model the modes are not pinned to zero energy. Analysis of the wavefunction of these zero energy modes showed states with amplitudes localized at the edges of the ladder and exponential decay into the bulk. We showed the chiral classes (BDI, AIII, and CII) are adiabatically connected through parameterization of the

interchain coupling as long as chiral symmetry isn't broken, i.e. chiral symmetry protects the topological state. In the case of DIII and CI the protecting symmetries are more complicated. We derived analytical expressions for the edge states in both cases. Using these analytical expressions we demonstrated the symmetry properties of each class appear in the properties of the edge states and give general properties of edge states for each class. We conclude that the topological insulator state can be constructed in a ladder model given careful application of symmetries and relative coupling strengths. The major conclusion of this section work is the results are general an can be applied to any arbitray number of coupled chains with chiral symmetry.

In the final chapter we constructed an interacting SSH-like model at $\upsilon = 1/4$ filling and showed the nontrivial properties of this topological state can arise as a mean field effect rather than a strong correlation one. In the case of reduced filling the lowest band has a quantized Zak phase in the topological regime when $\delta v = 0$. In the strong coupling picture this model resembles the spin-$1/2$ XXZ chain with $\mathbb{Z}_2$ symmetry breaking physics. The results from this line of research, unlike the previous set, is model specific and needs more work to generalize.

Outlook

While we have done good work here showing the ambiguity in the winding number and constructing classed topological insulator models using a systematic methodology there remain open questions. Expressions for generic chiral multichain model with N coupled chains using a combination of chiral operators is set out in [83]. We would also like to use this methodology to create models in all of the 10 universality classes, not just the chiral ones. We saw for the DIII class more than chiral symmetry was required to protect the edge state, so this may be an avenue to understanding how to create the other five classes.

As the winding number can be calculated and quantized in all odd dimensions, research has already been done to extend the methodology used in this work to 3D topological insulators with chiral symmetry, [99].

The models presented here are well suited for a study of the effects of interactions on the topological properties of this type of 1D systems. One can also decouple the hopping terms in the chains, such that they are independent of each other, say v and w on one chain and t and u on the other, and investigate the various phases that arise for different parameter sets. One can also ask about anisotropic interchain couplings where the hoppings are different intracell and intercell or different for $A-A$ and $B-B$ sublattice connections in the case of DIII and CI models.

The simplicity and power of these models should make it easy to add interactions. While there has been much work in this area, classifying and understanding the effect of interactions is a daunting task [100–102]. Our approach should provide a better framework on which to develop interacting models.

An extended analysis of the mean field in the SSH4 model would provide a complete picture of four band models at quarter filling with interactions. A study of the edge states in these reduced filling fractions and examination of subband gap states would provide a

complete mean field understanding. Additionally current cold atom set ups would be able to built and test these noninteracting models. As we noted in the introduction the field of cold atomic and trapped ion experiments is bringing these theoretical microscopic models into the tangible realm. While the SSH model has been extensively studied [25, 24], realization of the different universality classes has not, although this seems to be within reach with cold atoms.

The coupled SSH chains we have described here can be considered as spinful fermion models, where the two internal states can be considered as spins or two hyperfine states. This provides a path to experimentally study them via spin-orbit interactions (couplings) and some Zeeman terms accounting for the staggered amplitudes. These methods are covered in depth in [103–108].

While there is still much research to do on the theoretical side, bringing these microscopic models to life with experiment holds exciting prospects for the future.

References

[1] D. J. Thouless, *Topological Quantum Numbers in Nonrelativistic Physics*. WORLD SCIENTIFIC, 3 1998.

[2] F. D. M. Haldane, "Nobel lecture: Topological quantum matter," *Reviews of Modern Physics*, vol. 89, p. 040502, 10 2017.

[3] X.-G. Wen, "Colloquium : Zoo of quantum-topological phases of matter," *Reviews of Modern Physics*, vol. 89, p. 041004, 12 2017.

[4] R. B. Laughlin, "Quantized hall conductivity in two dimensions," *Physical Review B*, vol. 23, pp. 5632–5633, 5 1981.

[5] D. J. Thouless, M. Kohmoto, M. P. Nightingale, and M. den Nijs, "Quantized hall conductance in a two-dimensional periodic potential," *Physical Review Letters*, vol. 49, pp. 405–408, 8 1982.

[6] C. L. Kane and E. J. Mele, "Z2 topological order and the quantum spin hall effect," *Physical Review Letters*, vol. 95, p. 146802, 9 2005.

[7] B. A. Bernevig, T. L. Hughes, and S.-C. Zhang, "Quantum spin hall effect and topological phase transition in hgte quantum wells," *Science*, vol. 314, pp. 1757–1761, 12 2006.

[8] B. A. Bernevig and S.-C. Zhang, "Quantum spin hall effect," *Physical Review Letters*, vol. 96, p. 106802, 3 2006.

[9] M. Koenig, S. Wiedmann, C. Bruene, A. Roth, H. Buhmann, L. W. Molenkamp, X.-L. Qi, and S.-C. Zhang, "Quantum spin hall insulator state in hgte quantum wells," *Science*, vol. 318, pp. 766–770, 11 2007.

[10] L. Fu, C. L. Kane, and E. J. Mele, "Topological insulators in three dimensions," *Physical Review Letters*, vol. 98, p. 106803, 3 2007.

[11] X.-L. Qi, T. L. Hughes, and S.-C. Zhang, "Topological field theory of time-reversal invariant insulators," *Physical Review B*, vol. 78, p. 195424, 11 2008.

[12] D. Hsieh, D. Qian, L. Wray, Y. Xia, Y. S. Hor, R. J. Cava, and M. Z. Hasan, "A topological dirac insulator in a quantum spin hall phase," *Nature*, vol. 452, pp. 970–974, 4 2008.

[13] M. König, H. Buhmann, L. W. Molenkamp, T. Hughes, C.-X. Liu, X.-L. Qi, and S.-C. Zhang, "The quantum spin hall effect: Theory and experiment," *Journal of the Physical Society of Japan*, vol. 77, p. 031007, 3 2008.

[14] A. Roth, C. Brüne, H. Buhmann, L. W. Molenkamp, J. Maciejko, X.-L. Qi, and S.-C. Zhang, "Nonlocal transport in the quantum spin hall state," *Science*, vol. 325, pp. 294–297, 7 2009.

[15] D. Hsieh, Y. Xia, L. Wray, D. Qian, A. Pal, J. H. Dil, J. Osterwalder, F. Meier, G. Bihlmayer, C. L. Kane, Y. S. Hor, R. J. Cava, and M. Z. Hasan, "Observation of unconventional quantum spin textures in topological insulators," *Science*, vol. 323, pp. 919–922, 2 2009.

[16] D. Hsieh, Y. Xia, D. Qian, L. Wray, J. H. Dil, F. Meier, J. Osterwalder, L. Patthey, J. G. Checkelsky, N. P. Ong, A. V. Fedorov, H. Lin, A. Bansil, D. Grauer, Y. S. Hor, R. J. Cava, and M. Z. Hasan, "A tunable topological insulator in the spin helical dirac transport regime," *Nature*, vol. 460, pp. 1101–1105, 8 2009.

[17] Z. Wang, X.-L. Qi, and S.-C. Zhang, "Topological order parameters for interacting topological insulators," *Physical Review Letters*, vol. 105, p. 256803, 12 2010.

[18] A. Kitaev, V. Lebedev, and M. Feigel'man, "Periodic table for topological insulators and superconductors," vol. 1134, pp. 22–30, AIP, 2009.

[19] A. P. Schnyder, S. Ryu, A. Furusaki, and A. W. W. Ludwig, "Classification of topological insulators and superconductors in three spatial dimensions," *Physical Review B*, vol. 78, p. 195125, 11 2008.

[20] G. Akemann, J. Baik, and P. D. Francesco, eds., *The Oxford Handbook of Random Matrix Theory*. Oxford University Press, 9 2015.

[21] A. Hatcher, *Algebraic Topology*. Cambridge University Press, 2002.

[22] M. Nakahara, *Geometry, Topology and Physics*. CRC Press, 10 2018.

[23] W. P. Su, J. R. Schrieffer, and A. J. Heeger, "Solitons in polyacetylene," *Physical Review Letters*, vol. 42, pp. 1698–1701, 6 1979.

[24] M. Atala, M. Aidelsburger, J. T. Barreiro, D. Abanin, T. Kitagawa, E. Demler, and I. Bloch, "Direct measurement of the zak phase in topological bloch bands," *Nature Physics*, vol. 9, pp. 795–800, 12 2013.

[25] M. Leder, C. Grossert, L. Sitta, M. Genske, A. Rosch, and M. Weitz, "Real-space imaging of a topologically protected edge state with ultracold atoms in an amplitude-chirped optical lattice," *Nature Communications*, vol. 7, p. 13112, 10 2016.

[26] F. D. M. Haldane, "Model for a quantum hall effect without landau levels: Condensed-matter realization of the "parity anomaly"," *Physical Review Letters*, vol. 61, pp. 2015–2018, 10 1988.

[27] C. L. Kane and E. J. Mele, "Quantum spin hall effect in graphene," *Physical Review Letters*, vol. 95, p. 226801, 11 2005.

[28] M. Z. Hasan and C. L. Kane, "Colloquium: Topological insulators," *Reviews of Modern Physics*, vol. 82, pp. 3045–3067, 11 2010.

[29] X.-L. Qi and S.-C. Zhang, "Topological insulators and superconductors," *Reviews of Modern Physics*, vol. 83, pp. 1057–1110, 10 2011.

[30] S. Ryu, A. P. Schnyder, A. Furusaki, and A. W. W. Ludwig, "Topological insulators and superconductors: tenfold way and dimensional hierarchy," *New Journal of Physics*, vol. 12, p. 065010, 6 2010.

[31] B. A. Bernevig and T. L. Hughes, *Topological Insulators and Topological Superconductors*. Princeton University Press, 4 2013.

[32] S.-Q. Shen, *Topological Insulators*, vol. 187. Springer Singapore, 2 ed., 2017.

[33] A. W. W. Ludwig, "Topological phases: classification of topological insulators and superconductors of non-interacting fermions, and beyond," *Physica Scripta*, vol. T168, p. 014001, 12 2016.

[34] S. Barbarino, D. Rossini, M. Rizzi, R. Fazio, G. E. Santoro, and M. Dalmonte, "Topological devil's staircase in atomic two-leg ladders," *New Journal of Physics*, vol. 21, p. 043048, 4 2019.

[35] H. Guo and S.-Q. Shen, "Topological phase in a one-dimensional interacting fermion system," *Physical Review B*, vol. 84, p. 195107, 11 2011.

[36] J. Jünemann, A. Piga, S.-J. Ran, M. Lewenstein, M. Rizzi, and A. Bermudez, "Exploring interacting topological insulators with ultracold atoms: The synthetic creutz-hubbard model," *Physical Review X*, vol. 7, p. 031057, 9 2017.

[37] F. H. L. Essler, H. Frahm, F. Göhmann, A. Klümper, and V. E. Korepin, *The One-Dimensional Hubbard Model*. Cambridge University Press, 2 2005.

[38] R. Resta, "Macroscopic polarization in crystalline dielectrics: the geometric phase approach," *Reviews of Modern Physics*, vol. 66, pp. 899–915, 7 1994.

[39] F. Wilczek and A. Zee, "Appearance of gauge structure in simple dynamical systems," *Physical Review Letters*, vol. 52, pp. 2111–2114, 6 1984.

[40] S. Rachel, "Interacting topological insulators: a review," *Reports on Progress in Physics*, vol. 81, p. 116501, 11 2018.

[41] C. V. Kraus, M. Dalmonte, M. A. Baranov, A. M. Läuchli, and P. Zoller, "Majorana edge states in atomic wires coupled by pair hopping," *Physical Review Letters*, vol. 111, p. 173004, 10 2013.

[42] M. Tovmasyan, S. Peotta, P. Törmä, and S. D. Huber, "Effective theory and emergent su(2) symmetry in the flat bands of attractive hubbard models," *Physical Review B*, vol. 94, p. 245149, 12 2016.

[43] M. C. Strinati, E. Cornfeld, D. Rossini, S. Barbarino, M. Dalmonte, R. Fazio, E. Sela, and L. Mazza, "Laughlin-like states in bosonic and fermionic atomic synthetic ladders," *Physical Review X*, vol. 7, p. 021033, 6 2017.

[44] A. Petrescu, M. Piraud, G. Roux, I. P. McCulloch, and K. L. Hur, "Precursor of the laughlin state of hard-core bosons on a two-leg ladder," *Physical Review B*, vol. 96, p. 014524, 7 2017.

[45] E. M. Stoudenmire, J. Alicea, O. A. Starykh, and M. P. Fisher, "Interaction effects in topological superconducting wires supporting majorana fermions," *Physical Review B*, vol. 84, p. 014503, 7 2011.

[46] S. T. Carr, B. N. Narozhny, and A. A. Nersesyan, "Spinless fermionic ladders in a magnetic field: Phase diagram," *Physical Review B*, vol. 73, p. 195114, 5 2006.

[47] C.-W. Huang, S. T. Carr, D. Gutman, E. Shimshoni, and A. D. Mirlin, "Transport via double constrictions in integer and fractional topological insulators," *Physical Review B*, vol. 88, p. 125134, 9 2013.

[48] R. A. Santos and B. Béri, "Fractional topological insulator precursors in spin-orbit fermion ladders," *Physical Review B*, vol. 100, p. 235122, 12 2019.

[49] C. J. Kennedy, W. C. Burton, W. C. Chung, and W. Ketterle, "Observation of bose–einstein condensation in a strong synthetic magnetic field," *Nature Physics*, vol. 11, pp. 859–864, 10 2015.

[50] M. E. Tai, A. Lukin, M. Rispoli, R. Schittko, T. Menke, D. Borgnia, P. M. Preiss, F. Grusdt, A. M. Kaufman, and M. Greiner, "Microscopy of the interacting harper–hofstadter model in the two-body limit," *Nature*, vol. 546, pp. 519–523, 6 2017.

[51] M. Aidelsburger, M. Lohse, C. Schweizer, M. Atala, J. Barreiro, S. Nascimbène, N. Cooper, I. Bloch, and N. Goldman, "Measuring the chern number of hofstadter bands with ultracold bosonic atoms," *Nature Physics*, vol. 11, pp. 162–166, 2 2015.

[52] N. Cooper, J. Dalibard, and I. Spielman, "Topological bands for ultracold atoms," *Reviews of Modern Physics*, vol. 91, p. 015005, 3 2019.

[53] J. Struck, M. Weinberg, C. Ölschläger, P. Windpassinger, J. Simonet, K. Sengstock, R. Höppner, P. Hauke, A. Eckardt, M. Lewenstein, and L. Mathey, "Engineering ising-xy spin-models in a triangular lattice using tunable artificial gauge fields," *Nature Physics*, vol. 9, pp. 738–743, 11 2013.

[54] R. Citro, S. D. Palo, M. D. Dio, and E. Orignac, "Quantum phase transitions of a two-leg bosonic ladder in an artificial gauge field," *Physical Review B*, vol. 97, p. 174523, 5 2018.

[55] E. Orignac, R. Citro, M. D. Dio, and S. D. Palo, "Vortex lattice melting in a boson ladder in an artificial gauge field," *Physical Review B*, vol. 96, p. 014518, 7 2017.

[56] S. Barbarino, L. Taddia, D. Rossini, L. Mazza, and R. Fazio, "Magnetic crystals and helical liquids in alkaline-earth fermionic gases," *Nature Communications*, vol. 6, p. 8134, 9 2015.

[57] L. Taddia, E. Cornfeld, D. Rossini, L. Mazza, E. Sela, and R. Fazio, "Topological fractional pumping with alkaline-earth-like atoms in synthetic lattices," *Physical Review Letters*, vol. 118, p. 230402, 6 2017.

[58] F. Kolley, M. Piraud, I. P. McCulloch, U. Schollwöck, and F. Heidrich-Meisner, "Strongly interacting bosons on a three-leg ladder in the presence of a homogeneous flux," *New Journal of Physics*, vol. 17, p. 092001, 9 2015.

[59] M. Piraud, F. Heidrich-Meisner, I. P. McCulloch, S. Greschner, T. Vekua, and U. Schollwöck, "Vortex and meissner phases of strongly interacting bosons on a two-leg ladder," *Physical Review B*, vol. 91, p. 140406, 4 2015.

[60] A. Tokuno and A. Georges, "Ground states of a bose–hubbard ladder in an artificial magnetic field: field-theoretical approach," *New Journal of Physics*, vol. 16, p. 073005, 7 2014.

[61] A. Dhar, T. Mishra, M. Maji, R. V. Pai, S. Mukerjee, and A. Paramekanti, "Chiral mott insulator with staggered loop currents in the fully frustrated bose-hubbard model," *Physical Review B*, vol. 87, p. 174501, 5 2013.

[62] E. Orignac and T. Giamarchi, "Meissner effect in a bosonic ladder," *Physical Review B*, vol. 64, p. 144515, 9 2001.

[63] S. Barbarino, L. Taddia, D. Rossini, L. Mazza, and R. Fazio, "Synthetic gauge fields in synthetic dimensions: interactions and chiral edge modes," *New Journal of Physics*, vol. 18, p. 035010, 3 2016.

[64] S. Greschner, M. Piraud, F. Heidrich-Meisner, I. P. McCulloch, U. Schollwöck, and T. Vekua, "Symmetry-broken states in a system of interacting bosons on a two-leg ladder with a uniform abelian gauge field," *Physical Review A*, vol. 94, p. 063628, 12 2016.

[65] M. Atala, M. Aidelsburger, M. Lohse, J. T. Barreiro, B. Paredes, and I. Bloch, "Observation of chiral currents with ultracold atoms in bosonic ladders," *Nature Physics*, vol. 10, pp. 588–593, 8 2014.

[66] B. K. Stuhl, H.-I. Lu, L. M. Aycock, D. Genkina, and I. B. Spielman, "Visualizing edge states with an atomic bose gas in the quantum hall regime," *Science*, vol. 349, pp. 1514–1518, 9 2015.

[67] M. Mancini, G. Pagano, G. Cappellini, L. Livi, M. Rider, J. Catani, C. Sias, P. Zoller, M. Inguscio, M. Dalmonte, and L. Fallani, "Observation of chiral edge states with neutral fermions in synthetic hall ribbons," *Science*, vol. 349, pp. 1510–1513, 9 2015.

[68] D. Xie, W. Gou, T. Xiao, B. Gadway, and B. Yan, "Topological characterizations of an extended su–schrieffer–heeger model," *npj Quantum Information*, vol. 5, 12 2019.

[69] J. K. Asbóth, L. Oroszlány, and A. Pályi, *A Short Course on Topological Insulators*, vol. 919. Springer International Publishing, 2016.

[70] N. Batra and G. Sheet, "Physics with coffee and doughnuts," *Resonance*, vol. 25, pp. 765–786, 6 2020.

[71] H.-M. Guo, "A brief review on one-dimensional topological insulators and superconductors," *Science China Physics, Mechanics and Astronomy*, vol. 59, p. 637401, 3 2016.

[72] A. Altland and M. R. Zirnbauer, "Nonstandard symmetry classes in mesoscopic normal-superconducting hybrid structures," *Physical Review B*, vol. 55, pp. 1142–1161, 1 1997.

[73] M. R. Zirnbauer, "Riemannian symmetric superspaces and their origin in random-matrix theory," *Journal of Mathematical Physics*, vol. 37, pp. 4986–5018, 10 1996.

[74] P. Heinzner, A. Huckleberry, and M. Zirnbauer, "Symmetry classes of disordered fermions," *Communications in Mathematical Physics*, vol. 257, pp. 725–771, 8 2005.

[75] C. G. Velasco and B. Paredes, "Realizing and detecting a topological insulator in the aiii symmetry class," *Physical Review Letters*, vol. 119, p. 115301, 9 2017.

[76] H. Kramers, "Théorie générale de la rotation paramagnétique dans les cristaux," 1930.

[77] A. P. Schnyder, S. Ryu, A. Furusaki, A. W. W. Ludwig, V. Lebedev, and M. Feigel'man, "Classification of topological insulators and superconductors," vol. 1134, pp. 10–21, AIP, 2009.

[78] S. Ryu, J. E. Moore, and A. W. W. Ludwig, "Electromagnetic and gravitational responses and anomalies in topological insulators and superconductors," *Physical Review B*, vol. 85, p. 045104, 1 2012.

[79] D. S. Freed and G. W. Moore, "Twisted equivariant matter," *Annales Henri Poincaré*, vol. 14, pp. 1927–2023, 12 2013.

[80] R. Kennedy and M. R. Zirnbauer, "Bott–kitaev periodic table and the diagonal map," *Physica Scripta*, vol. T164, p. 014010, 12 2015.

[81] J. E. Marsden and M. J. Hoffman, *Basic complex analysis*. W.H. Freeman, third edition ed., 1998.

[82] S. Tewari and J. D. Sau, "Topological invariants for spin-orbit coupled superconductor nanowires," *Physical Review Letters*, vol. 109, p. 150408, 10 2012.

[83] P. Matveeva, T. Hewitt, D. Liu, K. Reddy, D. Gutman, and S. T. Carr, "One-dimensional noninteracting topological insulators with chiral symmetry," *Physical Review B*, vol. 107, p. 075422, 2 2023.

[84] V. Gurarie, "Single-particle green's functions and interacting topological insulators," *Physical Review B*, vol. 83, p. 085426, 2 2011.

[85] J. C. Budich and E. Ardonne, "Topological invariant for generic one-dimensional time-reversal-symmetric superconductors in class diii," *Physical Review B*, vol. 88, p. 134523, 10 2013.

[86] J. Zak, "Berry's phase for energy bands in solids," *Physical Review Letters*, vol. 62, pp. 2747–2750, 6 1989.

[87] F. Franchini, *The XXZ Chain*, vol. 940, pp. 71–92. Springer, Cham., 2017.

[88] T. Giamarchi, *Quantum Physics in One Dimension*. Oxford University Press, 12 2003.

[89] E. Fradkin, *Field Theories of Condensed Matter Physics*. Cambridge University Press, 2 2013.

[90] M. Takahashi, *Thermodynamics of One-Dimensional Solvable Models*. Cambridge University Press, 3 1999.

[91] R. Burden, *Numerical Analysis*. Australia; Pacific Grove, CA: Brooks/Cole, 2001.

[92] X. Zhou, J. S. Pan, and S. Jia, "Exploring interacting topological insulator in the extended su-schrieffer-heeger model," *Physical Review B*, vol. 107, 2 2023.

[93] M. Maffei, A. Dauphin, F. Cardano, M. Lewenstein, and P. Massignan, "Topological characterization of chiral models through their long time dynamics," *New Journal of Physics*, vol. 20, 1 2018.

[94] Y. He and C. C. Chien, "Non-hermitian generalizations of extended su-schrieffer-heeger models," *Journal of Physics Condensed Matter*, vol. 33, 12 2020.

[95] C.-K. Chiu, H. Yao, and S. Ryu, "Classification of topological insulators and superconductors in the presence of reflection symmetry," *Physical Review B*, vol. 88, p. 075142, 8 2013.

[96] M. V. Berry, "Quantal phase factors accompanying adiabatic changes," *Proceedings of the Royal Society of London. Series A, Mathematical and Physical Sciences*, vol. 392, pp. 45–57, 1984.

[97] D. Vanderbilt, *Berry Phases in Electronic Structure Theory*. Cambridge University Press, 10 2018.

[98] R. Resta, "Manifestations of berry's phase in molecules and condensed matter," *Journal of Physics: Condensed Matter*, vol. 12, pp. R107–R143, 3 2000.

[99] D. Liu, P. Matveeva, D. Gutman, and S. T. Carr, "Elementary models of 3d topological insulators with chiral symmetry," 2 2023.

[100] L. Fidkowski and A. Kitaev, "Effects of interactions on the topological classification of free fermion systems," *Physical Review B*, vol. 81, p. 134509, 4 2010.

[101] L. Fidkowski and A. Kitaev, "Topological phases of fermions in one dimension," *Physical Review B*, vol. 83, p. 075103, 2 2011.

[102] R. Verresen, R. Moessner, and F. Pollmann, "One-dimensional symmetry protected topological phases and their transitions," *Physical Review B*, vol. 96, p. 165124, 10 2017.

[103] Y.-J. Lin, K. Jiménez-García, and I. B. Spielman, "Spin–orbit-coupled bose–einstein condensates," *Nature*, vol. 471, pp. 83–86, 3 2011.

[104] L. W. Cheuk, A. T. Sommer, Z. Hadzibabic, T. Yefsah, W. S. Bakr, and M. W. Zwierlein, "Spin-injection spectroscopy of a spin-orbit coupled fermi gas," *Physical Review Letters*, vol. 109, p. 095302, 8 2012.

[105] D. L. Campbell, G. Juzeliūnas, and I. B. Spielman, "Realistic rashba and dresselhaus spin-orbit coupling for neutral atoms," *Physical Review A*, vol. 84, p. 025602, 8 2011.

[106] P. Wang, Z.-Q. Yu, Z. Fu, J. Miao, L. Huang, S. Chai, H. Zhai, and J. Zhang, "Spin-orbit coupled degenerate fermi gases," *Physical Review Letters*, vol. 109, p. 095301, 8 2012.

[107] M. Aidelsburger, M. Atala, M. Lohse, J. T. Barreiro, B. Paredes, and I. Bloch, "Realization of the hofstadter hamiltonian with ultracold atoms in optical lattices," *Physical Review Letters*, vol. 111, p. 185301, 10 2013.

[108] M. Aidelsburger, M. Atala, S. Nascimbène, S. Trotzky, Y.-A. Chen, and I. Bloch, "Experimental realization of strong effective magnetic fields in an optical lattice," *Physical Review Letters*, vol. 107, p. 255301, 12 2011.

Appendix A

Proof of winding number for 2N-band models

Consider a general 2N-band one-dimensional Hamiltonian with the prerequisite chiral symmetry in off-diagonal form,

$$\hat{H} = \begin{pmatrix} 0 & \hat{\Delta} \\ \hat{\Delta}^\dagger & 0 \end{pmatrix} \tag{A.1}$$

In the basis that $\hat{\Delta}$ is diagonal,

$$\hat{\Delta} = \begin{pmatrix} \epsilon_1 e^{i\theta_1} & 0 & \cdots & 0 & \\ 0 & \epsilon_2 e^{i\theta_2} & 0 & \cdots & 0 \\ 0 & 0 & \epsilon_3 e^{i\theta_3} & \cdots & 0 \\ \vdots & \vdots & \vdots & \ddots & \cdots \quad \vdots \\ 0 & 0 & \cdots & 0 & \epsilon_N e^{i\theta_N} \end{pmatrix} \tag{A.2}$$

where $\epsilon_m > 0$. The corresponding eigenstates of Eq. (A.1) are constructed as,

$$\Psi_n^\pm = \frac{e^{i\alpha}}{\sqrt{2}} \begin{pmatrix} \chi_n \\ \pm e^{-i\theta_j} \chi_n \end{pmatrix} \tag{A.3}$$

where χ_n is the N-component unit vector with $\chi_n^m = \delta_{mn}$ and α is an arbitrary phase factor. The eigensets are $\{\Psi_n^\pm, \pm\epsilon_n\}$. We can now construct the projector P_a onto a given band a with energy $-e_a$ using Eqs. (6.54) and (A.3). For $a = 1$ the projector is,

$$P_1 = (\Psi_1^-)^\dagger \Psi_1^- = \frac{1}{2} \begin{pmatrix} 1 & 0 & \cdots & -e^{i\theta_1} & \cdots & 0 \\ 0 & 0 & \cdots & 0 & \cdots & 0 \\ \vdots & \vdots & \ddots & \vdots & \cdots & 0 \\ -e^{i\theta_1} & 0 & \cdots & 1 & \cdots & 0 \\ \vdots & \vdots & \cdots & \vdots & \vdots & \vdots \\ 0 & 0 & \cdots & 0 & 0 & 0 \end{pmatrix} \tag{A.4}$$

The nonzero elements for a given a are $P_a^{aa} = P_a^{a+N,a+N} = 1$ and $P_a^{a,a+N} = (P_a^{a+N,a})^* = e^{i\theta_a}$. Performing the sum of projectors for all negative energy (filled) bands,

$$P = \sum_a (\Psi_a^-)^\dagger \Psi_a^- = \frac{1}{2}\begin{pmatrix} \mathbb{I}_N & -\bar{\Delta} \\ -\bar{\Delta}^* & \mathbb{I}_N \end{pmatrix} \tag{A.5}$$

where $\mathbb{I}_N$ is the identity matrix of dimension N. The $\bar{\Delta}$ block is given as the diagonal matrix,

$$\bar{\Delta} = \begin{pmatrix} e^{i\theta_1} & 0 & \cdots & 0 \\ 0 & e^{i\theta_2} & \cdots & 0 \\ \vdots & \vdots & \ddots & \vdots \\ 0 & \cdots & \cdots & e^{i\theta_N} \end{pmatrix} \tag{A.6}$$

To construct the winding number from here we follow the common Q-matrix method [30]. The Q-matrix is formed from the projector Eq. (A.5) as $Q = 1 - 2P(k)$. This matrix has a block off-diagonal structure which follows from the presence of chiral symmetry ($\{C, Q\}$) and C being block diagonal such that $C = \lambda\sigma_z$ where λ is some unitary matrix. The $Q(k)$ matrix is given as,

$$Q(k) = \begin{pmatrix} 0 & q(k) \\ q(k)^\dagger & 0 \end{pmatrix} \tag{A.7}$$

It is trivial to see that in our representation $\bar{\Delta} = q(k)$. Therefore the determinant of the $q(k)$ block is,

$$det[q(k)] = exp[i\sum_j \theta_j] \equiv e^{i\phi} \tag{A.8}$$

We know that $tr[q^{-1}\delta_k q] = \delta_k \ln det[q(k)] = i\delta_k\phi$, the winding number can be defined,

$$\nu = \frac{i}{2\pi}\int_{BZ} tr[q^{-1}\delta_k q]dk = -\frac{1}{2\pi}\int_{BZ} \delta_k\phi dk \tag{A.9}$$

Expressing the phase ϕ via its complex components using the determinant of $q(k)$,

$$\phi = arctan\left[\frac{\text{Im } det[q(k)]}{\text{Re } det[q(k)]}\right] \tag{A.10}$$

From equation (A.6) we can write $det[q(k)] = det[\bar{\Delta}(k)] = \Pi_j \epsilon_j e^{i\phi}$. Therefore the argument of Eq. (A.10) can be multiplied and divided by $\Pi_j\epsilon_j$ to get the final expression in terms of $\hat{\Delta}$,

$$\phi = arctan\left[\frac{\text{Im } det[\hat{\Delta}(k)]}{\text{Re } det[\hat{\Delta}(k)]}\right] \tag{A.11}$$

This leads nicely to a more tangible expression for calculating the winding number without having to diagonalize the Hamiltonian, equation (2.17).

Appendix B

Deriving symmetry operators

In this appendix we derive the operators for the T_+, T_-, P_+, and T_- symmetries for our generic ladder Hamiltonian given by equations (4.4). The operators will formed by two Pauli matrices, one acting in the unit cell basis (S_n) and the other acting in the chain basis (σ_n) where is from the standard set of Pauli matrices, i.e. $\{0, x, y, z\}$. There are 16 possible operator combinations of the form $S_n\sigma_m$, we will simply state and assert the correct combination for a given operator instead of performing the lengthy trial and error to find the correct one.

To dispel any ambiguity we list all the Pauli matrices here as they have been used throughout the thesis,

$$\sigma_0 = \begin{pmatrix} 1 & 0 \\ 0 & 1 \end{pmatrix} \quad \sigma_x = \begin{pmatrix} 0 & 1 \\ 1 & 0 \end{pmatrix} \quad \sigma_y = \begin{pmatrix} 0 & -i \\ i & 0 \end{pmatrix} \quad \sigma_z = \begin{pmatrix} 1 & 0 \\ 0 & -1 \end{pmatrix} \tag{B.1}$$

Note that the time-reversal and particle-hole symmetries are antiunitary and therefore they square to either +1 or −1. The operators are differentiated using subscript + for the +1 and subscript − for the −1 variants.

B.1 Time-reversal symmetry

A time-reversal invariant symmetry has the condition,

$$TH^*(-k)T^\dagger = H(k) \tag{B.2}$$

where T is the time-reversal symmetry operator and the Hamiltonians are,

$$\hat{H}(k) = \begin{pmatrix} \hat{h}_+ & \hat{\Delta}(k) \\ \hat{\Delta}_+(k) & \hat{h}_- \end{pmatrix} \quad \hat{H}^*(k) = \begin{pmatrix} \hat{h}_- & \hat{\Delta}^*(-k) \\ \hat{\Delta}^T(-k) & \hat{h}_+ \end{pmatrix} \tag{B.3}$$

where $\hat{h}_+$ is given by equation (4.1) and $\hat{h}_- = \hat{h}_+^*$.

The following subsections will derive and check the necessary conditions for the symmetry. The operator is denoted by $T = U_T^{\pm}K$ where K is the complex conjugation operator.

B.1.1 T_+ type symmetry

Given the time-reversal symmetry operation on the Hamiltonian, Eqs. (B.2) and (B.3), and the symmetry condition $T^2 = +1$ we derive a form for U_T^+ that meets these requirements. For this case the σ_x Pauli matrix provides the necessary chain basis operations and S_0 gives the required unit cell basis manipulations. The T_+ operator is then given by,

$$T_+ = U_T^+ K = S_0 \sigma_x K \tag{B.4}$$

We check this operator in the symmetry equation, Eq. (B.5),

$$S_0\sigma_x K H^*(-k) K \sigma_x^\dagger S_0^\dagger = H(k) \tag{B.5a}$$

$$S_0\sigma_x \begin{pmatrix} \hat{h}_- & \hat{\Delta}^*(-k) \\ \hat{\Delta}^T(-k) & \hat{h}_+ \end{pmatrix} \sigma_x^\dagger S_0^\dagger = H(k) \tag{B.5b}$$

$$S_0\sigma_x \begin{pmatrix} \hat{h}_- & \hat{\Delta}^*(-k) \\ \hat{\Delta}^T(-k) & \hat{h}_+ \end{pmatrix} \begin{pmatrix} 0 & S_0 \\ S_0 & 0 \end{pmatrix} = H(k) \tag{B.5c}$$

$$S_0\sigma_x \begin{pmatrix} \hat{\Delta}^*(-k)S_0 & \hat{h}_- S_0 \\ \hat{h}_+ S_0 & \hat{\Delta}^T(-k)S_0 \end{pmatrix} = H(k) \tag{B.5d}$$

$$\begin{pmatrix} S_0\hat{h}_+ S_0 & S_0\hat{\Delta}^T(-k)S_0 \\ S_0\hat{\Delta}^*(-k)S_0 & S_0\hat{h}_- S_0 \end{pmatrix} = H(k) \tag{B.5e}$$

$$\begin{pmatrix} \hat{h}_+ & \hat{\Delta}^T(-k) \\ \hat{\Delta}^*(-k) & \hat{h}_- \end{pmatrix} = H(k) \tag{B.5f}$$

The operator also returns +1 when squared,

$$\begin{aligned} (T_+)^2 &= (S_0\sigma_x K)(S_0\sigma_x K)^\dagger \\ &= (S_0\sigma_x\sigma_x S_0 K K) \qquad = +1 \end{aligned} \tag{B.6}$$

B.1.2 T_- type symmetry

In this section we derive the T_- operator which is necessary for the consideration of our CII class models studied in the main text. We follow the same procedure as the previous subsection and the operator for T_- is,

$$T_- = U_T^- K = i S_0 \sigma_y K \tag{B.7}$$

The operator adheres to the time-reversal symmetry equation, Eq. (B.2),

$$iS_0\sigma_y KH^*(-k)K(-i\sigma_y^\dagger S_0^\dagger) = H(k) \tag{B.8a}$$

$$S_0\sigma_y \begin{pmatrix} \hat{h}_- & \hat{\Delta}^*(-k) \\ \hat{\Delta}^T(-k) & \hat{h}_+ \end{pmatrix} \sigma_y^\dagger S_0^\dagger = H(k) \tag{B.8b}$$

$$S_0\sigma_y \begin{pmatrix} \hat{h}_- & \hat{\Delta}^*(-k) \\ \hat{\Delta}^T(-k) & \hat{h}_+ \end{pmatrix} \begin{pmatrix} 0 & -iS_0 \\ iS_0 & 0 \end{pmatrix} = H(k) \tag{B.8c}$$

$$S_0\sigma_y \begin{pmatrix} i\hat{\Delta}^*(-k)S_0 & -i\hat{h}_-S_0 \\ i\hat{h}_+S_0 & -i\hat{\Delta}^T(-k)S_0 \end{pmatrix} = H(k) \tag{B.8d}$$

$$\begin{pmatrix} S_0\hat{h}_+S_0 & -S_0\hat{\Delta}^T(-k)S_0 \\ -S_0\hat{\Delta}^*(-k)S_0 & S_0\hat{h}_-S_0 \end{pmatrix} = H(k) \tag{B.8e}$$

$$\begin{pmatrix} \hat{h}_+ & -\hat{\Delta}^T(-k) \\ -\hat{\Delta}^*(-k) & \hat{h}_- \end{pmatrix} = H(k) \tag{B.8f}$$

The operator squares to -1,

$$\begin{aligned} (T_-)^2 &= (iS_0\sigma_y K)(iS_0\sigma_y K)^\dagger \\ &= -(S_0\sigma_y\sigma_y S_0 KK) \qquad = -1 \end{aligned} \tag{B.9}$$

B.2 Particle-hole symmetry

A particle-hole invariant symmetry has the condition,

$$PH^*(-k)P^\dagger = -H(k) \tag{B.10}$$

where P is the time-reversal symmetry operator and the Hamiltonians are,

$$\hat{H}(k) = \begin{pmatrix} \hat{h}_+ & \hat{\Delta}(k) \\ \hat{\Delta}_+(k) & \hat{h}_- \end{pmatrix} \quad \hat{H}^*(k) = \begin{pmatrix} \hat{h}_- & \hat{\Delta}^*(-k) \\ \hat{\Delta}^T(-k) & \hat{h}_+ \end{pmatrix} \tag{B.11}$$

where $\hat{h}_+$ is given by equation (4.1) and $\hat{h}_- = \hat{h}_+^*$.

The following subsections will derive and check the necessary conditions for the symmetry. The operator is denoted by $P = U_P^\pm K$ where K is the complex conjugation operator.

B.2.1 P_+ type symmetry

Following the preceding subsections we calculate the P_+ operator and show it possesses the necessary symmetry operators on the Hamiltonian and squares to +1. The P_+ operator is given by,

$$P_+ = U_P^+ K = S_z\sigma_0 K \tag{B.12}$$

We confirm the operator manipulates our Hamiltonian correctly,

$$S_z\sigma_x KH^*(-k)K(\sigma_x^\dagger S_z^\dagger) = -H(k) \tag{B.13a}$$

$$S_z\sigma_x \begin{pmatrix} \hat{h}_- & \hat{\Delta}^*(-k) \\ \hat{\Delta}^T(-k) & \hat{h}_+ \end{pmatrix} \sigma_x^\dagger S_z^\dagger = -H(k) \tag{B.13b}$$

$$S_z\sigma_x \begin{pmatrix} \hat{h}_- & \hat{\Delta}^*(-k) \\ \hat{\Delta}^T(-k) & \hat{h}_+ \end{pmatrix} \begin{pmatrix} 0 & S_z \\ S_z & 0 \end{pmatrix} = -H(k) \tag{B.13c}$$

$$S_z\sigma_x \begin{pmatrix} \hat{\Delta}^*(-k)S_z & \hat{h}_- S_z \\ \hat{h}_+ S_z & \hat{\Delta}^T(-k)S_z \end{pmatrix} = -H(k) \tag{B.13d}$$

$$\begin{pmatrix} S_z\hat{h}_+ S_z & S_z\hat{\Delta}^T(-k)S_z \\ S_z\hat{\Delta}^*(-k)S_z & S_z\hat{h}_- S_z \end{pmatrix} = -H(k) \tag{B.13e}$$

$$\begin{pmatrix} -\hat{h}_+ & -S_z\hat{\Delta}^T(-k)S_z \\ -S_z\hat{\Delta}^*(-k)S_z & -\hat{h}_- \end{pmatrix} = -H(k) \tag{B.13f}$$

The operator squares to +1 as necessary,

$$\begin{aligned} (P_+)^2 &= (S_z\sigma_x K)(S_z\sigma_x K)^\dagger \\ &= (S_z\sigma_x\sigma_x S_z KK) \qquad = +1 \end{aligned} \tag{B.14}$$

B.2.2 P_- type symmetry

The P_- operator is given by,

$$P_- = U_P^- K = -iS_z\sigma_y K \tag{B.15}$$

The operator performs the necessary manipulations on our Hamiltonian,

$$-iS_z\sigma_y KH^*(-k)K(i\sigma_y^\dagger S_z^\dagger) = -H(k) \tag{B.16a}$$

$$-S_z\sigma_y \begin{pmatrix} \hat{h}_- & \hat{\Delta}^*(-k) \\ \hat{\Delta}^T(-k) & \hat{h}_+ \end{pmatrix} \sigma_y^\dagger S_z^\dagger = -H(k) \tag{B.16b}$$

$$-S_z\sigma_y \begin{pmatrix} \hat{h}_- & \hat{\Delta}^*(-k) \\ \hat{\Delta}^T(-k) & \hat{h}_+ \end{pmatrix} \begin{pmatrix} 0 & -iS_z \\ iS_z & 0 \end{pmatrix} = -H(k) \tag{B.16c}$$

$$-S_z\sigma_y \begin{pmatrix} i\hat{\Delta}^*(-k)S_z & -i\hat{h}_- S_z \\ i\hat{h}_+ S_z & -\hat{\Delta}^T(-k)S_z \end{pmatrix} = -H(k) \tag{B.16d}$$

$$-\begin{pmatrix} S_z\hat{h}_+ S_z & S_z\hat{\Delta}^T(-k)S_z \\ S_z\hat{\Delta}^*(-k)S_z & S_z\hat{h}_- S_z \end{pmatrix} = -H(k) \tag{B.16e}$$

$$\begin{pmatrix} -\hat{h}_+ & S_z\hat{\Delta}^T(-k)S_z \\ S_z\hat{\Delta}^*(-k)S_z & -\hat{h}_- \end{pmatrix} = -H(k) \tag{B.16f}$$

Finally, it returns -1 when the operator is squared,

$$\begin{aligned}(P_-)^2 &= (-iS_z\sigma_y K)(-iS_z\sigma_y K)^\dagger \\ &= (S_z\sigma_y\sigma_y S_z KK) \qquad\qquad = -1\end{aligned} \tag{B.17}$$

Appendix C

Deriving analytical edge state expressions

In this appendix we derive in detail the analytical expressions for the edge states of each chiral universality class, i.e. BDI, CII, DIII, and CI.

C.1 BDI and CII class models

The minimal model Hamiltonian for the BDI and CII classes is,

$$\begin{aligned}\hat{H}_1 = \hat{H}_0 + \hat{V}_1 = &\sum_{n\eta=1,2}^{N} (v c^{\dagger}_{An\eta} c_{Bn\eta} + w c^{\dagger}_{Bn\eta} c_{An+1\eta}) + \alpha \sum_{n\eta=1,2}^{N} (c^{\dagger}_{An\eta} c_{Bn-\eta} + c^{\dagger}_{Bn\eta} c_{A(n+1)-\eta}) \\ &+ \sum_{n\eta=1,2}^{N} (v^* c^{\dagger}_{Bn\eta} c_{An\eta} + w^* c^{\dagger}_{A(n+1)\eta} c_{Bn\eta}) + \alpha^* \sum_{n\eta=1,2}^{N} (c^{\dagger}_{Bn-\eta} c_{An\eta} + c^{\dagger}_{A(n+1)-\eta} c_{Bn\eta})\end{aligned} \tag{C.1}$$

where the sum n is over all unit cells N and η sums all chains, in this case (1,2). The general wavefunction ansatz for a two site unit cell,

$$|\Psi\rangle = \sum_{m=1}^{M} \sum_{\rho=1,2} a_{m\rho} |mA\rho\rangle + b_{m\rho} |mB\rho\rangle \tag{C.2}$$

Applying the Hamiltonian (Eq. (C.1)) to the general wavefunction (Eq. (C.2)),

$$\begin{aligned}\hat{H}_1|\Psi\rangle = &\sum_{mn\eta\rho}^{MN} v c^\dagger_{An\eta} c_{Bn\eta} a_{m\rho}|mA\rho\rangle + w c^\dagger_{Bn\eta} c_{An+1\eta} a_{m\rho}|mA\rho\rangle \\ &+ \alpha(c^\dagger_{An\eta} c_{Bn-\eta} a_{m\rho}|mA\rho\rangle + c^\dagger_{Bn\eta} c_{A(n+1)-\eta} a_{m\rho}|mA\rho\rangle) \\ &+ v^* c^\dagger_{Bn\eta} c_{An\eta} a_{m\rho}|mA\rho\rangle + w^* c^\dagger_{A(n+1)\eta} c_{Bn\eta} a_{m\rho}|mA\rho\rangle \\ &+ \alpha^*(c^\dagger_{Bn-\eta} c_{An\eta} a_{m\rho}|mA\rho\rangle + c^\dagger_{A(n+1)-\eta} c_{Bn\eta} a_{m\rho}|mA\rho\rangle) \\ &+ \sum_{mn\eta\rho}^{MN} v c^\dagger_{An\eta} c_{Bn\eta} b_{m\rho}|mB\rho\rangle + w c^\dagger_{Bn\eta} c_{An+1\eta} b_{m\rho}|mB\rho\rangle \\ &+ \alpha(c^\dagger_{An\eta} c_{Bn-\eta} b_{m\rho}|mB\rho\rangle + c^\dagger_{Bn\eta} c_{A(n+1)-\eta} b_{m\rho}|mB\rho\rangle) \\ &+ v^* c^\dagger_{Bn\eta} c_{An\eta} b_{m\rho}|mB\rho\rangle + w^* c^\dagger_{A(n+1)\eta} c_{Bn\eta} b_{m\rho}|mB\rho\rangle \\ &+ \alpha^*(c^\dagger_{Bn-\eta} c_{An\eta} b_{m\rho}|mB\rho\rangle + c^\dagger_{A(n+1)-\eta} c_{Bn\eta} b_{m\rho}|mB\rho\rangle)\end{aligned} \tag{C.3}$$

Eliminate all the zero overlap terms,

$$\begin{aligned}\hat{H}_1|\Psi\rangle = &\sum_{mn\eta\rho}^{MN} w c^\dagger_{Bn\eta} c_{An+1\eta} a_{m\rho}|mA\rho\rangle + \alpha c^\dagger_{Bn\eta} c_{A(n+1)-\eta} a_{m\rho}|mA\rho\rangle \\ &+ v^* c^\dagger_{Bn\eta} c_{An\eta} a_{m\rho}|mA\rho\rangle + \alpha^* c^\dagger_{Bn-\eta} c_{An\eta} a_{m\rho}|mA\rho\rangle \\ &+ \sum_{mn\eta\rho}^{MN} v c^\dagger_{An\eta} c_{Bn\eta} b_{m\rho}|mB\rho\rangle + \alpha(c^\dagger_{An\eta} c_{Bn-\eta} b_{m\rho}|mB\rho\rangle \\ &+ w^* c^\dagger_{A(n+1)\eta} c_{Bn\eta} b_{m\rho}|mB\rho\rangle + \alpha^* c^\dagger_{A(n+1)-\eta} c_{Bn\eta} b_{m\rho}|mB\rho\rangle\end{aligned} \tag{C.4}$$

Adjust the m and ρ indices in each term to match the annihilation operator indices (n and η),

$$\begin{aligned}\hat{H}_1|\Psi\rangle = &\sum_{n\eta}^{N} a_{n+1\eta} w c^\dagger_{Bn\eta} c_{An+1\eta}|n+1A\eta\rangle + a_{n+1-\eta}\alpha c^\dagger_{Bn\eta} c_{A(n+1)-\eta}|n+1A-\eta\rangle \\ &+ a_{n\eta} v^* c^\dagger_{Bn\eta} c_{An\eta}|nA\eta\rangle + a_{n\eta}\alpha^* c^\dagger_{Bn-\eta} c_{An\eta}|nA\eta\rangle \\ &+ \sum_{n\eta}^{N} b_{n\eta} v c^\dagger_{An\eta} c_{Bn\eta}|nB\eta\rangle + b_{n-\eta}\alpha c^\dagger_{An\eta} c_{Bn-\eta}|nB-\eta\rangle \\ &+ b_{n\eta} w^* c^\dagger_{A(n+1)\eta} c_{Bn\eta}|nB\eta\rangle + b_{n\eta}\alpha^* c^\dagger_{A(n+1)-\eta} c_{Bn\eta}|nB\eta\rangle\end{aligned} \tag{C.5}$$

Apply operators to kets,

$$\begin{aligned}\hat{H}_1|\Psi\rangle = \sum_{n\eta}^{N} & a_{n+1\eta}w|nB\eta\rangle + a_{n+1-\eta}\alpha|nB\eta\rangle + a_{n\eta}v^*|nB\eta\rangle + a_{n\eta}\alpha^*|nB-\eta\rangle \\ & + b_{n\eta}v|nA\eta\rangle + b_{n-\eta}\alpha|nA\eta\rangle + b_{n\eta}w^*|n+1A\eta\rangle + b_{n\eta}\alpha^*|n+1A-\eta\rangle\end{aligned} \tag{C.6}$$

Adjust indices in kets to prefactors,

$$\begin{aligned}\hat{H}_1|\Psi\rangle = \sum_{n\eta}^{N} & a_{n+1\eta}w|nB\eta\rangle + a_{n+1-\eta}\alpha|nB\eta\rangle + a_{n\eta}v^*|nB\eta\rangle + a_{n-\eta}\alpha^*|nB\eta\rangle \\ & + b_{n\eta}v|nA\eta\rangle + b_{n-\eta}\alpha|nA\eta\rangle + b_{n-1\eta}w^*|nA\eta\rangle + b_{n-1-\eta}\alpha^*|nA\eta\rangle\end{aligned} \tag{C.7}$$

Expand the chain sum η (1,2),

$$\begin{aligned}\hat{H}_1|\Psi\rangle = \sum_{n\eta}^{N} & a_{n+1,1}w|nB,1\rangle + a_{n+1,2}\alpha|nB,1\rangle + a_{n,1}v^*|nB,1\rangle + a_{n,2}\alpha^*|nB,1\rangle \\ & + b_{n,1}v|nA,1\rangle + b_{n,2}\alpha|nA,1\rangle + b_{n-1,1}w^*|nA,1\rangle + b_{n-1,2}\alpha^*|nA,1\rangle \\ & + a_{n+1,2}w|nB,2\rangle + a_{n+1,1}\alpha|nB,2\rangle + a_{n,2}v^*|nB,2\rangle + a_{n,1}\alpha^*|nB,2\rangle \\ & + b_{n,2}v|nA,2\rangle + b_{n,1}\alpha|nA,2\rangle + b_{n-1,2}w^*|nA,2\rangle + b_{n-1,1}\alpha^*|nA,2\rangle\end{aligned} \tag{C.8}$$

These terms decouple nicely and can be handled separately. We are looking for the equations of motion at zero energy, which are given by,

$$\begin{aligned}|nB,1\rangle: &\quad a_{n,1}v^* + a_{n+1,1}w + a_{n+1,2}\alpha + a_{n,2}\alpha^* = 0 \\ |nB,2\rangle: &\quad a_{n,2}v + a_{n+1,2}w^* + a_{n+1,1}\alpha + a_{n,1}\alpha^* = 0 \\ |nA,1\rangle: &\quad b_{n,1}v + b_{n-1,1}w^* + b_{n,2}\alpha + b_{n-1,2}\alpha^* = 0 \\ |nA,2\rangle: &\quad b_{n,2}v^* + b_{n-1,2}w + b_{n,1}\alpha + b_{n-1,1}\alpha^* = 0\end{aligned} \tag{C.9}$$

To be concrete in this derivation we will consider only the left edge of a semi-infinite ladder. Determining the right edge would give an analogous calculation and conclusions. The general form of the wavefunction on a given site n,

$$\psi_n = \sum_{i=1,2} \vartheta_i(-\lambda)^n \vec{u}_i \tag{C.10}$$

consists of the linear combination of the amplitudes on both chains. Here $\vartheta_{1,2} \in \mathbb{C}$ represent the prefactor of each component, λ is the eigenvalue of the recurrence matrix, Eq. (6.11), and $\vec{u}_i$ is the wavefunction component. The most general form would be a four component sum however as we have restricted the calculation to the left edge (two sites), the sum is only over two elements.

We will derive the eigenvalue and eigenvector components of the recurrence matrix to construct our analytical edge state wavefunction in the following paragraphs. For the left

edge in the thermodynamic limit we expect states to be only on the A-sublattice such that all b_n coefficients should be 0 for all n. This gives us the boundary condition $b_0 = 0$. So we work with the $|nB,1\rangle$, $|nB,2\rangle$ sets. The A-site coefficients (a_n) need to decay into the bulk otherwise the state is unnormalizable. Here we will solve for only the A-site coefficients ($a_{n,(1,2)}$), which should decay from the left edge to zero on the right edge. Equally the B-sublattice amplitudes will be the reverse, decaying from the right edge to the left edge.

The next steps are to solve the recurrence relation eigensets to build the analytical wavefunctions. Collect like cell index terms from equations (C.9),

$$\begin{aligned} a_{n+1,1}w + a_{n+1,2}\alpha &= -(a_{n,1}v^* + a_{n,2}\alpha^*) \\ a_{n+1,1}\alpha + a_{n+1,2}w^* &= -(a_{n,1}\alpha^* + a_{n,2}v) \end{aligned} \tag{C.11}$$

What we have produced here is a recurrence relation that gives us the coefficients for the next cell based on the current cell. Expressed as matrices,

$$\begin{pmatrix} w & \alpha \\ \alpha & w^* \end{pmatrix} \begin{pmatrix} a_{n+1,1} \\ a_{n+1,2} \end{pmatrix} = - \begin{pmatrix} v^* & \alpha^* \\ \alpha^* & v \end{pmatrix} \begin{pmatrix} a_{n,1} \\ a_{n,2} \end{pmatrix} \tag{C.12}$$

Rearranging and simplifying, C represents the 2x2 matrix on the left side, D the same on the right side.

$$\vec{a}_{n+1} = -C^{-1}D\vec{a}_n \tag{C.13}$$

We can define the recurrence matrix T, by combining C and D matrices,

$$\vec{a_{n+1}} = -T\vec{a}_n \tag{C.14}$$

where,

$$T = \frac{1}{|w|^2 - \alpha^2} \begin{pmatrix} w^*v^* - |\alpha|^2 & w^*\alpha^* - \alpha v \\ w\alpha^* - v^*\alpha & wv - |\alpha|^2 \end{pmatrix} \tag{C.15}$$

Calculate the eigenvalues of the transfer matrix as this will tell us the parts for each chain,

$$\begin{pmatrix} w^*v^* - |\alpha|^2 - \lambda & w^*\alpha^* - \alpha v \\ w\alpha^* - v^*\alpha & wv - |\alpha|^2 - \lambda \end{pmatrix} \tag{C.16}$$

Solve for the eigenvalues,

$$\begin{aligned} (w^*v^* - \alpha\alpha^* - \lambda)(wv - \alpha\alpha^* - \lambda) - (w^*\alpha^* - \alpha v)(w\alpha^* - v^*\alpha) &= 0 \\ \lambda^2 - (2|\alpha|^2 - w^*v^* - wv)\lambda + |w|^2|v|^2 - |w|^2\alpha*^2 - |v|^2\alpha^2 + |\alpha|^4 &= 0 \end{aligned} \tag{C.17}$$

$$\lambda_{1,2} = \frac{-(2|\alpha|^2 - w^*v^* - wv) \pm i\sqrt{|\Omega|}}{2} \tag{C.18a}$$

$$\Omega = -4w^*v^*|\alpha|^2 - 4wv|\alpha|^2 + (w^*v^*)^2 + (wv)^2 - 2|w|^2|v|^2 + 4|w|^2\alpha^{*2} + 4|v|^2\alpha^2 \tag{C.18b}$$

We also define the decay length of the edge state and oscillating part of the wavefunction by taking the real and imaginary part of the logarithm of the eigenvalue, $\delta = ln(\lambda)$.

Additionally we can make the assertion that at the high symmetry points (i.e. time-reversal symmetry points) of $\alpha = \{0, \pi/2\}$ then $\lambda_1 = \lambda_2^*$ and vice versa. For this assertion to be true the sign of the square root term needs to change and as none of the terms under the square root change this is indicating that the sign of the square root must always be negative at the time-reversal symmetry points. The eigenvectors $\vec{u}_{1,2}$ of the transfer matrix are derived via,

$$\begin{pmatrix} t & u \\ v & w \end{pmatrix} \begin{pmatrix} a_1 \\ a_2 \end{pmatrix} = \lambda_i \begin{pmatrix} a_1 \\ a_2 \end{pmatrix} \tag{C.19}$$

where we have used generic variables,

$$ta_1 + ua_2 = \lambda_i a_1 \tag{C.20}$$

$$va_1 + wa_2 = \lambda_i a_2 \tag{C.21}$$

$$(\frac{-t}{u} + \frac{\lambda}{u})a_1 = a_2 \tag{C.22}$$

Thus the two (complex) eigenvectors are,

$$\vec{u}_{1,2} = \begin{pmatrix} 1 & \frac{wv - w^*v^* \pm \sqrt{|\Omega|}}{2(w^*\alpha* - \alpha v)} \end{pmatrix} \tag{C.23}$$

Then the most generic solution for this is, since an eigenvector can be a linear combination of other eigenvectors,

$$\vec{\psi}_n = \sum_{i=1,2} \vartheta_i (-\lambda)^n \vec{u}_i \tag{C.24}$$

where $\vartheta_{1,2} \in \mathbb{C}$.

$$\psi_{A,n} = \begin{pmatrix} a_{n,1} \\ a_{n,2} \end{pmatrix} = \vartheta_1 (-\lambda_1)^n \vec{u}_1 + \vartheta_2 (-\lambda_2)^n \vec{u}_2 \tag{C.25}$$

The ϑs are the contribution factors for the eigenvectors. These eigenvectors represent to edge states present on the left edge and since they are degenerate we can take any linear combination however the choice of a symmetric and antisymmetric combinations is useful to demonstrate some properties of the edge states.

In order to do that consider $\vartheta_1 = \pm\vartheta_2$ and have the following definitions,

$$\begin{aligned} \psi_+ &\Rightarrow \vartheta_1 = \vartheta_2 \\ \psi_- &\Rightarrow \vartheta_1 = -\vartheta_2 \end{aligned} \tag{C.26}$$

Refine the equation to a simpler notation where the minus has been incorporated into the eigenvalues (λ_i) and the eigenvectors are $\vec{u}_{1,2}$ with basis (A_1, A_2),

$$\vec{\Psi}_{\pm} = (\lambda_1)^n \vec{u}_1 \pm (\lambda_2)^n \vec{u}_2 \tag{C.27}$$

The edge states are normalizable if they decay (from the left in this case) into the bulk, i.e. $|\lambda_{1,2}| < 1$, which corresponds to the topological phase.

The symmetry properties of the model must be reflected in the properties of the edge states wave functions. We can demonstrate these properties analytically by studying how they transform under the action of time-reversal symmetry. Then we propose the conjectures that for the BDI class, application of the time-reversal symmetry will transform the state back to itself. For the CII class, to comply with Kramers theorem, the state will transform to its counterpart with a ±1 prefactor. Mathematically,

$$\begin{array}{rll} BDI: & T^+ |\Psi_+\rangle = |\Psi_+\rangle & T_+ = \sigma_0 S_x K \\ & T_+ |\Psi_-\rangle = -|\Psi_-\rangle & \\ CII: & T_- |\Psi_+\rangle = \pm |\Psi_-\rangle & T_- = i\sigma_0 S_y K \\ & T_- |\Psi_-\rangle = \pm |\Psi_+\rangle & \end{array} \tag{C.28}$$

$$BDI: \quad T_+ \phi_{\pm} \propto \phi_{\pm} \quad T_+ = S_0 \sigma_x K, \tag{C.29}$$

$$CII: \quad T_- \phi_{\pm} \propto \phi_{\mp} \quad T_- = i S_0 \sigma_y K \tag{C.30}$$

As the two edge states are degenerate one can take any linear combination, however our choice of $\Psi_{\pm}$ is useful to demonstrate the symmetry properties of these edge states.

So then if we have the state $\Psi = \begin{pmatrix} a \\ b \end{pmatrix}$ in the chain basis $\Psi = \begin{pmatrix} 1 \\ 2 \end{pmatrix}$ basis,

$$T_+ \Psi = \sigma_0 S_x K \begin{pmatrix} a \\ b \end{pmatrix} = \begin{pmatrix} b^* \\ a^* \end{pmatrix}, \quad T_- \Psi = i\sigma_0 S_y K \begin{pmatrix} a \\ b \end{pmatrix} = \begin{pmatrix} -b^* \\ a^* \end{pmatrix} \tag{C.31}$$

σ_0 applies to the A/B-sublattice so nothing changes there. In the T_+ (BDI) case we would need $a = b^*$. In the T_- case then we need $a = -b$.

Let us demonstrate these expressions explicitly using the eigenvectors $\vec{u}_{1,2}$,

$$T_+ \vec{u}_1 = S_0 \sigma_x K \begin{pmatrix} 1 \\ \frac{w^* v^* - wv + i\sqrt{|\Omega|}}{2(v^* a^* - wa)} \end{pmatrix} \tag{C.32}$$

$$= \begin{pmatrix} \frac{wv - w^* v^* - i\sqrt{|\Omega|}}{2(va - w^* a^*)} \\ 1 \end{pmatrix} = \vec{u}_2 \tag{C.33}$$

It is trivial to check that $T_+ \phi_- = -\phi_-$. Thusly $T_+ \phi_{\pm} = \pm \phi_{\pm}$ which is consistent with the aforementioned conjectures. By acting with T_- on the eigenstates $\vec{u}_1$ and $\vec{u}_2$ we get,

$$T_{-}\vec{u}_1 = iS_0\sigma_y K \begin{pmatrix} 1 \\ \frac{w^*v^* - wv + i\sqrt{|\Omega|}}{2(v^*a^* - wa)} \end{pmatrix} \tag{C.34}$$

$$= \begin{pmatrix} \frac{wv - w^*v^* - i\sqrt{|\Omega|}}{2(va - w^*a^*)} \\ -1 \end{pmatrix} = -\vec{u}_2 \tag{C.35}$$

Thus our conjectures hold for the CII model since operating on one of the eigenstates gives a minus sign needed to transform ϕ_+ to ϕ_-.

C.2 DIII and CI class models

In this section we will derive the analytical wavefunction expressions for the DIII and CI universality class models that have C_2 chiral symmetry. We follow the same procedure as the previous section.

The corresponding Hamiltonian is given by,

$$\begin{aligned}\hat{H}_2 = \hat{H}_0 + \hat{V}_1 = &\sum_{n\eta=1,2}^{N} (vc^\dagger_{An\eta}c_{Bn\eta} + wc^\dagger_{Bn\eta}c_{An+1\eta}) + \beta \sum_{n\eta=1,2}^{N-1} (c^\dagger_{An\eta}c_{A(n+1)-\eta} + c^\dagger_{Bn\eta}c_{B(n+1)-\eta}) \\ &+ \sum_{n\eta=1,2}^{N} (v^*c^\dagger_{Bn\eta}c_{An\eta} + w^*c^\dagger_{A(n+1)\eta}c_{Bn\eta}) + \beta^* \sum_{n\eta=1,2}^{N-1} (c^\dagger_{A(n+1)-\eta}c_{An\eta} + c^\dagger_{B(n+1)-\eta}c_{Bn\eta})\end{aligned} \tag{C.36}$$

where the operators are summed over all cells n and chains η. We apply the Hamiltonian (Eq. (C.36)) to the generic wavefunction,

$$|\Psi\rangle = \sum_{m\rho=1,2}^{M} a_{m\rho}\,|mA\rho\rangle + b_{m\rho}\,|mB\rho\rangle \tag{C.37}$$

where the wavefunction is summed over all unit cells m on all chains ρ. This gives,

$$\begin{aligned}\hat{H}_2|\Psi\rangle = &\sum_{mn\eta\rho}^{MN} v c^\dagger_{An\eta} c_{Bn\eta} a_{m\rho}|mA\rho\rangle + w c^\dagger_{Bn\eta} c_{An+1\eta} a_{m\rho}|mA\rho\rangle \\ &+ \beta(c^\dagger_{An\eta} c_{A(n+1)-\eta} a_{m\rho}|mA\rho\rangle + c^\dagger_{Bn\eta} c_{B(n+1)-\eta} a_{m\rho}|mA\rho\rangle) \\ &+ v^* c^\dagger_{Bn\eta} c_{An\eta} a_{m\rho}|mA\rho\rangle + w^* c^\dagger_{A(n+1)\eta} c_{Bn\eta} a_{m\rho}|mA\rho\rangle \\ &+ \beta^*(c^\dagger_{A(n+1)-\eta} c_{An\eta} a_{m\rho}|mA\rho\rangle + c^\dagger_{B(n+1)-\eta} c_{Bn\eta} a_{m\rho}|mA\rho\rangle) \\ &+ \sum_{mn\eta\rho}^{MN} v c^\dagger_{An\eta} c_{Bn\eta} b_{m\rho}|mB\rho\rangle + w c^\dagger_{Bn\eta} c_{An+1\eta} b_{m\rho}|mB\rho\rangle \\ &+ \beta(c^\dagger_{An\eta} c_{A(n+1)-\eta} b_{m\rho}|mB\rho\rangle + c^\dagger_{Bn\eta} c_{B(n+1)-\eta} b_{m\rho}|mB\rho\rangle) \\ &+ v^* c^\dagger_{Bn\eta} c_{An\eta} b_{m\rho}|mB\rho\rangle + w^* c^\dagger_{A(n+1)\eta} c_{Bn\eta} b_{m\rho}|mB\rho\rangle \\ &+ \beta^*(c^\dagger_{A(n+1)-\eta} c_{An\eta} b_{m\rho}|mB\rho\rangle + c^\dagger_{B(n+1)-\eta} c_{Bn\eta} b_{m\rho}|mB\rho\rangle)\end{aligned} \tag{C.38}$$

Eliminate zero overlap terms,

$$\begin{aligned}\hat{H}_2|\Psi\rangle = &\sum_{mn\eta\rho}^{MN} w c^\dagger_{Bn\eta} c_{An+1\eta} a_{m\rho}|mA\rho\rangle + \beta(c^\dagger_{An\eta} c_{A(n+1)-\eta} a_{m\rho}|mA\rho\rangle) \\ &+ v^* c^\dagger_{Bn\eta} c_{An\eta} a_{m\rho}|mA\rho\rangle + \beta^*(c^\dagger_{A(n+1)-\eta} c_{An\eta} a_{m\rho}|mA\rho\rangle) \\ &+ \sum_{mn\eta\rho}^{MN} v c^\dagger_{An\eta} c_{Bn\eta} b_{m\rho}|mB\rho\rangle + \beta(c^\dagger_{Bn\eta} c_{B(n+1)-\eta} b_{m\rho}|mB\rho\rangle) \\ &+ w^* c^\dagger_{A(n+1)\eta} c_{Bn\eta} b_{m\rho}|mB\rho\rangle + \beta^*(c^\dagger_{B(n+1)-\eta} c_{Bn\eta} b_{m\rho}|mB\rho\rangle)\end{aligned} \tag{C.39}$$

Adjust indices in the kets to match annihilation operators indices,

$$\begin{aligned}\hat{H}_2|\Psi\rangle = &\sum_{n\eta}^{N} w c^\dagger_{Bn\eta} c_{An+1\eta} a_{n+1\eta}|n+1A\eta\rangle + \beta(c^\dagger_{An\eta} c_{A(n+1)-\eta} a_{n+1-\eta}|n+1A-\eta\rangle) \\ &+ v^* c^\dagger_{Bn\eta} c_{An\eta} a_{n\eta}|nA\eta\rangle + \beta^*(c^\dagger_{A(n+1)-\eta} c_{An\eta} a_{n+1\eta}|n+1A\eta\rangle) \\ &+ \sum_{n\eta}^{N} v c^\dagger_{An\eta} c_{Bn\eta} b_{n\eta}|nB\eta\rangle + \beta(c^\dagger_{Bn\eta} c_{B(n+1)-\eta} b_{n+1-\eta}|n+1B-\eta\rangle) \\ &+ w^* c^\dagger_{A(n+1)\eta} c_{Bn\eta} b_{n\eta}|nB\eta\rangle + \beta^*(c^\dagger_{B(n+1)-\eta} c_{Bn\eta} b_{n\eta}|nB\eta\rangle)\end{aligned} \tag{C.40}$$

Apply operators,

$$\begin{aligned}\hat{H}_2|\Psi\rangle = &\sum_{n\eta}^{N} w a_{n+1\eta}|nB\eta\rangle + \beta(a_{n+1-\eta}|nA\eta\rangle) + v^* a_{n\eta}|nB\eta\rangle + \beta^*(a_{n+1\eta}|n+1A-\eta\rangle) \\ &+ \sum_{n\eta}^{N} v b_{n\eta}|nA\eta\rangle + \beta(b_{n+1-\eta}|nB\eta\rangle) + w^* b_{n\eta}|n+1A\eta\rangle + \beta^*(b_{n\eta}|n+1B-\eta\rangle)\end{aligned} \tag{C.41}$$

Adjust n and η indices,

$$\begin{aligned}\hat{H}_2|\Psi\rangle = &\sum_{n\eta}^{N} w a_{n+1\eta}|nB\eta\rangle + \beta(a_{n+1-\eta}|nA\eta\rangle) + v^* a_{n\eta}|nB\eta\rangle + \beta^*(a_{n-1-\eta}|nA\eta\rangle) \\ &+ \sum_{n\eta}^{N} v b_{n\eta}|nA\eta\rangle + \beta(b_{n+1-\eta}|nB\eta\rangle) + w^* b_{n-1\eta}|nA\eta\rangle + \beta^*(b_{n-1-\eta}|nB\eta\rangle)\end{aligned} \tag{C.42}$$

Expanding the chain sums (i.e. 1 for the top chain, 2 for the bottom one),

$$\begin{aligned}\hat{H}_2|\Psi\rangle = &\sum_{n,1}^{N} w a_{n+1,1}|nB,1\rangle + \beta(a_{n+1-\eta}|nA,1\rangle) + v^* a_{n,1}|nB,1\rangle + \beta^*(a_{n-1,2}|nA,1\rangle) \\ &+ \sum_{n,1}^{N} v b_{n,1}|nA,1\rangle + \beta(b_{n+1,2}|nB,1\rangle) + w^* b_{n-1,1}|nA,1\rangle + \beta^*(b_{n-1,2}|nB,1\rangle) \\ = &\sum_{n,2}^{N} w a_{n+1,2}|nB,2\rangle + \beta(a_{n+1,1}|nA,2\rangle) + v^* a_{n,2}|nB,2\rangle + \beta^*(a_{n-1,1}|nA,2\rangle) \\ &+ \sum_{n,2}^{N} v b_{n,2}|nA,2\rangle + \beta(b_{n+1,1}|nB,2\rangle) + w^* b_{n-1,2}|nA,2\rangle + \beta^*(b_{n-1,1}|nB,2\rangle)\end{aligned} \tag{C.43}$$

Finally we arrive at the equations of motion,

$$|nA,1\rangle: \quad b_{n,1}v + b_{n-1,1}w^* + a_{n+1,2}\beta + a_{n-1,2}\beta^* = \epsilon|nA,1\rangle \tag{C.44a}$$

$$|nA,2\rangle: \quad b_{n,2}v^* + b_{n-1,2}w + a_{n+1,1}\beta + a_{n-1,1}\beta^* = \epsilon|nA,2\rangle \tag{C.44b}$$

$$|nB,1\rangle: \quad a_{n,1}v^* + a_{n+1,1}w + b_{n+1,2}\beta + b_{n-1,2}\beta^* = \epsilon|nB,1\rangle \tag{C.44c}$$

$$|nB,2\rangle: \quad a_{n,2}v + a_{n+1,2}w^* + b_{n+1,1}\beta + b_{n-1,1}\beta^* = \epsilon|nB,2\rangle \tag{C.44d}$$

Unlike the previous BDI/CII case, these equations do not decouple nicely if we focus on the natural A-B sublattice and zero energy. However they decouple in the C_2 basis, i.e. in the chiral basis where $A \to A'$, $B \to B'$ on the top chain and on the bottom chain $A \to B'$, $B \to A'$, see Fig. 4.1. We convert the prefactors in equations (C.44) accordingly and we come to a set of decoupled equations at zero energy,

$$\begin{aligned} a'_{n,1}v^* + a'_{n+1,1}w + a'_{n+1,2}\beta + a'_{n-1,2}\beta^* &= 0 \\ a'_{n,2}v^* + a'_{n-1,2}w + a'_{n+1,1}\beta + a'_{n-1,1}\beta^* &= 0 \end{aligned} \tag{C.45}$$

$$\begin{aligned} b'_{n,2}v + b'_{n+1,2}w^* + b'_{n+1,1}\beta + b'_{n-1,1}\beta^* &= 0 \\ b'_{n,1}v + b'_{n-1,1}w^* + b'_{n+1,2}\beta + b'_{n-1,2}\beta^* &= 0 \end{aligned} \tag{C.46}$$

If we think about the state vector on cell n being of the form $\Psi_n = \begin{pmatrix} a'_{n,1} & a'_{n,2} & b'_{n,1} & b'_{n,2} \end{pmatrix}^T$ and if we expect the solution in the form of plane waves then we can take the state amplitudes at cell '0' and then apply an 'evolution' parameter that will give us the amplitude at any cell in the system. Thus we can define the following ansatz,

$$\Psi_n = \Psi_0 e^{i\lambda n} \quad \Psi_n = \begin{pmatrix} a'_{n,1} \\ a'_{n,2} \\ b'_{n,1} \\ b'_{n,2} \end{pmatrix} \quad \Psi_0 = \begin{pmatrix} a'_{0,1} \\ a'_{0,2} \\ b'_{0,1} \\ b'_{0,2} \end{pmatrix} \tag{C.47}$$

where the exponential is the decay factor and λ is the decay rate which is essentially the eigenvalues of the transfer matrix. If we break the vectors down further into the component sets we are interested in,

$$\Psi_n \rightarrow \Psi_n^{(1)} = \begin{pmatrix} a'_{n,1} \\ b'_{n,2} \end{pmatrix} \quad \Psi_n^{(2)} = \begin{pmatrix} a'_{n,2} \\ b'_{n,1} \end{pmatrix} \tag{C.48}$$

If we define $Z = e^{i\lambda}$ then we can propogate our equations as above. Looking at the first set of two equations, equations (C.44a) and (C.44b), and defining each as per equations (C.47) gives the wavefunctions as a function of Z,

$$\begin{aligned} a'_{0,1}Z^n v^* + a'_{0,1}wZ^{n+1} + b'_{0,2}\beta Z^{n+1} - b'_{0,2}\beta^* Z^{n-1} &= 0 \\ a'_{0,1}\beta Z^{n+1} + a'_{0,1}\beta^* Z^{n-1} + b'_{0,2}Z^n v^* + b'_{0,2}wZ^{n-1} &= 0 \end{aligned} \tag{C.49}$$

Divide out Z^n and consiladate into matrix form,

$$\begin{aligned} a'_{0,1}v^* + a'_{0,1}wZ + b'_{0,2}\beta Z + b'_{0,2}\beta^* Z^{-1} &= 0 \\ a'_{0,1}\beta Z + a'_{0,1}\beta^* Z^{-1} + b'_{0,2}v^* + b'_{0,2}wZ^{-1} &= 0 \end{aligned} \tag{C.50}$$

$$\begin{aligned} (v^* + wZ)a'_{0,1} + (\beta Z + \beta^{*1}/z)b'_{0,2} &= 0 \\ (\beta Z + \beta^{*1}/z)a'_{0,1} + (v^* + w^1/z)b'_{0,2} &= 0 \end{aligned}$$

$$\begin{pmatrix} (v^* + wZ) & (\beta Z + {}^{\beta^*}/_Z) \\ (\beta Z + {}^{\beta^*}/_Z) & (v^* + {}^{w}/_Z) \end{pmatrix} \begin{pmatrix} a'_{n,1} \\ b'_{n,2} \end{pmatrix} = \begin{pmatrix} 0 \\ 0 \end{pmatrix} \tag{C.51}$$

This is the recurrence relation transfer matrix for DIII. The determinant gives the allowed values for Z, and subsequently the eigenvalues of the analytical edge states. The determinant gives,

$$v^{*2} + \frac{wv^*}{Z} + wv^*Z - (\beta Z)^2 - 2|\beta|^2 - \frac{\beta^{*2}}{Z^2} = 0 \tag{C.52}$$

Multiply through by Z^2 and rearrange,

$$-\beta^2 Z^4 + wv^*Z^3 + v^{*2}Z^2 - 2|\beta|^2 Z^2 + wv^*Z - \beta^{*2} = 0 \tag{C.53}$$

This can be reduced to a quadratic, if the left side is a polynomial in Z then one may write the identity,

$$\begin{aligned} aZ^4 + bZ^3 + cZ^2 + dZ + e = 0 \\ \frac{P(Z)}{Z^2} = (aZ^2 + \frac{e}{Z^2}) + (bZ + \frac{d}{Z}) + c \end{aligned} \tag{C.54}$$

Assume $a = e$ and $b = d$, which should be true in our case,

$$\frac{P(Z)}{Z^2} = a(Z^2 + \frac{1}{Z^2}) + b(Z + \frac{1}{Z}) + c \tag{C.55}$$

This can be reduced to a simple quadratic by setting,

$$x = Z + {}^1\!/\!_Z \tag{C.56}$$

Which gives,

$$\frac{P(Z)}{Z^2} = ax^2 + bx + c \tag{C.57}$$

Solving for x gives, explicitly,

$$\begin{aligned} x_1 &= \frac{wv^* + \sqrt{(wv^*)^2 + 4(v^*\beta)^2 - 8|\beta|^2\beta^2 + 4(w\beta)^2 + 8\beta^2}}{2\beta^2} \\ x_2 &= \frac{wv^* - \sqrt{(wv^*)^2 + 4(v^*\beta)^2 - 8|\beta|^2\beta^2 + 4(w\beta)^2 + 8\beta^2}}{2\beta^2} \end{aligned} \tag{C.58}$$

We then solve for Z by multiplying equation (C.56) by Z giving,

$$Z^2 - x_1 Z + 1 = 0 \quad Z^2 - x_2 Z + 1 = 0 \tag{C.59}$$

The full solutions for Z are,

$$Z = \frac{-x_{1,2} \pm \sqrt{x_{1,2}^2 - 4}}{2}$$

$$Z_{1a,b}^{(1)} = \frac{-wv^* + \sqrt{(wv^*)^2 + 4(v^*\beta)^2 - 8|\beta|^2\beta^2 + 4(w\beta)^2 + 8\beta^2}}{4\beta^2} \pm \frac{\sqrt{(\frac{-wv^* + \sqrt{(wv^*)^2+4(v^*\beta)^2-8|\beta|^2\beta^2+4(w\beta)^2+8\beta^2}}{4\beta^2}) - 4}}{2}$$

$$Z_{2a,b}^{(1)} = \frac{-wv^* - \sqrt{(wv^*)^2 + 4(v^*\beta)^2 - 8|\beta|^2\beta^2 + 4(w\beta)^2 + 8\beta^2}}{4\beta^2} \pm \frac{\sqrt{(\frac{-wv^* - \sqrt{(wv^*)^2+4(v^*\beta)^2-8|\beta|^2\beta^2+4(w\beta)^2+8\beta^2}}{4\beta^2}) - 4}}{2} \tag{C.60}$$

Where the superscript on the Zs indicates these solutions are for equations (C.44a) and (C.44b), and the subscripts denote the two possible solutions for each. These allowed values have the relations $Z_{1a} = {}^1/_{Z_{1b}}$ and $Z_{2a} = {}^1/_{Z_{2b}}$. Now that we have a definition for Z, can now calculate the eigenvectors of the 2x2 transfer matrix from above where Z can be any of the four allowed values for Z equations (C.60),

$$\begin{pmatrix} a'_{0,1} \\ b'_{0,2} \end{pmatrix}_1 = \begin{pmatrix} 1 \\ \frac{-(v^* + wZ)}{\beta Z + \beta^* / Z} \end{pmatrix} \quad \begin{pmatrix} a'_{0,1} \\ b'_{0,2} \end{pmatrix}_2 = \begin{pmatrix} 1 \\ \frac{-(v^* + w/Z)}{\beta Z + \beta^* / Z} \end{pmatrix} \tag{C.61}$$

It is trivial to see that time-reversal will turn one edge state into the other, that is,

$$\begin{pmatrix} a'_{n,1} \\ b'_{n,2} \end{pmatrix} \rightarrow \begin{pmatrix} a'_{n,2} \\ b'_{n,1} \end{pmatrix} \tag{C.62}$$

And vice-versa.

Appendix D

Mean field calculations and SSH4

Here we derive the necessary mean field equations for a two site unit cell case and then for a four site unit cell case.

D.1 2-site unit cell case

Begin with a Hamiltonian with uniform coupling A and interaction U, and convert to momentum space,

$$\hat{H} = A\sum_{n}^{N}(c_{nA}^{\dagger}c_{nB} + c_{nB}^{\dagger}c_{n+1A} + h.c.) + U\sum_{n}^{N}(c_{nA}^{\dagger}c_{nA}c_{nB}^{\dagger}c_{nB} + c_{n+1A}^{\dagger}c_{n+1A}c_{nB}^{\dagger}c_{nB}) \tag{D.1}$$

$$= A\sum_{k}^{BZ}(c_{kA}^{\dagger}c_{kB} + c_{nB}^{\dagger}c_{kA}e^{ik} + h.c.) + U\sum_{k}^{N}(c_{kA}^{\dagger}c_{kA}c_{kB}^{\dagger}c_{kB})e^{ik_1 n}e^{-ik_2 n}e^{ik_3 n}e^{-ik_4 n} \tag{D.2}$$

$$= A\sum_{k}^{BZ}(c_{kA}^{\dagger}c_{kB} + c_{nB}^{\dagger}c_{kA}e^{ik} + h.c.) + U\sum_{k}^{BZ}(c_{kA}^{\dagger}c_{kA}c_{kB}^{\dagger}c_{kB})\delta(k_1 - k_2 + k_3 - k_4) \tag{D.3}$$

$$= A\sum_{k}^{BZ}(c_{kA}^{\dagger}c_{kB} + c_{nB}^{\dagger}c_{kA}e^{ik} + h.c.) + U\sum_{kpq}^{BZ}(c_{kA}^{\dagger}c_{k+qA}c_{pB}^{\dagger}c_{p-qB}(1 + e^{-iq})) \tag{D.4}$$

where we have parameterized $k_1 = k, k_2 = k+q, k_3 = p, k_4 = p-q$. Diagonalize $H = C_k^{\dagger}\tilde{U}D\tilde{U}^{-1}C_k$ where $\tilde{U}^{-1}C_k = (c_- c_+)^T$ with $-$ and $+$ representing the lower and upper bands respectively. Also have $C^{\dagger}\tilde{U} = (c_-^{\dagger}c_+^{\dagger})$. The $\tilde{U}$s are the eigenvectors of H and are unitary such that $\tilde{U}^{-1} = \tilde{U}^{\dagger}$ and are all functions of k.

$$\tilde{U} = \begin{pmatrix} u_{11} & u_{21} \\ u_{12} & u_{22} \end{pmatrix} \tag{D.5}$$

where the first eigenvector is the first column $(u_{11}\ u_{12})$ and the second eigenvector $(u_{21}\ u_{22})$ in the second column. Transform the momentum space operators to the band basis,

$$c_{kA}^{\dagger} = u_{11}^{*} c_{-}^{\dagger} + u_{21}^{*} c_{+}^{\dagger} \tag{D.6}$$
$$c_{kB}^{\dagger} = u_{12}^{*} c_{-}^{\dagger} + u_{22}^{*} c_{+}^{\dagger} \tag{D.7}$$
$$c_{kA} = u_{11} c_{-} + u_{21} c_{+} \tag{D.8}$$
$$c_{kB} = u_{12} c_{-} + u_{22} c_{+} \tag{D.9}$$

We are at half-filling so will only be interested in the (-,-) terms. Calculate expectation values of the kinetic operators,

$$\langle c_{kA}^{\dagger} c_{kB} \rangle = (u_{11}^{*} c_{-}^{\dagger} + u_{21}^{*} c_{+}^{\dagger})(u_{12} c_{-} + u_{22} c_{+}) \tag{D.10}$$
$$= u_{11}^{*} u_{12} c_{-}^{\dagger} c_{-} + u_{11}^{*} u_{22} c_{-}^{\dagger} c_{+} + u_{21}^{*} u_{12} c_{+}^{\dagger} c_{-} + u_{21}^{*} u_{22} c_{+}^{\dagger} c_{+} \tag{D.11}$$
$$= u_{11}^{*} u_{12} c_{-}^{\dagger} c_{-} \tag{D.12}$$

And the $c_{kB}^{\dagger} c_{kA}$ term is just the complex conjugate of above. To save ourselves calculating all of the components in the four operator interacting term we use the half-filling condition to know that the only nonzero terms are $\langle c_{-}^{\dagger} c_{-} c_{-}^{\dagger} c_{-} \rangle$ and $\langle c_{-}^{\dagger} c_{+} c_{+}^{\dagger} c_{-} \rangle$ which occur when $q = 0$ and $q = p - k$, respectively.

$$\langle c_{-}^{\dagger} c_{-} c_{-}^{\dagger} c_{-} \rangle = \begin{cases} |u_{11}|^2 |u_{11}|^2 & if \;\; q = 0 \\ u_{11}^{*} u_{21} u_{22}^{*} u_{12} & if \;\; q = p - k \\ 0 & otherwise \end{cases} \tag{D.13}$$

Establish the mean field integrals for kinetic and interacting terms,

$$\langle \hat{H}_{kin} \rangle = A \int_{BZ} [u_{11}^{*} u_{22} (1 + e^{ik} + u_{11} u_{22}^{*} (1 + e^{-ik})] \frac{dk}{2\pi} \tag{D.14}$$

$$\langle \hat{H}_{int} \rangle = U \int_{BZ} \int_{BZ} [2|u_{11}|^2 |u_{11}|^2 + u_{11}^{*} u_{21} u_{22}^{*} u_{12} (1 + e^{i(k-p)})] \frac{dk}{2\pi} \tag{D.15}$$

$$\hat{H}_1^{MF} = \begin{pmatrix} c_{kA}^{\dagger} & c_{kB}^{\dagger} \end{pmatrix} \begin{pmatrix} \delta w & -t(1 + e^{-ik}) \\ -t(1 - e^{ik}) & -\delta w \end{pmatrix} \begin{pmatrix} c_{kA} \\ c_{kB} \end{pmatrix} \tag{D.16}$$

In general performing the integrals analytically is not advised so we stick to simple numerical integration using the trapezoidal rules in both one and two dimensions. Obviously one could use one of the more accurate Simpsons rules but this one is accurate enough for our purposes.

$$\int_a^b f(x) = \frac{\Delta x}{2} [f(x_0) + 2f(x_1) + 2f(x_2) + \cdots + 2f(x_{N-1}) + f(x_N)] \tag{D.17}$$

$$\int_a^b \int_c^d f(x,y)dxdy = \frac{\Delta x \Delta y}{4}[f(a,c)+f(b,c)+f(a,d)+f(b,d)+2\sum_i f(x_i,c)+2\sum_i f(x_i,d) \\ +2\sum_j f(a,y_j)+2\sum_j f(b,y_j)+4\sum_j\sum_i f(x_i,y_j)] \tag{D.18}$$

where $\Delta x(y) = \frac{b-a}{N}$.

D.2 4-site unit cell case

Here we construct the mean field theory for a four site unit cell Hamiltonian,

$$\hat{H}_{kin} = A\sum_n^N (c^\dagger_{nA}c_{nB} + c^\dagger_{nA'}c_{nB'} + h.c.) + B\sum_n^N (c^\dagger_{nB}c_{nA'} + c^\dagger_{nB'}c_{n+1A} + h.c.) \tag{D.19}$$

$$\hat{H}_{int} = U\sum_n^N (c^\dagger_{nA}c_{nA}c^\dagger_{nB}c_{nB} + c^\dagger_{nA'}c_{nA'}c^\dagger_{nB'}c_{nB'}) \tag{D.20}$$

Convert to momentum space,

$$\hat{H}_{kin}(k) = A\sum_k^{BZ} (c^\dagger_{kA}c_{kB} + c^\dagger_{kA'}c_{kB'} + h.c.) + B\sum_k^{BZ} (c^\dagger_{kB}c_{kA'} + c^\dagger_{kB'}c_{kA}e^{ik} + h.c.) \tag{D.21}$$

$$\hat{H}_{int}(k) = U\sum_k^{BZ} (c^\dagger_{kA}c_{k+qA}c^\dagger_{pB}c_{pp-qB} + c^\dagger_{kA'}c_{k+qA'}c^\dagger_{pB'}c_{p-qB'}) \tag{D.22}$$

We label the four bands from lowest to highest as 1,2,3,4. We give the matrix of eigenvectors (columns),

$$\tilde{U} = \begin{pmatrix} u_{11} & u_{21} & u_{31} & u_{41} \\ u_{12} & u_{22} & u_{32} & u_{42} \\ u_{13} & u_{23} & u_{33} & u_{43} \\ u_{14} & u_{24} & u_{34} & u_{44} \end{pmatrix} \tag{D.23}$$

Construct the vector of operators,

$$C_k = \tilde{U}C_\pm = \begin{pmatrix} u_{11} & u_{21} & u_{31} & u_{41} \\ u_{12} & u_{22} & u_{32} & u_{42} \\ u_{13} & u_{23} & u_{33} & u_{43} \\ u_{14} & u_{24} & u_{34} & u_{44} \end{pmatrix} \begin{pmatrix} c_1 \\ c_2 \\ c_3 \\ c_4 \end{pmatrix} \tag{D.24}$$

Define the annihilation operators in terms of the basis of bands,

$$c_{kA} = u_{11}c_1 + u_{21}c_2 + u_{31}c_3 + u_{41}c_4 \tag{D.25}$$
$$c_{kB} = u_{12}c_1 + u_{22}c_2 + u_{32}c_3 + u_{42}c_4 \tag{D.26}$$
$$c_{kA'} = u_{13}c_1 + u_{23}c_2 + u_{33}c_3 + u_{43}c_4 \tag{D.27}$$
$$c_{kB'} = u_{14}c_1 + u_{24}c_2 + u_{34}c_3 + u_{44}c_4 \tag{D.28}$$

On to calculating the expectation values of each term. Since we are working at quarter filling ($\upsilon = 1/4$) this cuts down the number of nonzero terms significantly. We will only write these nonzero terms to save time. The only nonzero expectation value terms from the kinetic Hamiltonian, Eq. (7.31a), involve $\langle c_1^\dagger c_1 \rangle$,

$$\langle c_{kA}^\dagger c_{kB} \rangle = u_{11}^* u_{12} \langle c_1^\dagger c_1 \rangle \tag{D.29a}$$
$$\langle c_{kA'}^\dagger, c_{kB'} \rangle = u_{13}^* u_{14} \langle c_1^\dagger c_1 \rangle \tag{D.29b}$$
$$\langle c_{kB}^\dagger c_{kA'} \rangle = u_{12}^* u_{13} \langle c_1^\dagger c_1 \rangle \tag{D.29c}$$
$$\langle c_{kB'}^\dagger c_{kA} \rangle = u_{14}^* u_{11} \langle c_1^\dagger c_1 \rangle \tag{D.29d}$$

We have also parameterized the momentums in the same way as the 2x2 case which leads to the only nonzero interacting expectation value terms are those involving,

$$\langle c_1^\dagger c_1 c_1^\dagger c_1 \rangle \tag{D.30a}$$
$$\langle c_1^\dagger c_2 c_2^\dagger c_1 \rangle \tag{D.30b}$$
$$\langle c_1^\dagger c_3 c_3^\dagger c_1 \rangle \tag{D.30c}$$
$$\langle c_1^\dagger c_4 c_4^\dagger c_1 \rangle \tag{D.30d}$$

All other operator combinations are zero. For $q = 0$,

$$\langle c_{kA}^\dagger c_{kA} c_{pB}^\dagger c_{pB} \rangle = |u_{11k}|^2 |u_{12p}|^2 \langle c_1^\dagger c_1 c_1^\dagger c_1 \rangle \tag{D.31}$$

and for $q = p - k$,

$$\langle c_{kA'}^\dagger, c_{kA'} c_{pB'}^\dagger, c_{pB'} \rangle = |u_{13k}|^2 |u_{14p}|^2 \langle c_1^\dagger c_1 c_1^\dagger c_1 \rangle \tag{D.32}$$
$$\langle c_{kA}^\dagger c_{pA} c_{pB}^\dagger c_{kB} \rangle = u_{11k}^* u_{21p} u_{22p}^* u_{12k} \langle c_1^\dagger c_2 c_2^\dagger c_1 \rangle + u_{11k}^* u_{31p} u_{32p}^* u_{12k} \langle c_1^\dagger c_3 c_3^\dagger c_1 \rangle + u_{11k}^* u_{41p} u_{42p}^* u_{12k} \langle c_1^\dagger c_4 c_4^\dagger c_1 \rangle \tag{D.33}$$
$$\langle c_{kA'}^\dagger, c_{pA'} c_{pB'}^\dagger, c_{kB'} \rangle = u_{13k}^* u_{23p} u_{24p}^* u_{14k} \langle c_1^\dagger c_2 c_2^\dagger c_1 \rangle + u_{13k}^* u_{33p} u_{34p}^* u_{14k} \langle c_1^\dagger c_3 c_3^\dagger c_1 \rangle + u_{13k}^* u_{43p} u_{44p}^* u_{14k} \langle c_1^\dagger c_4 c_4^\dagger c_1 \rangle \tag{D.34}$$

Then the mean field expectation value integrals are,

$$\langle \hat{H}_{kin} \rangle = \int_{BZ} [A(u_{11}^* u_{12} + u_{13}^* u_{14} + h.c.) + B(u_{12}^* u_{13} + u_{14}^* u_{11} e^{ik} + h.c.)] \frac{dk}{2\pi} \tag{D.35}$$

$$\begin{aligned}\langle \hat{H}_{int} \rangle = U \int_{BZ} \int_{BZ} [&|u_{11k}|^2 |u_{12p}|^2 + |u_{13k}|^2 |u_{14p}|^2 + u_{11k}^* u_{21p} u_{22p}^* u_{12k} + u_{11k}^* u_{31p} u_{32p}^* u_{12k} \\ &+ u_{11k}^* u_{41p} u_{42p}^* u_{12k} + u_{13k}^* u_{23p} u_{24p}^* u_{14k} + u_{13k}^* u_{33p} u_{34p}^* u_{14k} \\ &+ u_{13k}^* u_{43p} u_{44p}^* u_{14k}] \frac{dk}{2\pi} \frac{dp}{2\pi}\end{aligned} \tag{D.36}$$

Use the mean field chain Eq. (7.18) Hamiltonian,

$$\hat{h}(k) = \begin{pmatrix} 0 & (v+\delta v) & 0 & (w-\delta w)e^{-ik} \\ (v+\delta v) & 0 & (w+\delta w) & 0 \\ 0 & (w+\delta w) & 0 & (v-\delta v) \\ (w-\delta w)e^{ik} & 0 & (v-\delta v) & 0 \end{pmatrix} \tag{D.37}$$

D.3 SSH4 model

The Hamiltonian for this is then,

$$\begin{aligned}\hat{H}_{SSH4} = &\sum_j^N ((v+\delta v) c_{jA}^\dagger c_{jB} + (w+\delta w) c_{jB}^\dagger c_{jC} + (v-\delta v) c_{jC}^\dagger c_{jD}) + \sum_j^N ((w-\delta w) c^\dagger c_{j+1,A} + (w-\delta w) c_{j+1,A}^\dagger c_{jD}) \\ &+ \sum_j^N ((v+\delta v) c_{jB}^\dagger c_{jA} + (w+\delta w) c_{jC}^\dagger c_{jB} + (v-\delta v) c_{jD}^\dagger c_{jC})\end{aligned} \tag{D.38}$$

Convert to momentum space,

$$\hat{H}_{SSH4(k)} = (v+\delta v) \frac{1}{N} \sum_{kk'n}^{BZ} c_{kA}^\dagger c_{k'B} e^{-ikn} e^{ik'n} + (w+\delta w) \frac{1}{N} \sum_{kk'n}^{BZ} c_{kB}^\dagger c_{kC} e^{-ikn} e^{ik'n} \tag{D.39}$$

$$+ (v-\delta v) \frac{1}{N} \sum_{kk'n}^{BZ} c_{kC}^\dagger c_{k'D} e^{-ikn} e^{ik'n} + (v+\delta v) \frac{1}{N} \sum_{kk'n}^{BZ} c_{kB}^\dagger c_{k'A} e^{-ikn} e^{ik'n} \tag{D.40}$$

$$+ (w+\delta w) \frac{1}{N} \sum_{kk'n}^{BZ} c_{kC}^\dagger c_{k'B} e^{-ikn} e^{ik'n} + (v-\delta v) \frac{1}{N} c_{kD}^\dagger c_{k'C} e^{-ikn} e^{ik'n} \tag{D.41}$$

$$+ (w-\delta w) \frac{1}{N} (\sum_{kk'n}^{BZ} c_{kD}^\dagger c_{k'A} e^{-ikn} e^{ik'(n+1)} + c_{kA}^\dagger c_{k'D} e^{-ik(n+1)} e^{ik'n}) \tag{D.42}$$

Sum the exponentials,

$$\hat{H}_{SSH4(k)} = (v+\delta v)\sum_{k}^{BZ}(c_{kA}^{\dagger}c_{kB} + c_{kB}^{\dagger}c_{kA}) + (v-\delta v)\sum_{k}^{BZ} c_{kC}^{\dagger}c_{kD} + c_{kD}^{\dagger}c_{kC}) \tag{D.43}$$

$$+ (w+\delta w)\sum_{k}^{BZ}(c_{kB}^{\dagger}c_{kC} + c_{kC}^{\dagger}c_{kB}) + (w-\delta w)\sum_{k}^{BZ}(c_{kD}^{\dagger}c_{kA}e^{ik} + c_{kA}^{\dagger}c_{kD}e^{-ik}) \tag{D.44}$$

This can be brought into a block off-diagonal form by rearranging the basis such that it is $\{A\ C\ B\ D\}$,

$$\hat{h}_{SSH4}(k) = \begin{pmatrix} 0 & 0 & (v+\delta v) & (w-\delta w)e^{ik} \\ 0 & 0 & (w+\delta w) & (v-\delta v) \\ (v+\delta v) & (w+\delta w) & 0 & 0 \\ (w-\delta w)e^{-ik} & (v-\delta v) & 0 & 0 \end{pmatrix} \tag{D.45}$$